Student thesis series INES nr 301

Modeling the Evolution of Wildfire: An Analysis of Short Term Wildfire Events and their Relationship to Meteorological Variables.

Sean Gardner Demet

2014
Department of
Physical Geography and Ecosystems Science
Lund University
Sölvegatan 12
S-223 62 Lund
Sweden

Seminar series nr 301

Sean Gardner Demet (2014). Modeling the Evolution of Wildfire: An Analysis of Short Term Wildfire Events and their Relationship to Meteorological Variables.
Master degree thesis, 30 credits in *Physical Geography and Ecosystem Analysis*
Department of Physical Geography and Ecosystems Science, Lund University

Modeling the Evolution of Wildfire: An Analysis of Short Term Wildfire Events and their Relationship to Meteorological Variables.

Sean Gardner Demet
Master degree thesis, 30 credits, in Physical Geography and Ecosystem Analysis

Supervisor:
Dr. Veiko Lehsten
Department of Physical Geography and Ecosystems Science
Lund University

Abstract

Wildfire events are expected to increase with the changing climate; thereby increasing atmospheric, economic, and anthropogenic impacts. Gaining a real-time understanding of the evolution of wildfire events can benefit regional meteorology models, global atmospheric models, and hazard warning systems. As a result, an attempt at modeling the evolution of wildfire was undertaken utilizing 8 years of daily meteorological variables and fire radiative power (FRP) provided by the European Centre for Medium-Range Weather Forecasting from 2003 to 2010.

Fire Radiative Power (FRP) measures the rate of radiative energy emitted by active wildfire events across the globe. FRP is observed from MODIS sensors aboard the sun-synchronous Terra and Aqua satellites and provides a unique way to incorporate active wildfire information into climate models and weather forecasting. Observations have shown that the amount of FRP is related to the rate at which fuel is being consumed, linking it directly to the fuel load of ecosystems. The impact of meteorological variables on the behavior of FRP, on a daily basis, is expected to show an observable relationship. Modeling this relationship is the primary objective of the thesis.

Meteorological variables and a time-delayed FRP value were established as independent variables for linear regression modeling. The relative change in FRP (ΔFRP) functioned as the dependent variable. Three distinct ecosystems (Equatorial, Warm Temperate, and Boreal) were included to account for vegetation structure and fuel load. Ecosystem selection was performed using the climate based Köppen-Geiger Climate Classification which created approximately homogeneous ecosystems based off of observed temperature and precipitation values.

Covariate analysis showed no significant correlation between the independent variables and ΔFRP. Mann-Whitney U Tests identified ecosystems where statistically significant trends were observed and suggested opportunities for successful linear regression modeling. Both linear and non-linear relationships were accounted for in the application of a Bayesian Information Criteria to the linear regression modeling. The linear regression results did not produce a successful model and the impact of meteorological variables on FRP was not observable.

Acknowledgements

I'd like to recognize my family and friends, for their positive encouragement, emotional support and inspiration throughout this process. Most of all, I'd like to thank my grandma, Margadette Demet, for her keen editorial eye, constant support, and gentle encouragement along the way.

Finally, I'd like to acknowledge my advisor, Veiko Lehsten. Without his help and guidance this would not have been possible. His unceasing patience, flexibility, and availability proved critical in every step of the effort.

Table of Contents

Abstract....3
Acknowledgements....4
Introduction....7
Hypothesis....10
Data....10
Computer Programs....10
Fire Radiative Power....10
Meteorological Variables....12
Köppen-Geiger Climate Classification....12
Methods....13
Zone Selection....15
Additional Data....16
Relative Humidity....16
Angstrom Index....16
Temporal Aspects and ΔFRP....17
Covariate Analysis....18
Histograms....18
Correlation Coefficients....18
Scatterplots & R2....18
Box Plots....18
Mann-Whitney U test....19
Model Development and evaluation....20
Results....21
Spatial Arrangements....21
Autocorrelation and Correlation Coefficients....24
Histograms....27
Box Plot Results....29
Mann-Whitney U Test Results....31
Model Results....33
Discussion....34

Variable Comparison & Performance....36
FRP, FRP0 & ΔFRP....36
Moisture Variables....38
Movement Variables....41
Ecosystem Impacts....44
Impacts of the Köppen-Geiger Climate Classification....46
Conclusion....48
Bibliography....50
Appendix 1: Köppen-Geiger Climate Map....53
Appendix 2: Mapped Variables....54
Appendix 2: Autocorrelation Tables....64
Appendix 3: Independent Variable Correlations....65
Appendix 4: Scatterplots....66
Appendix 5: Histograms....67
Appendix 6: Box Plots....70
Appendix 7: Mann-Whitney U Test Results....71
Appendix 8: BIC and Modeling....76
Appendix 9: Computer Script....78

Introduction

Fire is a natural component of the earth's carbon system and plays an integral part in maintaining ecosystems by influencing vegetation distribution and structure (Bowman, Balch, & Artaxo, 2009). Fire is also utilized as an anthropogenic landscape management tool to control vegetation structure and clear land for agriculture. According to Golding (2011), "wildfires oxidize 1.7 to 4.1 GtC per year which represents about 3-8% of total terrestrial Net Primary Productivity" of atmospheric carbon. Whether natural or anthropogenic forces ignite wildfires, their occurrence poses several problems that impact the surrounding landscape, atmosphere, and population centers.

Wildfire events generate significant emissions of greenhouse gases such as methane and carbon dioxide which contribute directly to the greenhouse effect. In addition to greenhouse gases, fires are a significant source of black carbon and aerosol particles (Werd et al., 2004; Ramanathan & Carmichael, 2008; Vermote et al., 2009). Wildfires create a significant impact on the larger earth system and atmosphere, while also generating a significant impact on the human scale. Peterson (2013) states that fires may interact with meteorological processes a great distance away. Fine particulate matter and aerosols emitted by wildfire poses a direct risk to human health by impacting air quality and visibility (Kinney, 2008; Konovalov, Beekmann, Kuznetsova, Yurova, & Zvyagintsev, 2011). Wildfire occurring in the urban-rural interface also creates significant economic damage to property, agriculture, and forestry (Barker, 2007). Fire frequency, size, intensity and seasonality shape forest composition and production, controlling and limiting economic gain and altering the ecosystem (Easterling, Aggarwal, & Batima, 2007).

According to Bowman et al. (2009), "at the landscape scale, fire responds predictability to variation in fuel types, vegetation structure, topographic features and weather conditions." An active wildfire event intersects these factors thereby influencing the atmosphere, biosphere and hydrosphere. Each fire event is in turn impacted by the fuel type, moisture content and combustion type which are subject to temperature and available oxygen (Bowman et al., 2009). Additionally work by Golding (2011) determined that temperature, precipitation, relative humidity and wind speed are the key meteorological factors that affect wildfires. Fire responds to complex mechanisms and is very challenging to model.

On a daily scale, climate primarily effects the moisture content of fuel, but the impact of climate extends beyond that when considering longer time scales. Over a medium time scale (seasonal to yearly), climate is poised to alter the vegetation structure and subsequently the fuel type of a given region. Over a longer time scale, climate can impact topographic features of the region. The short term effects of climate are of primary consideration for this thesis; however, with a changing climate, the medium term impacts of climate are expected to dictate seasonal occurrence of wildfire events (Easterling et al., 2007).

Meteorological variables impacting fires fall into two primary groups; moisture and movement. Both of these groups are critical in determining fuel moisture and fire spread. It is unclear which group will be more pertinent for this modeling effort. Typically, variables in the moisture group directly impact fuel moisture and exhibit an inverse relation to fire growth. Increases in fuel moisture decrease fire growth and vice versa. Additionally, precipitation drives the net primary productivity effectively increasing fuel load (Lehsten, Harmand, Palumbo, & Arneth, 2010). Variables in the movement group interact with fuel moisture via evaporation and exhibit a direct relationship with the fire growth, e.g. increased wind and increased air temperature leads to drier fuel and increase fire growth.

The impact of both variable groups is effective over different time scales varying from daily to seasonal (Freeborn, Wooster, & Roberts, 2011). Climate variables such as air temperature and wind speed influence the diurnal behavior of fires while precipitation events have an immediate effect when present. The immediate impact of precipitation events enable easier forecasting of the decay of fire events compared to the growth of fire events (Peterson et al., 2013). Drought conditions represent a seasonal impact. Suppressed precipitation and high temperatures over a season effect the lifespan of wildfire events. According to Peterson et al. (2013), "the duration of dry conditions typically has a much stronger relation to burned area observations than the total seasonal precipitation and therefore sets the stage for active fire weather conditions." Both variable groups, moisture and movement, impact fire conditions on short term and long term timescales. It is unclear which has the greater impact and this uncertainty serves as a motivation for the research.

Expectations for significant meteorological variables that dictate the behavior of fire were obtained from pre-existing fire indices. Evaluating these indices guide the focus of the research and illuminate the important meteorological variables in regard to wildfire events. The meteorological variables utilized by the Canadian Forest Fire Danger Rating System (CFFDRS) include surface temperature, relative humidity, rainfall, and wind speed. The goal of the CFFDRS is to determine biomass moisture content; thereby predicting daily fire potential and spread in the unique boreal ecosystem (Peterson et al., 2013). Two other fire indices, the McArthur Forest Fire Danger Index (FFDI) and Canadian Fire Weather Index (FWI) were compared by Dowdy et al. (2009) and determined to be similar on the broad scale and complementary, even though they were developed for Australia (FFDI) and Canada (FWI). Dowdy also determined that fire indices were most sensitive to wind speed, followed by relative humidity, and temperature. Furthermore the Angstrom Index utilizes temperature and relative humidity, in addition to precipitation to determine ignition likelihood. Golding (2011) goes onto note that "changes in land cover and vegetation will strongly influence how the FFDI applies in practice. Other non-meteorological changes, such as population, will also influence the risk of forest fires." The impacts of climate change on fire occurrence and persistence are unpredictable due to the effects expected on both the meteorological variables and the vegetation structure.

According to Easterling et al. (2007), authors of the *Food Fibre and Forest Products* chapter in the fourth assessment from the IPCC, "there is uncertainty associated with the studies of climate change and forest fires; however, current modeling studies suggest that increased temperatures and longer growing seasons will elevate fire risk in connection with increased aridity." They go on to cite the work of Crozier and Dwyer (2006) and Flannigan et al. (2005) who both predict an increase wildfire occurrence. Crozier and Dwyer focused on the United States in a changing climate and indicated the "possibility of a 10% increase in the seasonal severity of fire hazard". While Flannigan et al. focused on the burned area in Canada and "projected as much as 74-118% increase of the area burned in Canada by the end of the 21st century". Similarly, Golding (2011) states that the largest proportional increases of fire danger is expected under the A1B scenarios for Europe, Amazonia and parts of North America and East Asia. The primary mechanism that Golding cites for increases in fire danger is the increasing temperatures which increase daily maximum temperatures, and also reduce relative humidity. Needless to say, with the global rise in temperature, decreased soil moisture, extended periods of drought and a longer growing season, the occurrence of wild fire is most likely to increase. And fire induced emissions will influence future climate scenarios and fire weather (Bowman et al., 2009; Easterling et al., 2007; Westerling, Hidalgo, Cayan, & Swetnam, 2006).

The particular impacts of climate change on specific meteorological variables can be challenging to predict and model and require specific attention. Easterling et al., (2007) highlights a particularly

hard to model process that is expected to increase. The positive feedback observed between deforestation, forest fragmentation, wildfire occurrence and increased frequency of droughts exists in the Amazon basin. Which is an area expected to experience temperature increases which may trigger massive deforestation. Complex feedback loops, insects and extreme events are identified by Easterling as challenging drivers to model. This challenge is further when considering the impact of climate change on wind and precipitation (Golding & Caesar, 2011). Incorporating these complex drivers requires models focusing on a longer time scale than that considered for this thesis. However; a sound understanding of short-term effects of meteorological variables on fire radiative power (FRP) would be beneficial to managing increased fire occurrence through predictive modeling of fire evolution.

Similar research and attempts have been made to model the evolution of fires. Peterson et al., (2013) states that common attempts at modeling focus primarily on ignition events and are assessed on a seasonal or monthly basis, which is concurrent with the literature review. This seasonal and monthly focus has provided a robust understanding of meteorological drivers and missing components poised to improve modeling. Research, performed by Golding (2011), has established the "primary meteorological driver of projected changes in forest fire danger on a global scale is generally temperature, followed by relative humidity which itself is strongly influenced by temperature." Additionally, Easterling et al. (2007) has acknowledged the absence of key ecological processes typically modeled by dynamic global vegetation models. Inclusion of fire effects into these vegetation models allow better predictions of climate-induced vegetative change. This will also help to highlight the importance of temperature, relative humidity, and vegetation structure in modeling efforts.

There was one modeling effort similar to, but more detailed than this research, which was discovered after the establishment and execution of the methods for this research. Peterson et al., (2013) made the first attempt at a numerical weather prediction (NWP) to characterize the impact of meteorological conditions on the following day fire activity. They included ignition and spread potential to enhance the forecasting of smoke emission over large spatial scales.

They were prompted to explore usage of NWP data to capture day-to-day changes in fire activity by the 2008 paper from Mölders where a Weather Research and Forecasting model successfully calculated fire weather indices at a spatiotemporal resolution of 1.0º and 6-h for interior Alaska. The focus of the Peterson et al. (2013) paper was focused on the North American boreal forest. Using fire count data recorded from the MODIS sensors aboard the Terra and Aqua satellites, the objective was to establish an empirical relationship between weather, fire ignition and fire evolution. The objective was achieved through inclusion of a fire weather index, initial spread index, fine fuel moisture content, synoptic index, moisture index and relative humidity. Their approach to modeling fire evolution was more detailed than this research and helped to illuminate the challenges of predicting fire evolution.

Considering the complex nature of fire modeling. It is the objective of this thesis to explore the relationships between meteorological variables and FRP. Focusing on a global scale and highlighting three distinct ecosystems will enable a better understanding of the evolution of wildfire events. Variables related to both movement and moisture will be included in the research. Through covariate analysis and Mann-Whitney U tests, the relationships between FRP and meteorological variables will be determined. This knowledge can be applied to linear regression modeling with a Bayesian Information Criteria to generate predictive models for each major ecosystem. This process will be done for three ecosystems where fire is featured prominently in the landscape, those being the Boreal ecosystem, Mediterranean ecosystem, and Equatorial ecosystems.

Hypothesis

The predicted increase in wildfire activity due to long term climate trends and the poor predictability of the evolution of wildfires limits the accuracy of multi-day forecasts (Easterling et al., 2007; J. W. Kaiser et al., 2012). Furthermore, there are differing opinions as to which meteorological variable has the strongest impact on the evolution of fire evolution. These uncertainties serve as the primary motivation for this research.

As a result they have prompted the establishment of two hypotheses guiding the research. First, meteorological data can be used to predict future FRP values and improve realtime forecasting of wildfire events. Second, considering the prominent meteorological variables in existing indices, moisture variables will have a more significant impact on FRP than movement variables.

Data

There were three primary sources of data required for analysis and development of the short term wildfire model; fire radiative power (FRP) values, meteorological values, and land classification values. All data used in the analysis and development was provided over the whole globe in grid cells measuring 0.5° x 0.5°. Daily values were used for model development and evaluation from 2003 to 2010, with the years 2003-2007 serving as the development dataset and 2008-2010 serving as the evaluation dataset. Unlike most other research regarding the relationship between meteorological variables and wildfire evolution, the linear regression modeling was conducted for daily variables rather than monthly or seasonally. All of the raw data used in the model development and analysis was provided by the European Centre for Medium-Range Weather Forecasting (ECMWF).

Computer Programs

Dataset construction required the use of Climate Data Operators (CDO) while the covariate analysis and model development and evaluation were performed with the statistical computing software R. CDO provided the means by which to join the two independent datasets of FRP values and meteorological variables through bilinear interpolation. Preceding this, the latitude and longitude were corrected to remain uniform throughout the dataset, and the 8x daily meteorological variables were transformed to represent single day values by selecting the maximum, minimum, or total value for each day. Furthermore, zone selection was conducted through CDO when the two datasets were joined. At this point, the R program was utilized to add the time delayed information, calculate the ΔFRP, and select short-term wildfire events by the ΔFRP. Additionally, R was used for table formation, generation of graphics, statistical analysis, model development and model evaluation.

Fire Radiative Power

FRP is the rate of radiative energy emitted by an active fire in W/m^2. The Global Fire Assimilation System (GFASv1.0) uses FRP observations to determine current fire events and calculate biomass burning emissions. According to Csiszar et al (2009), there is a strong empirical relationship between rate of combustion that allows CO2 emission rates from a fire to be estimated from FRP observations. Furthermore, ground-truthing for small-scale experimental fires have shown that the amount of FRP is related to the rate at which fuel is being consumed (Csiszar 2009).

These observations are made using the Moderate Resolution Imaging Spectrometer (MODIS) aboard the Terra and Aqua satellites (J. Kaiser, Suttie, & Flemming, 2009; J. W. Kaiser et al., 2012).

Specifically, the FRP observations are obtained by measuring the thermal emissive bands at 3.9 µm and 11.0 µm and represent the rate of release of fire radiative energy (Freeborn et al., 2011; Giglio, 2010; Ichoku & Kaufman, 2005). By comparing the difference of the mid infrared spectral range of the fire pixel radiance to the background radiance of surrounding pixels the same pixel, the proportional FRP can be determined. These measurements over each pixel generate a grid-related data layer summarizing the fire pixel information (Giglio et al. 2003; Justice et al. 2003). While the process of determining FRP is performed for each pixel, the FRP values assumed to represent the whole grid cell. MODIS observations include two dimensions to each measurement: the primary FRP value along with a secondary value detailing the effective satellite observations of each grid cell (J. W. Kaiser et al., 2012; Konovalov et al., 2011; Wooster, Roberts, Perry, & Kaufman, 2005). Effective satellite passes are limited by the sun-synchronous orbit of the Terra and Aqua satellites. MODIS observations are limited to cloud free days and disregard observations over snow, ice, and bodies of water (Kaiser et al. 2012).

The original format for FRP measurements were as Network Common Data Form (NetCDF) files. The raw FRP data were as daily values for 2003-2010 with corresponding latitudes and longitudes to match other data. Applications of these FRP values can be visualized in Figure 1, where they were used to calculate the average distribution of carbon combustion (gC a^{-1} m^{-2}) over the years 2003-2008 (J. W. Kaiser et al., 2012).

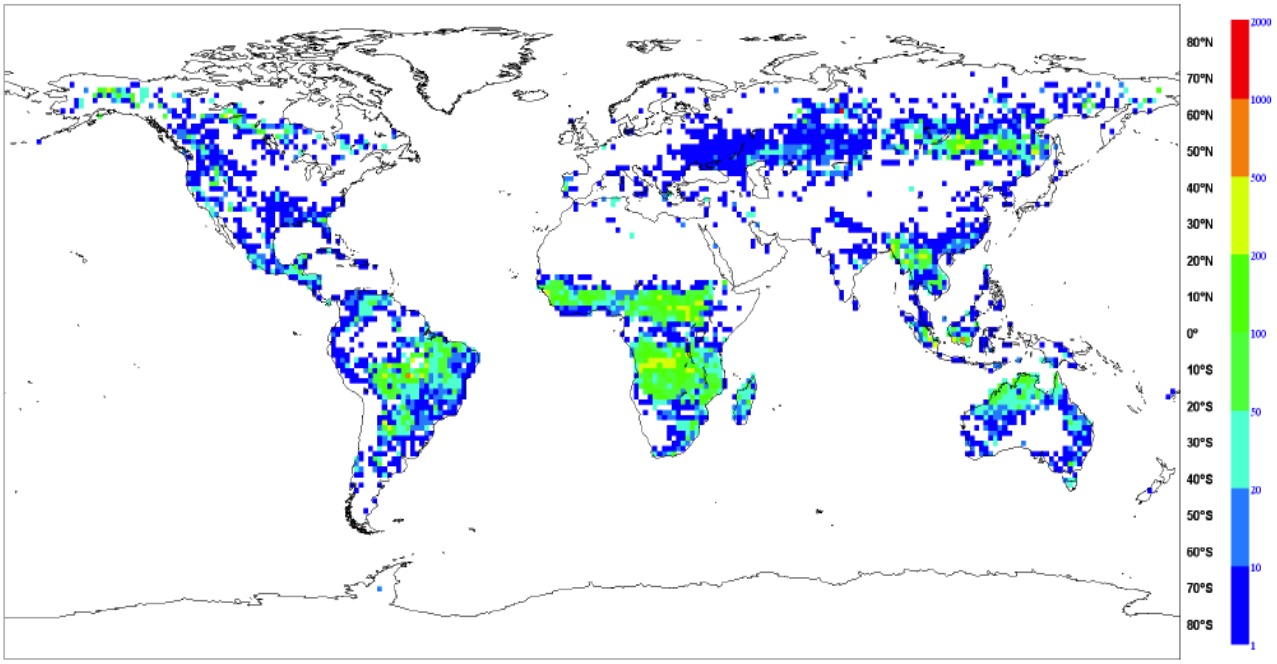

Figure 1: This map, from Kaiser et al., 2012, was consulted to aid in the selection of Köppen-Geiger Climate regions for modeling. This map shows the average distribution of carbon combustion (gC a^{-1} m^{-2}) over the years 2003-2008. Selection of regions for the analysis was done visually and in an attempt to cover critical areas where carbon combustion was observed (Kaiser et al., 2012).

The effective satellite passes of FRP measurements were included in the NetCDF files and were immediately evaluated in the dataset using CDO; selecting all FRP events with the effective satellite passes greater than zero (J. W. Kaiser et al., 2012). These FRP measurements were used in conjunction with meteorological variables as well as land type classes in an attempt to predict the change in FRP from one day to the next, highlighting significant relationships between FRP and explanatory meteorological variables.

It should be noted that, for all intents and purposes, the terms *wildfire size* and *wildfire intensity* are used interchangeably in this paper. Acknowledging the fact that these two concepts are vastly different, the resolution of the 0.5º grid cell and lack of spatial autocorrelation in analysis effectively draw these two concepts together in regards to FRP. Whether the wildfire event is more intense or it covers a larger percentage of the grid cell cannot be determined from the data; the corresponding FRP value is the same. Thereby, when discussing *large* fire events, this primarily refers to large FRP values and does not speak to the size or intensity of the wildfire event.

Meteorological Variables

The ECMWF provided the six meteorological variables that were used to analyze the behavior of fire events. These variables were produced from the Integrated Forecast System from ECMWF which is an operational meteorological forecasting model. The six variables included in the analysis were the volumetric soil water content, 10 meter wind gusts, large scale precipitation, convective precipitation, 2 meter air temperature, and 2 meter dew point temperature measurements. According to *IFS Documentation IV. Physical Processes* published by ECMWF, the wind gusts, air temperature, and dew point temperature are calculated in the post-processing of ECMWF's turbulent transport and interactions model. The convective precipitation and large scale precipitation is derived from cloud microphysics related to the cloud and convection model. This approach does not differentiate between snow and rain as forms of precipitation. Snow and rain both impact the evolution of wildfire in the same way, thus there is no distinction made in this research. Finally, soil water content was determined from surface parameterization accounting for interception, soil properties, runoff, and water transport in frozen soil (ECMWF 2012).

Table 1: Summarization of the six meteorological variables used in the analysis and provided by the ECMWF. Modification refers to the way in which variables were transformed from 4 hour (8x daily) measurements to 24 hour (daily) measurements.

Shortname	Variable	Units	Modification	Source
swc	volumetric soil water content	$m^3 * m^{-3}$	minimum	modelled
wind	10 meter wind gusts	$m * s^{-1}$	maximum	modelled
lsp	large-scale precipitation	m	summation	modelled
cp	convective precipitation	m	summation	modelled
t	2 meter temperature	K	maximum	modelled
d	2 meter dew point temperature	K	maximum	modelled

The original data format for the meteorological variables were as a GRIB file, with eight daily values per variable and covering the globe in 0.5° x 0.5° grid cells. Modifications for the variables were required to match the daily values of the FRP measurements. Table 1 summarizes actions taken for each variable to modify the eight daily variables into one. There was no interpolation performed for this raw data; rather, maximum daily values, minimum daily values and summated values were used to represent the meteorological variables over an individual day. Once the meteorological variables were converted to daily values, a bilinear interpolation was performed with CDO to insure grid cells matched that of the FRP values. With the two data sets combined, the relationship between FRP and the meteorological variables was investigated and will be discussed in the methods section.

Köppen-Geiger Climate Classification

The primary role for the Köppen-Geiger Climate Classification was to control for the variation inherent in the world's ecosystems. Accounting for ecosystem type is important when considering

how crucial fuel load and vegetation structure is to fire behavior. In addition to weather conditions, the behavior and response of fires is closely linked to fuel type and vegetation structures present in each ecosystem (Bowman et al., 2009). Applying this classification to the data allowed for consideration and evaluation of the effects of weather conditions on fires in specific ecosystems.

The Köppen-Geiger Climate Classification was based on the 5 vegetation zones determined by French botanist De Candolle. These groups are the equatorial zone, arid zone, warm temperate zone, snow zone and polar zone. The determination of these vegetation groups were based temperature and precipitation. The classification presents a unique connection between climatological variables and vegetation type. The index for precipitation includes the fully humid, dry summer, dry winter, and monsoon designations for equatorial, warm temperate, and snow zones. While the precipitation index for the arid and polar zones respectively are steppe and desert, frost and tundra designations respectively. The temperature index for the equatorial, warm temperate, and snow zones are hot summer, warm summer, cool summer, cold winter and extremely continental. While the arid zones have hot and cold classifications, polar has one temperature designation. The combinations of zone, temperature, and precipitation indices result in 31 distinct vegetation types unique to each region, and thus provide a means select specific regions and measure the impact of weather conditions. A detailed map of the classifications can be found in Appendix 1: Köppen-Geiger Climate Map. From the inception of the concept by Vladimir Köppen in 1884, the classification system has been updated to incorporate a more robust body of information valid for the second half of the 20th century (Kottek, Grieser, Beck, Rudolf, & Rubel, 2006).

In the analysis and model development, the Köppen-Geiger Climate Classification map represented the years 1976-2000. These climate classifications, determined over a 0.5º grid globally, were generated with observed global temperature and precipitation values. Observed temperature observations were provided by the Climatic Research Unit of the University of East Anglia and precipitation observations were provided by the Global Precipitation Climatology Center (Rubel & Kottek, 2010). For the analysis, selected regions accounted for ecosystems of the Warm Temperate zones in the Mediterranean, Snow zones in the boreal regions, and Equatorial zones over the equator.

Methods

The whole data set, from 2003 to 2010, was divided into two parts to allow for covariate analysis, model development and model evaluation. Data used for the covariate analysis and model development was from 2003-2007. The goal of model development was two-fold. First, there was an interest in identifying the significant meteorological variables influencing the behavior of fire events and second, to determine if these meteorological variables were the same over all ecosystems. The model evaluation used the three final years of data, 2008-2010. In addition to the temporal separation of the data, nine climate classification regions were selected to represent three distinct zones based off of the Köppen-Geiger Climate Classification. To appropriately evaluate wildfire events and their relationship with the meteorological variables, selection of the active events was necessary. This was done through R by selecting all FRP measurements greater than zero and including corresponding meteorological data.

Figure 2 is a flow chart detailing the work undertaken for the analysis, highlighting the processes, datasets and output. It was necessary to expand the covariate analysis because of the absence of significant trends prohibiting clear conclusions. The covariate analysis led to selection of regions where the best relationships were observed in order to streamline the modeling process. After the

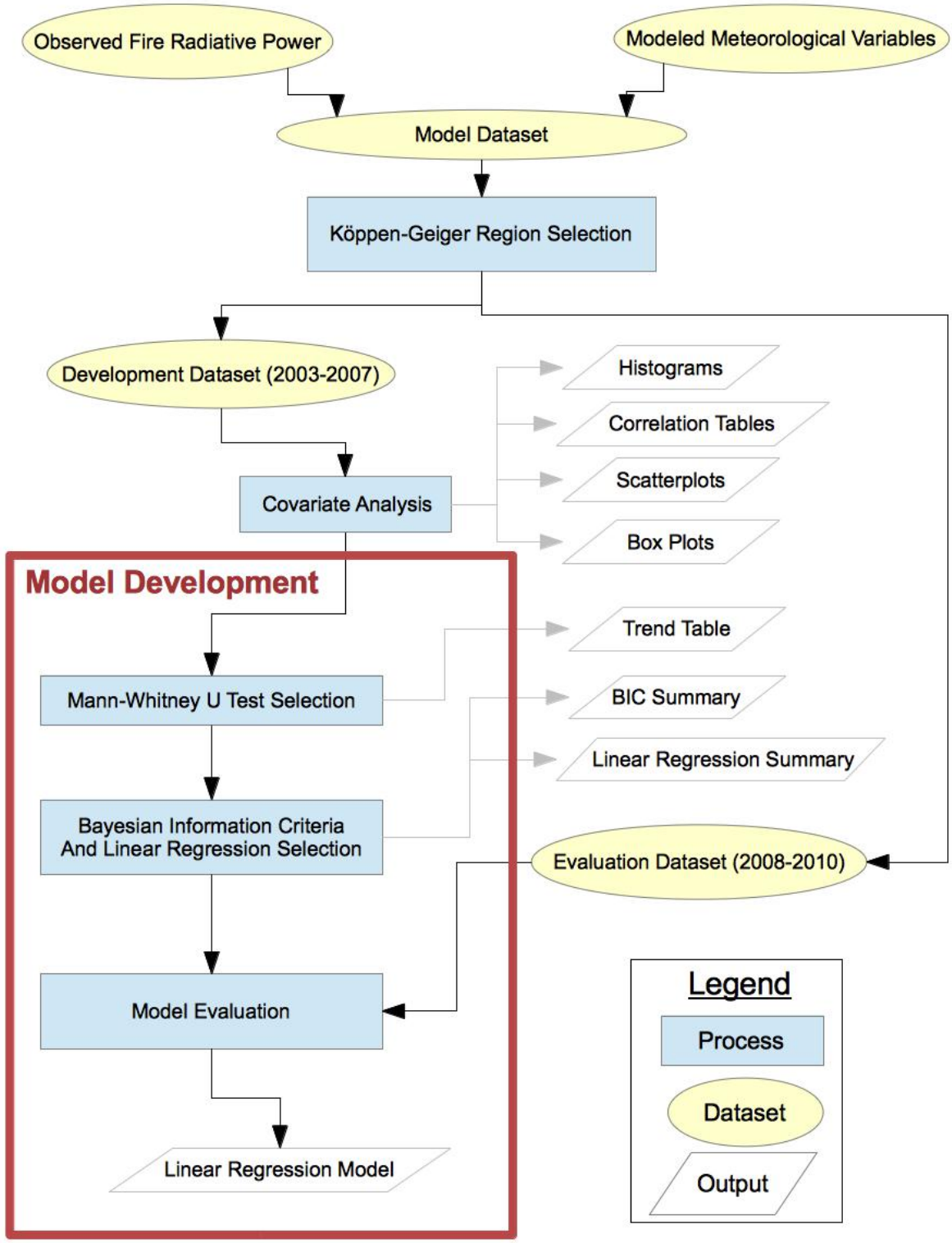

Figure 2: Flow chart detailing the stages of analysis to develop the linear regression model to predict FRP behavior. The flowchart includes: changes and modifications to the dataset (yellow circles), statistical and analytical processes applied to the data (blue rectangles), output from analysis for interpretation, both as tables and graphs (white parallelograms), and specific steps for the development of the linear regression model (red box border).

final selection, linear modeling was possible and a brief analysis was performed.

Zone Selection

The impact of vegetation structure and fuel type on fire behavior is clear. The means by which to incorporate this significant component dictating fire size and behavior was achieved through the selection of different Köppen-Geiger classes, in an effort to create a more uniform vegetation distribution. Region selection provided an opportunity to evaluate the meteorological impacts for different regions and also created a way to compare the impact of different meteorological variables between different vegetation distributions.

Table 2: Summary of the full names, according to the Köppen-Geiger Classification, for each region selected in the analysis. The three zones are separated by the first qualifier in each row. The regions making up the Equatorial zone differ by humidity and precipitation, while the regions comprising the warm temperate and snow zones differ by air temperature.

Class	Full Description
Af	Equatorial : Fully Humid
Am	Equatorial : Monsoon
Aw	Equatorial : Winter Dry
Csa	Warm Temperate : Summer Dry : Hot Summer
Csb	Warm Temperate : Summer Dry : Warm Summer
Csc	Warm Temperate : Summer Dry : Cool Summer
Dfa	Snow : Fully Humid : Hot Summer
Dfb	Snow : Fully Humid : Warm Summer
Dfc	Snow : Fully Humid : Cool Summer

The selection of regions was performed by visually comparing two maps (Figure 1 and the map found in Appendix 1: Köppen-Geiger Climate Map) with three goals. The primary goal was to select regions where there had been FRP values observed in the past. The secondary goal was to select significantly different main climates. Typical climate conditions, fuel loads and ecosystems types were the primary differences that were highlighted through this selection. The final goal was to offer a range of different FRP intensities. Equatorial regions showed the highest FRP averages while polar latitudes exhibited lower but measurable FRP averages. Furthermore, precipitation and temperature trends were considered for the selection based on their intricate role in the creation of the Köppen-Geiger Climate Classification.

Table 3: Summary of the different precipitation and temperature criterion of each region are presented in the table above. These criteria were transcribed from the updated Köppen-Geiger Climate Classification paper from Kottek et al., 2006.

Class	Precipitation Criteria	Temperature Criteria
Af	$P_{min} \geq 60$mm	$T_{min} \geq +18\,^{\circ}C$
Am	$P_{ann} \geq 25(100\text{-}P_{min})$	$T_{min} \geq +18\,^{\circ}C$
Aw	$P_{min} < 60$mm in winter	$T_{min} \geq +18\,^{\circ}C$
Csa	$P_{smin} < 40$ mm	$T_{max} \geq +22\,^{\circ}C$
Csb	$P_{smin} < 40$ mm	not (a) and atleast 4 $T_{mon} \geq +10\,^{\circ}C$
Csc	$P_{smin} < 40$ mm	not (b) and $T_{min} > -38\,^{\circ}C$
Dfa	$P_{smin} > 40$ mm	$T_{min} \leq -3\,^{\circ}C$, $T_{max} \geq +22\,^{\circ}C$
Dfb	$P_{smin} > 40$ mm	$T_{min} \leq -3\,^{\circ}C$, not (a) and atleast 4 $T_{mon} \geq +10\,^{\circ}C$
Dfc	$P_{smin} > 40$ mm	$T_{min} \leq -3\,^{\circ}C$, not (b) and $T_{min} > -38\,^{\circ}C$

With these goals in mind, three of the five main climates, identified by Köppen-Geiger, were selected. These three main climates selected for model development were the Equatorial, Warm

Temperate, and Snow Climates. Furthermore, from each main climate, three regions were chosen to offer a representation of the main climate. Table 2, provides the full description of the 9 regions selected along with the class identifier for each Köppen-Geiger Climate Classification. The regions that composed each zone differed either by temperature or precipitation, not both. The criteria for the precipitation and temperature developed by Köppen and modified by Geiger is listed in Table 3 (Kottek et al., 2006). Regions composing the Equatorial zone varied over the precipitation gradient, while the regions composing the Warm Temperate and Snow zones varied in their temperature designations.

Additional Data

Although meteorological data from the ECMWF provide a robust picture of the daily weather at each location, there were several additional variables calculated to assist in covariate analysis and model development. Most importantly, ΔFRP was generated at this stage. ΔFRP quantified the change in FRP values from one day to the next; it also incorporated the temporal nature of the research objective. In an effort to predict the percentage change, ΔFRP was calculated as a ratio. As such, ΔFRP represents the dependent variable for the model, the variable that model development was directed towards.

Relative Humidity

Relative humidity was included in the model development because of it's pertinent representation of water vapor in the air, it's ability to relate air temperature and moisture, and it's frequent inclusion in various fire indices. While the dew point temperature was provided by the ECMWF, relative humidity was needed for the Angstrom Index calculation. Determining relative humidity is a simple calculation utilizing 2 meter air temperature and 2 meter dew point temperature values provided by the ECMWF. Equation 1 was used to calculate relative humidity in R that was later used for Angstrom Index calculations and model development.

$$RH = 100 * \frac{\exp\left(\frac{a\,T_d}{b\,T_d}\right)}{\exp\left(\frac{a\,T}{b\,T}\right)}$$

Equation 1:Relative Humidity

Where a = 17.271 and b = 237.7. This formula was based on the August-Roche-Magnus approximation and is considered a highly accurate conversion (Lawrence, 2005). Furthermore, this conversion is considered valid for 0 ºC < T < 60 ºC & 0 ºC < T_d < 50 ºC which accounts for most of the FRP events.

Angstrom Index

The Angstrom Index was also included in model development in hopes that a pre-existing and validated index can be used in modeling of the ΔFRP. The Angstrom Index (Equation 2) is a Swedish based fire ignition index developed for Scandinavia (Chandler et al. 1983). It is based on temperature and relative humidity and identifies favorable ignition conditions for fire events. As this

is developed for Scandinavia, it is expected to perform best for the Snow zone. The expected response of fire, based on the Angstrom Index is detailed below in Table 4. Lower values indicate an increased opportunity of fire occurrence while larger values indicate that fire is unlikely. As a general benchmark, it provides another way to determine if the behavior of FRP and ΔFRP are acting logically.

$$AI = \left(\frac{RH}{20}\right) + \left(\frac{27 - T}{10}\right)$$

Equation 2: Angstrom Index

Table 4: Scale for the Angstrom Index, indicating the probability of fire events.

Class	Ignition Index
Fire occurrence unlikely	> 4.0
Fire conditions unfavorable	2.5 - 4.0
Fire conditions favorable	2.0 - 2.5
Fire conditions very likely	< 2.0

Temporal Aspects and ΔFRP

A temporal autocorrelation was performed for the dataset and focused on the behavior of FRP, large scale precipitation and convective precipitation. Prompted by the evaluation of these autocorrelations and expected behavior of the independent variables, four additional variables reflecting the prior day's value were included. In each stage of the analysis and model development, the preceding day's FRP variable (FRP_0) was included in the dataset. While FRP_0 is directly used in the generation of the dependent variable, it's role in explaining the behavior is critically important. As a result, FRP_0 is considered an independent variable because of it's explanatory role in the behavior of ΔFRP. Furthermore, the autocorrelation was evaluated for all regions and zones and summarizes the values from the autocorrelation of FRP for the three zones (Equatorial, Warm Temperate, and Snow) in Table 5 found in the results section. From the evaluation of the autocorrelation, it was evident that the inclusion of the temporal aspects of FRP values would be prudent.

$$\Delta FRP = \frac{FRP}{FRP_0}$$

Equation 3: Formula for ΔFRP

To reflect this autocorrelation and generate a value upon which to focus the modeling effort, the FRP_0 values were used in conjunction with the present FRP value to yield the ΔFRP. The ΔFRP functioned as the dependent variable in model development. The formula used to generate the ΔFRP is shown in Equation 3. Essentially, ΔFRP shows the relative percentage of the FRP signal remaining after one time-step, or in the case of this research, per day. Low ΔFRP values (< 0.50) indicate large decreases in the FRP signal, while high ΔFRP values (> 0.50) indicate a smaller decrease in FRP. For ΔFRP > 1, an increase in the FRP signal over the period between measurements is represented. ΔFRP, as a ratio, was established as a dependent variable that, at the onset, appeared to be easier to apply once determined by using the percentage change to calculate the new value over each time step. The issues of using a ratio as a dependent variable will be discussed later.

In addition to the FRP_0, the preceding day's precipitation values were also included as independent variables for the analysis. This accounted for the residual effects of precipitation and the possibility of precipitation events occurring before or after the FRP measurements. Total precipitation, large scale precipitation, and convective precipitation from the preceding day were included in the analysis.

Covariate Analysis

Before a focused modeling effort began, it was necessary to gain a better understanding of the relationships between the ΔFRP and the independent variables. This was achieved through evaluation of correlation coefficients, scatter plots, histograms, and box plots. This analysis was undertaken for each of the nine regions and then for the three zones. The analysis and modeling, in addition to model creation, was generated with the data analysis suite R. For analysis and model development, the ΔFRP was capped at 2 to provide a working dataset. This ΔFRP selection retained ~98% of the FRP events and allowed for easier interpretation of covariate analysis.

Global maps were generated for all variables to establish an expected range of values specific to each variable. Additionally, the maps provided insight into the spatial differences among the variables and allowed for easy comparison between the zones. These maps (presented in the results section) were generated with the data analysis suite R.

Histograms

Histograms were generated from the dataset for both independent and dependent variables. Primarily, histograms, cumulative and otherwise, were used in analysis to aid in understanding the distribution of variables. The histograms offered insight into the behavior of the variables, enabled the differentiation between regions and zones and verified the appropriate behavior of variables. Furthermore, the histograms assisted in the determination of the mean state and general distribution of the variables. Cumulative histograms were prepared for ΔFRP of the three zones.

Correlation Coefficients

There were two primary correlation coefficients evaluated in the analysis. Meteorological variables generally covary (Peterson et al., 2013). Accordingly, the first the relationship between the independent variables was assessed to evaluate preexisting relationships. Second, relationships between the independent variables and the ΔFRP were also calculated to examine their relationship on a basic level, in hopes that a cursory understanding of the relationship between variables would guide the research and explain observed behavior.

Scatterplots & R^2

Further understanding of the relationship between independent and dependent variables can be gained from scatterplots that were generated for each independent variable and ΔFRP. The scatterplots provided a best fit line with the corresponding R^2. The best fit line represents the overall trend observed between two variables and the R^2 value indicates the amount of variance explained by the independent variable. The overall trends provided a benchmark to determine if the observed behavior between variables was logical and R^2 indicated how effectively this behavior can be explained.

Box Plots

The vast amount of data points was prohibitive in visually interpreting the scatter plots; box plots provided an easier way to visually interpret the behavior of the relationships. Generation of box plots was achieved through a two-step process. Initially, the whole dataset pertaining to each independent variable was divided into quantiles. With the quantile limits identified, four unique box

plots comparing independent variables and the ΔFRP were generated for each quantile. The four box plots were presented sequentially in order to visualize the change/trend from one quantile to the next. This step allowed for evaluation of the distribution of the ΔFRP over the change in independent variable.

A range of 1.5 x Inner Quartile Range was included for the box plot, which dictated the extent to which "whiskers" extended. All points beyond the "whiskers" represent possible outliers. While the interior boxes detail the distribution of the ΔFRP values, highlighting the median. The upper boundary of the box is the 75th percentile and the lower boundary of the box is the 25th percentile. Box plots further explained the trends observed in the scatterplots while improving the interpretation of the trends and relationships between variables.

Mann-Whitney U test

The Mann-Whitney U test was the first step in model development. It furthered the investigation of the relationship between variables, but unlike previous steps, the Mann-Whitney U test determined if the difference between data groups were statistically significant. The Mann-Whitney U test is a non-parametric test that determines if two populations are stochastically larger than one another. The null hypothesis is establishes that two populations that are the same. Furthermore, it is effective with both normal and non-normal distributions. (Mann & Whitney 1947) By evaluating the difference in stochastic behavior among the selected population segments of the independent variable, a trend of ΔFRP can be observed. The presence of statistical significance determined whether or not observed trends were sufficient to form a conclusion.

Unlike box plots, which only evaluated quartiles, the distribution of independent variable was divided into six unique groups for each Mann-Whitney U Test. The independent variables were divided at the 5%, 25%, 50%, 75% and 95% to yield the six groups as shown in Figure 3. For the U test, each percentile of the independent variable and the corresponding ΔFRP from that selection was tested against the adjoining section's ΔFRP. Additionally, the extreme 5th percentile and 95th percentile were tested against the remaining dataset. This yielded 7 unique comparisons for each variable of each region. Each percentile was given a roman numeral label. U tests designated as I:II means that the 5th percentile was compared to the 25th percentile.

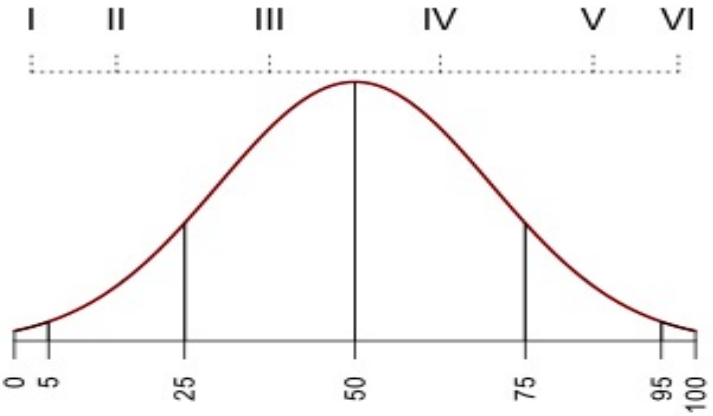

Figure 3: Percentage breakdown for the Mann-Whitney U tests performed for all zones and regions, with corresponding group designations above. Groups I-VI are represented in the figure above, while VII is the summation of the last 5 groups (from 5-100%) and VIII is the summation of the first five groups (from 0-95%).

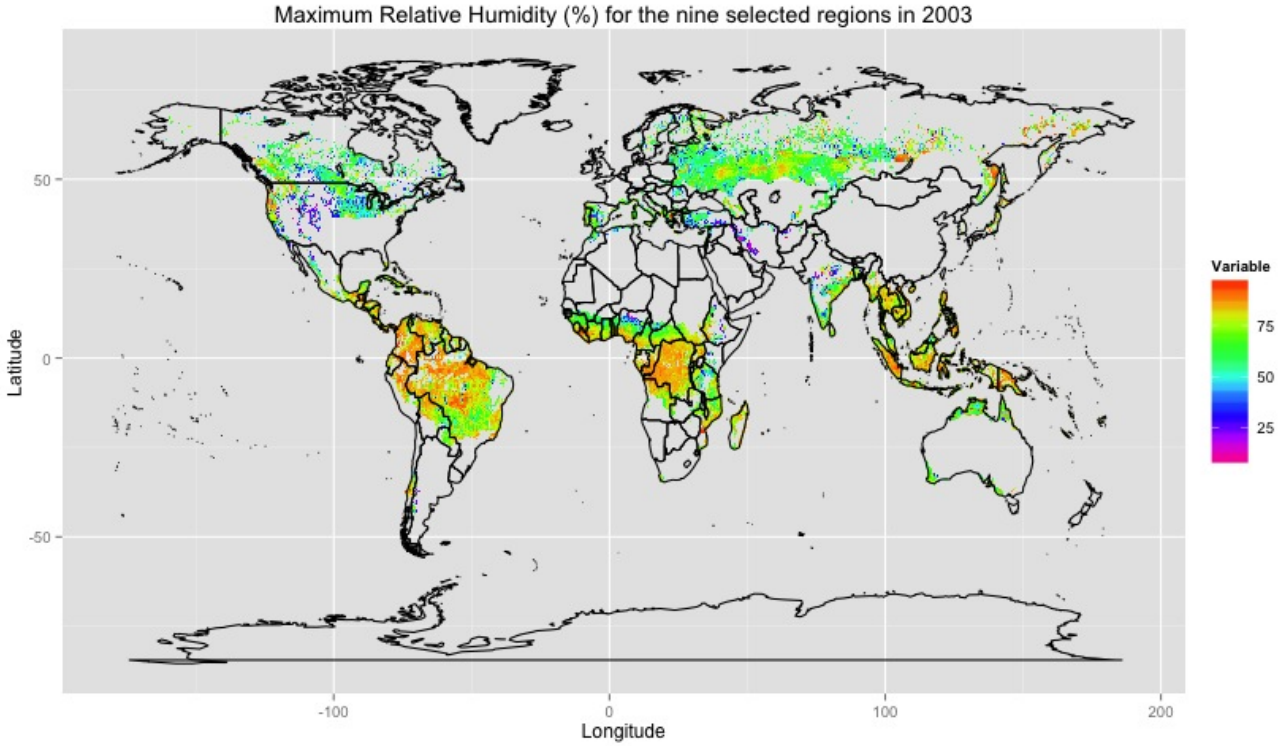

Figure 4: Map of maximum daily Relative Humidity values for the year 2003. The largest observed Relative Humidity value is 97.96%. Resolution of the map is 0.5° lat/lon.

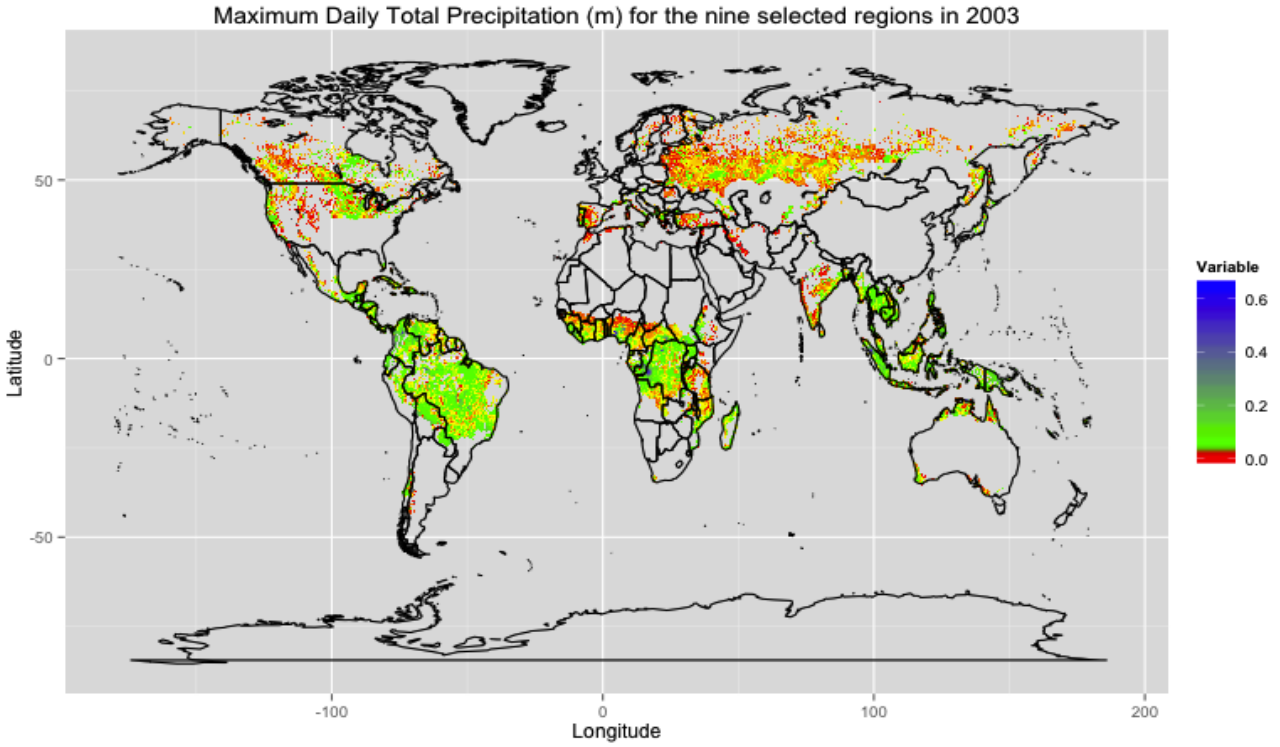

Figure 5: Map of maximum daily Total Precipitation values for the year 2003. Maximum daily Total Precipitation is 0.6644 m. Resolution of the map is 0.5° lat/lon.

As stated, the goal of the U test was to determine if the behavior of ΔFRP was significantly different from one another. In addition to the significance test, the median of each section was compared to determine the trend of ΔFRP across the percentiles. This comparison was performed from left to right, to correspond with the increasing independent variables. By evaluating the change in median for each group, a statistically significant trend could be determined. The traditional confidence interval used in U tests is 0.05. However, due to the multiple U tests performed for each dataset and the familywise error rate, a Bonferroni correction was used to correct the confidence intervals and account for the problem of multiple comparisons. (Dunn 1961) Considering each independent-dependent variable relationship unique, there were still seven different tests applied to the same population. This lowered the confidence interval from 0.05 to 0.007 when dividing by the number of tests performed for each Variable-to-ΔFRP comparison.

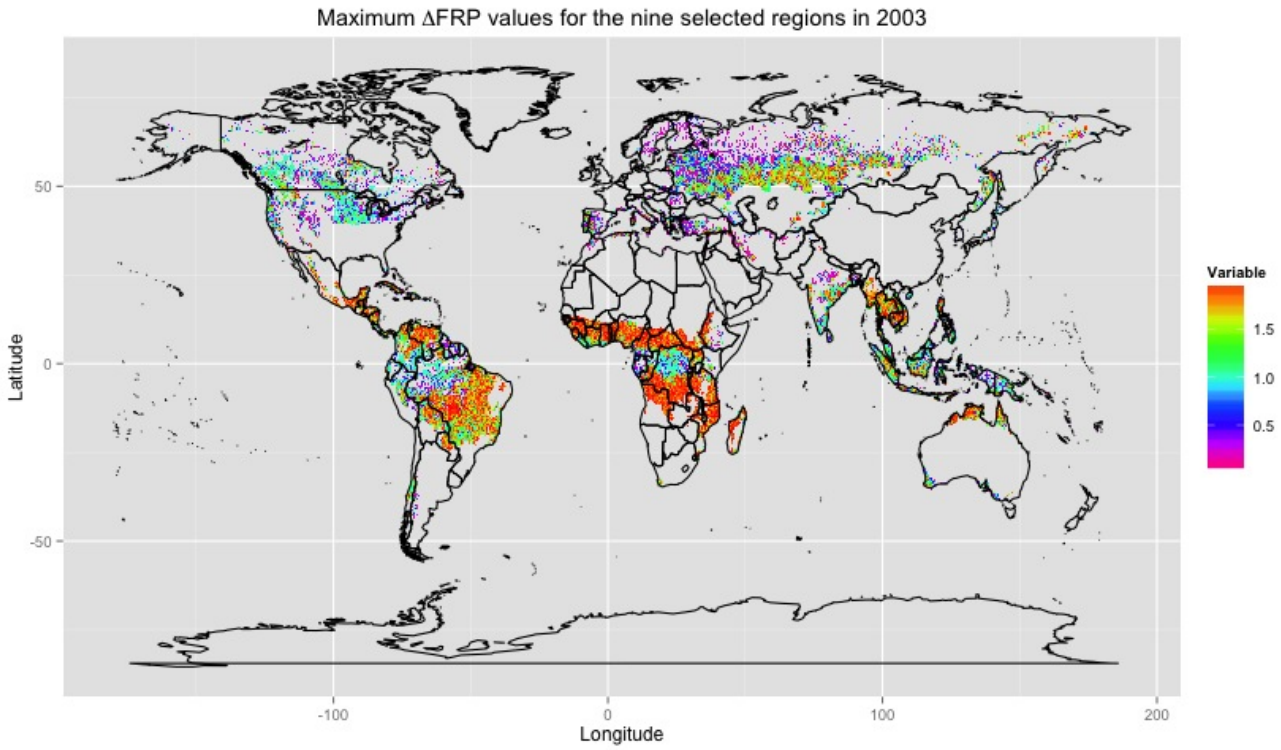

Figure 6: Map of maximum daily ΔFRP values for the year 2003. Maximum daily ΔFRP values occur around the Equator. Resolution of the map is 0.5° lat/lon.

Model Development and evaluation

Reviewing the results of the Mann-Whitney U tests was the first step in model development. Regions and zones that failed more than 20% of the Mann-Whitney U tests, were removed from consideration. For the remaining regions and zones, a linear regression was run for the datasets from 2003-2007.

The parameters for the multiple linear regression were determined by applying a Bayesian Information Criteria (BIC). The BIC was included to determine the best number of parameters to use in modeling and avoid over fitting. BIC is based off of the Akaike Information Criteria, which measured the relative quality of the statistical model and balances the goodness of fit and the complexity of the model. (Akaike 1974) BIC evaluates the leading terms of the asymptotic expansion and includes a penalty term based off the number of parameters in a model. (Schwarz 1978) The BIC is suited well for this dataset and was limited to the selection of five variables.

The BIC takes into account nonlinearity by including a squared version of each meteorological variable in addition to a linear representation. The BIC selected variables were recorded to determine what explanatory variables were most preferred in the model development. Before evaluation, model development was assessed by calculating the R^2 value for the fitted variables with the actual results among the 2003-2007 data. The linear regression formula developed from the development dataset was then applied to the evaluation datasets from 2008-2010.

For this research, model evaluation was performed for the region with the highest R^2 value from the development stage. Using the `predict` command in R, the fit value along with the lower and upper boundary were modeled to predict the behavior within a confidence interval of 95%. Of these three variables, the fitted ΔFRP values were compared to the measured ΔFRP values and the corresponding R^2 was evaluated.

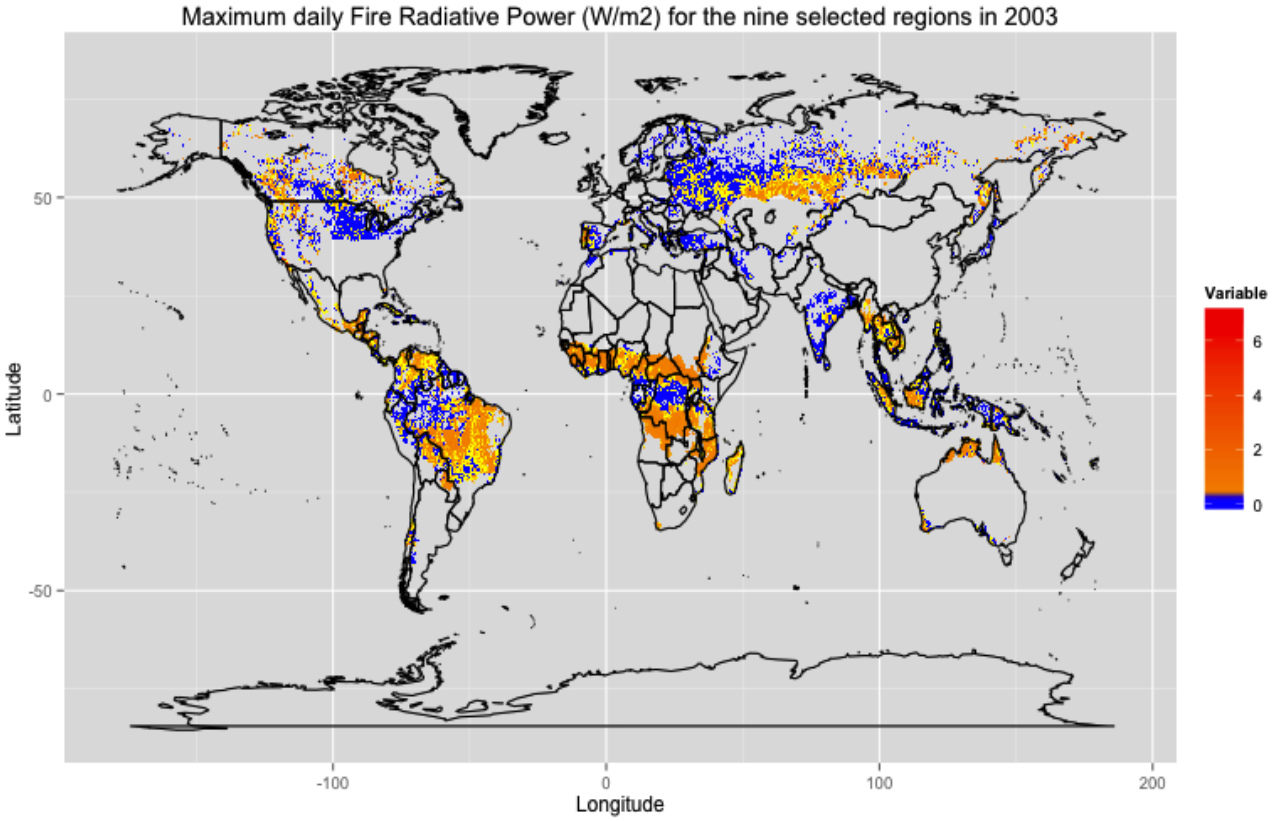

Figure 7: Map of maximum daily FRP values for the year 2003. Maximum daily FRP value 7.36 W/m². Resolution of the map is 0.5° lat/lon.

Results

Spatial Arrangements

Maps displaying dependent and independent variables were generated to insure that the initial data frame was created properly. These maps show the spatial distribution of the Köppen-Geiger regions selected for analysis. The maximum daily value of each cell is displayed in each map. FRP, ΔFRP and meteorological variables for the year 2003 are displayed here and the remaining years (2004-2007) are included in Appendix 2: Mapped Variables.

The dependent variable, ΔFRP, offers a more dynamic map than that of FRP in Figure 6. Evaluating

the maximum daily ΔFRP from 2003 shows interesting behavior and striking differences based on location. The location of fire events that showed substantial increases in FRP (ΔFRP > 1) occur primarily in the Equatorial rainforest and savannah. Interestingly, fire events occurring over the equator do not show the same maximum daily ΔFRP values. There is a band in central Russia, on the 50th parallel, where substantial fires occurred and persisted unlike other boreal wildfire events in North America and Scandinavia. The remoteness of the Siberian boreal forests may be the cause. Boreal forests show maximum daily ΔFRP values less than one, which is also observed among populated subtropical latitudes in the Mediterranean region. These observations suggest brief wildfire events ended by precipitation or the prevalence of anthropogenic extinguishing.

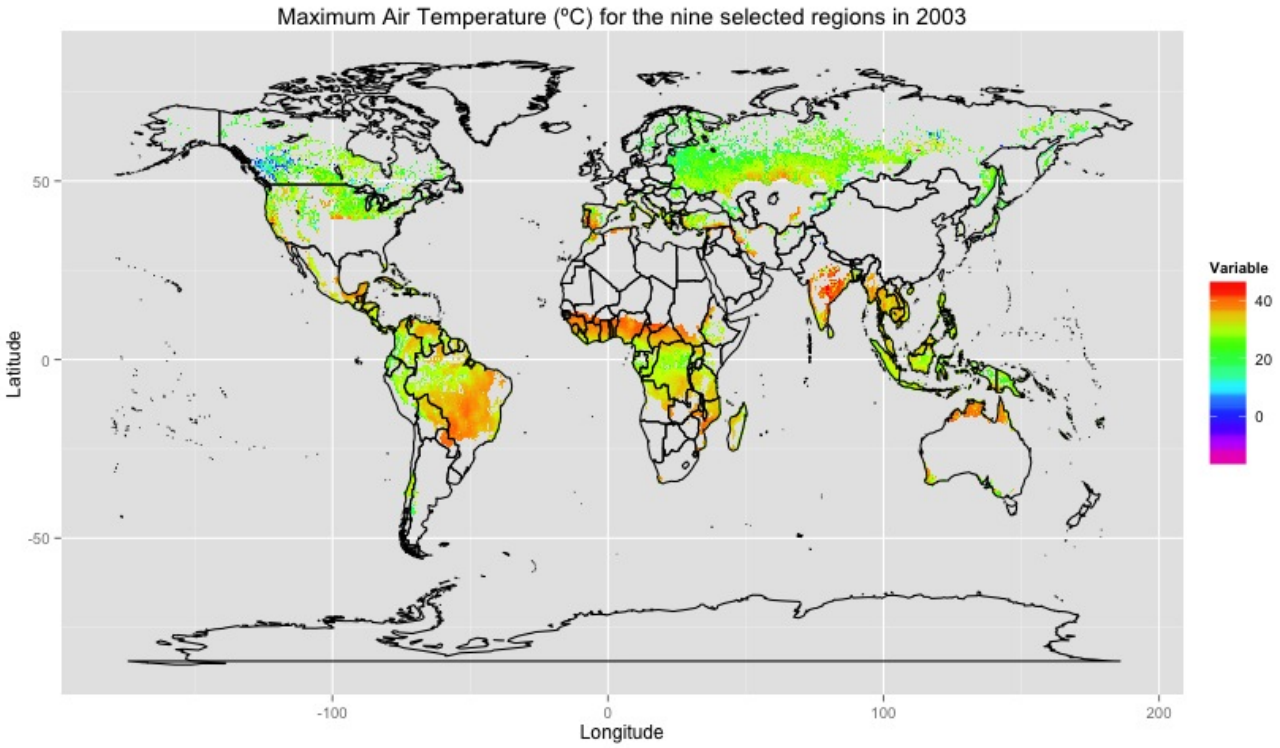

Figure 8: Map of maximum daily Air Temperature values for the year 2003. Maximum daily Air Temperature is 45.75 ºC. Resolution of the map is 0.5º lat/lon.

In Figure 7, locations of larger FRP events mirror the location of maximum daily ΔFRP events. Maximum daily FRP values occur on the 50th latitude north in Asia, and straddling the equator in South America and Africa. Similar to ΔFRP measurements, FRP measurements occurring on the equator exhibited lower FRP values and wildfire events occurring above the 60th latitude north also show substantially lower FRP values. The impact of anthropogenic fire control can possible be seen in low FRP values found in the Great Lakes region of the United States, eastern India, and Turkey.

The map of maximum daily relative humidity in Figure 4 corresponds to general expectations. More humid environments are observed along the equator. Moderately humid environments are evident in the boreal regions, and low relative humidity is observed in the Middle East, and North American Rockies. These values only represent relative humidity observed during active fire events, prohibiting strong conclusions. One question, that cannot be answered with this limited knowledge is: How do these values compare to typical relative humidities observed? Essentially, it is uncertain whether or not we are observing drought conditions, which would be unlikely, because the maximum daily relative humidity values are shown.

The map of maximum daily total precipitation (Figure 5) shows no distinct difference across the three ecosystems. There are pockets where larger rain events occurred, such as Oceania and pockets of the Equatorial rainforest. But there is little variation in maximum daily total precipitation across the globe. These observations correspond to active fire events only and do not reflect the possibility of drought like conditions on the ground. The map of maximum daily air temperatures can be found in Figure 8. Active fires occurring in conjunction with high temperatures (around 40º C) are observed in the equatorial regions and northern Australia. The 50th parallel north shows a presumed heat wave occurring in Russia in conjunction with the observed intense fires. In the boreal region fire events occur in more mild temperatures, around 20º C.

Autocorrelation and Correlation Coefficients

The autocorrelation of FRP was calculated for each zone and region. For each test of autocorrelation, it was determined that a lag of one should be included in the modeling efforts. The Lag 1 values showed a maximum autocorrelation of 0.59 and a minimum autocorrelation of 0.15 with an average autocorrelation of 0.49. The average autocorrelation of the Lag 2 values was 0.31, putting these below the threshold to warrant consideration for the analysis. Table 5 summarizes the FRP autocorrelation results from the Snow Zone along with the three corresponding regions that make up that zone (Dfa, Dfb, and Dfc). Here you can see the decreasing trend of autocorrelation over the number of lags, and the reason that only a lag of one, represented as FRP_0, was included in the analysis. The summaries of the FRP autocorrelation for the other zones and regions can be found in Appendix 2: Autocorrelation Tables.

Table 5: Autocorrelation values of FRP measurements for the snow zone along with the Dfa, Dfb, and Dfc regions (Snow:Fully Humid:Hot/Warm/Cool Summer) for a lag of 4 days.

Lag (days)	Dfa	Dfb	Dfc	Snow
0	1.00	1.00	1.00	1.00
1	0.34	0.44	0.54	0.49
2	0.15	0.22	0.32	0.28
3	0.08	0.05	0.19	0.13
4	0.04	0.03	0.09	0.07

The decision to include time delayed precipitation values was also based on the autocorrelation of convective precipitation and large scale precipitation. The autocorrelation values of convective precipitation for the Dfa, Dfb, and Dfc regions (Snow:Fully Humid:Hot, Warm, & Cool Summer) and Snow zone, displayed in Table 6, provided a clear argument for inclusion. The average Lag 1 autocorrelation value of 0.43, across all regions and zones, and a maximum and minimum autocorrelation of 0.65 and 0.27 respectively warranted the inclusion of Lag 1 of convective precipitation values.

The large scale precipitation autocorrelation figures for the snow zone and corresponding regions (Dfa, Dfb, & Dfc = Snow:Fully Humid:Hot, Warm, & Cool Summer)) are summarized in Table 7. Including all regions and zones, the autocorrelation values were less significant but maintained an average of 0.29, with a maximum and minimum autocorrelation of 0.44 and 0.22 respectively. Based upon these autocorrelation values, a 1 day lag of large scale precipitation values were included in the analysis.

Table 6: Autocorrelation values for convective precipitation values of the snow zone and corresponding regions (Snow:Fully Humid:Hot/Warm/Cool Summer).

Lag (days)	Dfa	Dfb	Dfc	Snow
0	1.00	1.00	1.00	1.00
1	0.27	0.32	0.29	0.31
2	0.08	0.12	0.12	0.12
3	0.05	0.08	0.11	0.09
4	0.05	0.06	0.08	0.08

Table 7: Autocorrelation values for large scale precipitation values of the snow zone and corresponding regions (Snow:Fully Humid:Hot/Warm/Cool Summer).

Lag (days)	Dfa	Dfb	Dfc	Snow
0	1.00	1.00	1.00	1.00
1	0.22	0.25	0.26	0.25
2	0.04	0.05	0.07	0.06
3	0.03	0.04	0.07	0.05
4	0.03	0.03	0.05	0.04

The second aspect evaluated through correlation coefficients were the relationships between the independent variables used in the model generation. Initially, this was undertaken to mitigate the effects of colinearity in the analysis and offer a more detailed understanding of the interconnections between variables. Once the Bayesian Information Criteria was adopted as a means of model selection, the impact of colinearity became less significant. The correlation coefficients among independent variables were still important for the overall understanding of the model. Correlation tables for independent variables were calculated for the three zones and all of the independent variables were used. This included the raw data provided by the ECMWF and the additional data of total precipitation, the preceding day's value of convective precipitation, large scale precipitation, and total precipitation, relative humidity, and angstrom index. Furthermore, FRP_0 was included in the correlation coefficient table to guide the analysis. Table 8 shows the correlation coefficients for the snow zone.

Table 8: Summary of the correlation coefficients for the independent variables produced from the snow zone. For raw data directly provided by ECMWF, the highest correlation of 0.74 was observed between air temperature (t) and dew point temperature (d) for the snow zone.

Variable	FRP_0	lsp	lsp_0	cp	cp_0	tp	tp_0	t	d	swc	wind	rh	ai
FRP_0	1.00	-0.00	-0.01	-0.01	-0.02	-0.01	-0.02	0.01	-0.02	0.01	0.02	-0.03	-0.03
lsp	-0.00	1.00	0.31	0.44	0.21	0.87	0.31	-0.21	0.03	0.23	0.16	0.39	0.35
lsp_0	-0.01	0.31	1.00	0.12	0.44	0.26	0.86	-0.22	-0.05	0.27	0.09	0.27	0.29
cp	-0.01	0.44	0.12	1.00	0.37	0.82	0.28	0.03	0.32	0.21	0.06	0.42	0.22
cp_0	-0.02	0.21	0.44	0.37	1.00	0.33	0.83	-0.01	0.21	0.27	0.04	0.31	0.18
tp	-0.01	0.87	0.26	0.82	0.33	1.00	0.35	-0.12	0.19	0.26	0.14	0.48	0.34
tp_0	-0.02	0.31	0.86	0.28	0.83	0.35	1.00	-0.14	0.09	0.32	0.08	0.34	0.28
t	0.01	-0.21	-0.22	0.03	-0.01	-0.12	-0.14	1.00	**0.74**	-0.46	-0.11	-0.37	-0.86
d	-0.02	0.03	-0.05	0.32	0.21	0.19	0.09	**0.74**	1.00	-0.19	-0.22	0.32	-0.31
swc	0.01	0.23	0.27	0.21	0.27	0.26	0.32	-0.46	-0.19	1.00	0.05	0.36	0.50
wind	0.02	0.16	0.09	0.06	0.04	0.14	0.08	-0.11	-0.22	0.05	1.00	-0.14	-0.00
rh	-0.03	0.39	0.27	0.42	0.31	0.48	0.34	-0.37	0.32	0.36	-0.14	1.00	0.80
ai	-0.03	0.35	0.29	0.22	0.18	0.34	0.28	-0.86	-0.31	0.50	-0.00	0.80	1.00

There were limited amounts of correlation among independent variables used in the analysis further implying that colinearity would not impact results of the analysis. FRP_0 exhibited no correlation to any of the variables. For the equatorial zone, convective precipitation was weakly correlated to the dew point temperature (0.54) and soil water content (0.52) (Appendix 3: Independent Variable Correlations;Table 27). The significant relationships observed in the equatorial zone were not observed for the warm temperate zone. The warm temperate zone exhibited a weak correlation between large scale precipitation and convective precipitation (0.52) (Appendix 3: Independent Variable Correlations;Table 28). In the snow zone, neither of the relationships from the equatorial

or warm temperate zone were observed. While, as evident in Table 8, the air temperature and dew point temperature were moderately correlated (0.74). Across all of the zones, the observed relationships with the highest correlation values make sense on an intrinsic level.

The relationship between ΔFRP and independent variables were explored in two ways, through the use of scatterplots to determine R^2 values as well as a correlation table. The R^2 valued from the scatterplots and the correlation coefficients did not indicate any correlation or significant relationships between the ΔFRP and the independent variables. Correlation coefficients were calculated for all independent variables and their relationship with the ΔFRP. This was performed for all three zones, and summarized in Table 9. The largest correlation occurred between the ΔFRP and relative humidity and ΔFRP and dew point temperature in the Warm Temperate zone. These relationships both yielded coefficients of -0.15.

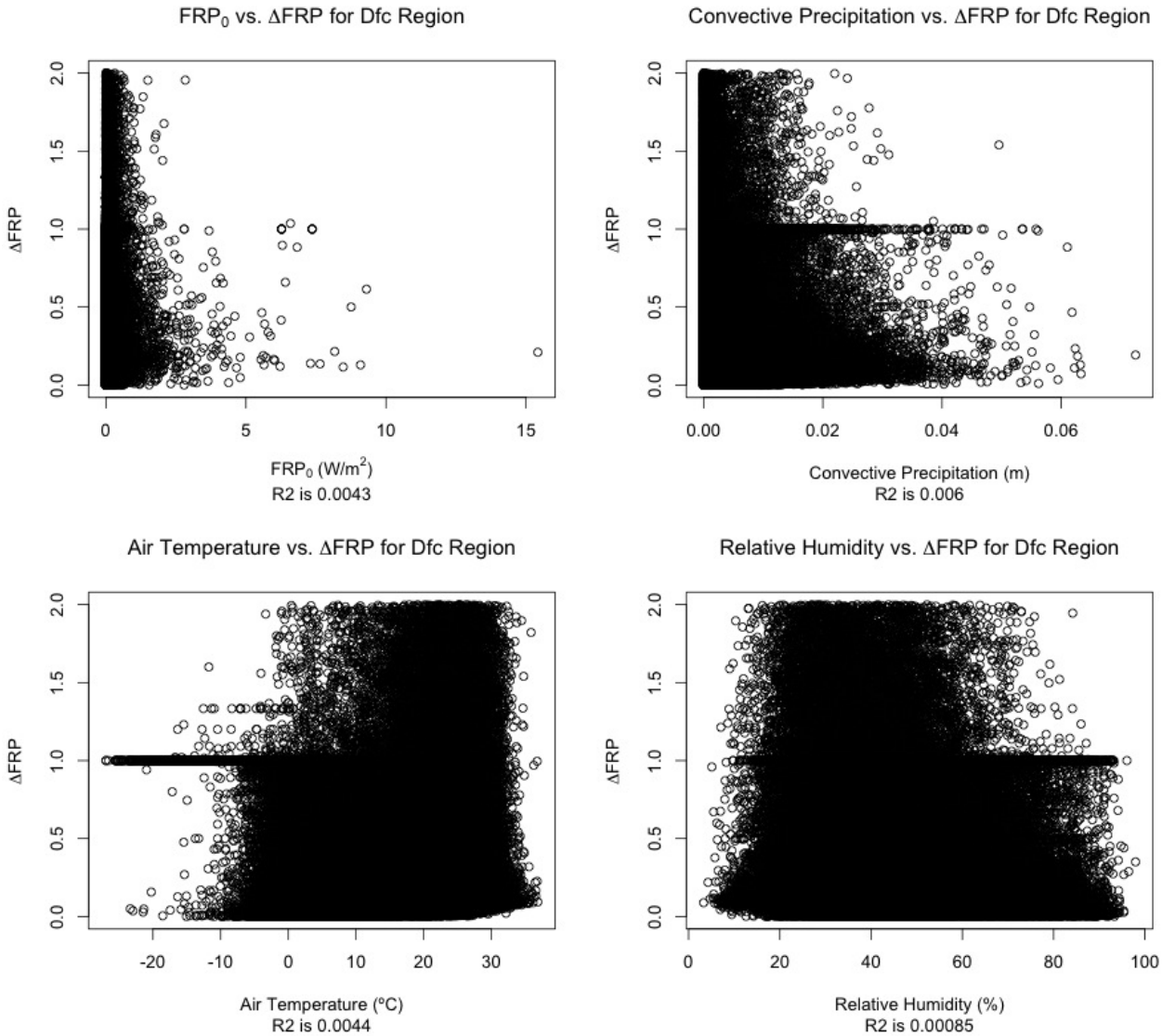

Figure 9: Scatterplots of four independent variables (FRP_0, convective precipitation, air temperature, and relative humidity) and their relation to ΔFRP for the Dfc region (Snow:Fully Humid:Cool Summer). The R^2 is reported below each scatterplot, and in all cases R^2 is miniscule.

Furthermore, scatterplots show insignificant R^2 values for the independent variables in relation to ΔFRP. The scatterplots displayed in Figure 9 were generated for four variables from the data for the Dfc region (Snow:Fully Humid:Cool Summer). (Remaining scatterplots can be found in Appendix 4: Scatterplots) No visual trends were evident in the initial evaluation of the scatterplots, which was common across all regions and zones.

Table 9: Correlation coefficients between ΔFRP and the independent variables used in analysis. Values from the three zones were used to represent an expected value for the corresponding regions.

Variable	Equatorial	Warm Temperate	Snow
ΔFRP	1.00	1.00	1.00
FRP_0	0.06	0.09	0.06
lsp	**0.11**	-0.01	**0.08**
lsp_0	-0.04	-0.04	-0.01
cp	-0.01	-0.06	0.02
cp_0	-0.09	-0.09	-0.04
tp	0.06	-0.04	0.06
tp_0	-0.08	-0.07	-0.03
t	-0.08	0.09	-0.01
d	-0.09	**-0.15**	-0.04
swc	0.05	-0.07	0.02
wind	-0.00	0.05	0.03
rh	0.01	**-0.15**	-0.01
ai	0.06	-0.14	-0.00

The R^2 values for each meteorological value related to ΔFRP was calculated and summarized in Table 10. The primary objective was to determine if any meteorological value, in any region or zone, exhibited a significant capability of determining ΔFRP. The results suggest no significant determining factor of any meteorological variables, where the highest R^2 value, outside of the Csc region, was 0.0227. The Csc region (Warm Temperate:Summer Dry:Cool Summer) exhibited the highest R^2 values, but ultimately due to the small sample size (n=164) the data was discarded for analysis.

Table 10: Summary of the R^2 values of the adjusted best fit line for each independent variable and its relation to ΔFRP. In addition to considering every independent variable, the table accounts for every region and zone (Ez = Equatorial Zone, Wtz = Warm Temperate Zone, & Sz = Snow Zone). As seen with the scatterplots from the Dfc region (Snow:Fully Humid:Cool Summer), R^2 values are miniscule; not including the Csc (Warm Temperate:Summer Dry:Cool Summer) region due to its sample size.

Variable	Af	Am	Aw	Ez	Csa	Csb	Csc	WTz	Dfa	Dfb	Dfc	Sz
FRP_0	0.00451	0.00529	0.00815	0.00852	0.00201	0.00652	-0.00751	0.00355	0.00489	0.00247	0.00433	0.00355
lsp	0.00162	0.00016	0.00026	0.00015	0.00130	0.0141	0.167	0.00589	0.0208	0.0113	0.00609	0.0118
lsp_0	1.85e-5	0.00051	0.00157	0.0015	0.00053	1.06e-5	0.0102	0.00013	0.00022	0.00167	0.00525	0.00162
cp	0.00347	1.49e-5	0.00448	0.00357	6.6e-6	0.00182	0.00767	0.00035	0.00377	0.00015	0.00602	0.00015
cp_0	5.61e-5	0.00146	0.00855	0.00808	0.00156	0.00118	-0.00728	0.00139	0.00322	0.00918	0.0189	0.00866
tp	0.00304	0.00011	0.00232	0.00163	0.00051	0.0112	0.131	0.0038	0.0144	0.00378	4.32e-5	0.00384
tp_0	4.34e-5	0.00121	0.00599	0.00544	0.00125	0.00026	0.00157	0.00061	0.00168	0.00612	0.0154	0.00592
t	0.00057	0.0068	0.00593	0.00803	1.72e-5	0.00078	0.0529	7.75e-5	0.00541	0.00497	0.00437	0.00649
d	0.00032	0.00306	0.0222	0.0227	0.00123	0.00186	-0.00627	0.00146	0.00485	0.00848	0.00815	0.00788
swc	7.28e-6	8.11e-5	0.00461	0.00419	5.11e-6	0.00122	0.0201	0.00029	0.00074	0.00063	6.35e-5	0.0026
wind	1.1e-5	0.00067	0.00181	0.00259	0.00027	0.00177	0.0413	0.00077	0.00017	-1.76e-6	6.07e-5	1.89e-5
rh	5.35e-5	0.00582	0.0221	0.0224	0.00059	5.47e-5	0.0232	0.00013	0.00075	0.00014	0.00085	3.18e-5
ai	1.36e-6	0.00699	0.0191	0.0204	0.00031	0.00036	0.0449	4.56e-7	0.00408	0.00156	0.00075	0.00311

Histograms

Histograms of for all of the variables were consulted to assist in interpretation of the observed

relationships between variables. As histograms are helpful in assessing the distribution of variables, they were evaluated to determine the central tendency, skewness, and the presence of outliers or multiple nodes of each variable. In addition to simple histograms, cumulative histograms were evaluated for the ΔFRP of each zone.

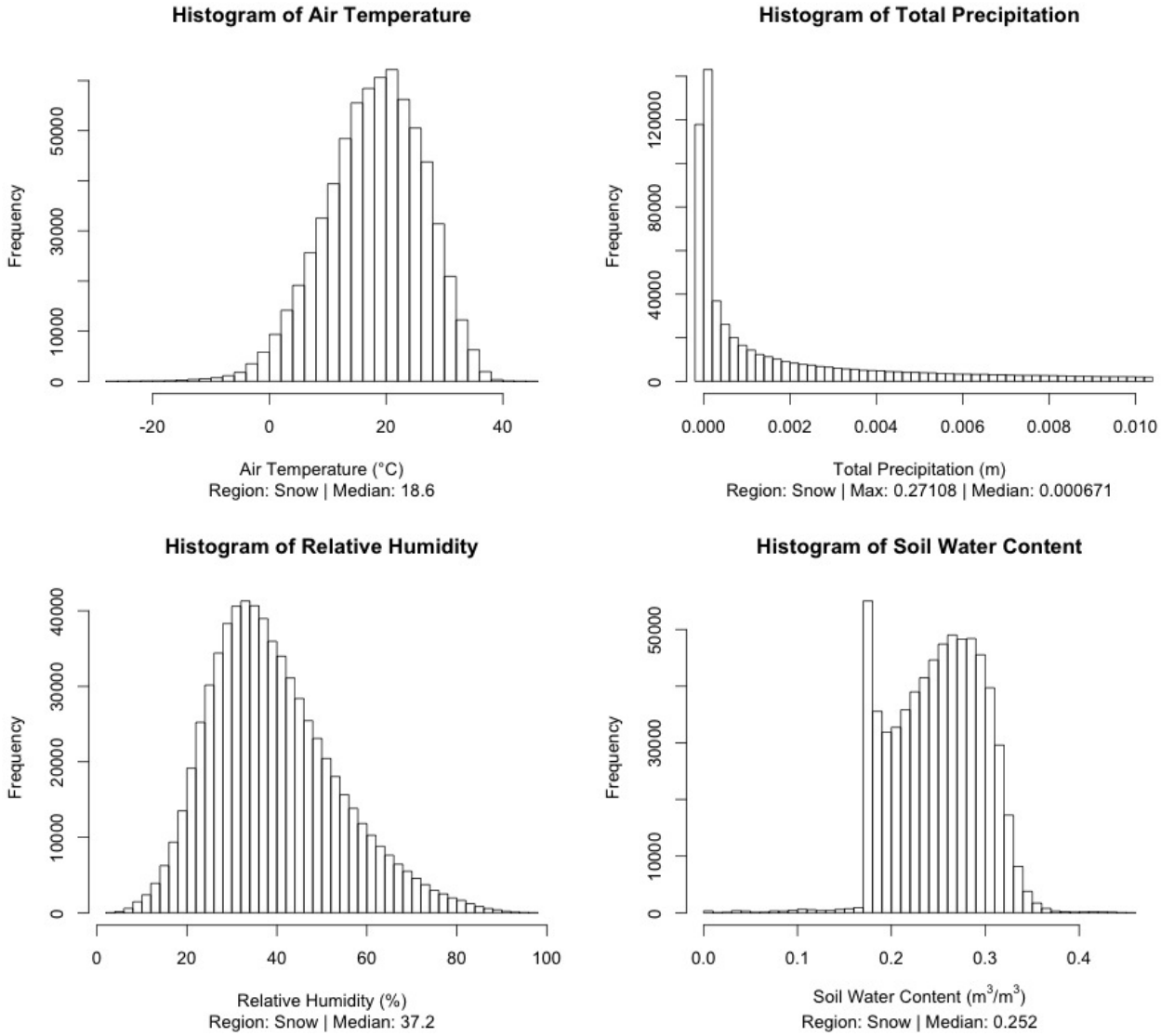

Figure 10: Histograms of four independent variables (air temperature, total precipitation, relative humidity, and soil water content) for the snow zone. The Median of each variable is included in the histograms. For air temperature and relative humidity, a normal distribution is observed, while total precipitation exhibits a skewed distribution. The distribution of soil water content (Median = 0.252) suggests the possibility of a bimodal distribution.

The simple histograms for the snow zone revealed significant characteristics of each variable included in the analysis. Figures 10 & 11 show the distributions of five independent variables used in the analysis (the additional histograms are included in Appendix 5: Histograms). Wind, air temperature, and angstrom index all exhibited a normal distribution for the snow zone. The central tendency of wind was around 9 m/s and there is no evidence of outliers nor of multiple modes of the variable. Similarly, the central tendency of air temperature was around 20ºC. It was curious to see measurements of temperature below zero, as it is unlikely for fire events to occur during those

temperatures. The angstrom index had a central tendency around 2.5. This is right on the cusp between favorable and unfavorable conditions outlined by the index.

Large scale precipitation and soil water content exhibited distributions other than normal. In the case of soil water content, an absence of values less than 0.18 was observed in Figure 10. Similarly, there was an over abundance of values at ~0.18. The central tendency, were this a normal distribution, would suggest a value of 0.28. Large scale precipitation suggests the majority of precipitation events occur around 0.0001. But is also clear that there are larger rain events occurring during the development data.

Finally, a cumulative histogram of ΔFRP was generated (Figure 11). It is important to grasp this distribution in order to achieve a successful model. Reflecting on this cumulative histogram showed two primary results. First, that over half of the ΔFRP values are smaller than 0.25 which represents a significant decrease in FRP of around 75%. Furthermore, nearly 90% of the ΔFRP values are smaller than 0.50, or a decrease of FRP by 50%. Considering these values represent a time series of one day, the observed FRP events appear to have a short time span. The presumed magnitude of decrease for FRP events is substantial. These significant decreases may not be explainable by the small variations of the independent variables. The cumulative histogram of the ΔFRP exhibits odd behavior at 1, suggesting repeat measurements. The cumulative histograms for the warm temperate and equatorial zone can be found in Appendix 5: Histograms;Figure 47, where the common distribution of the ΔFRP is evident.

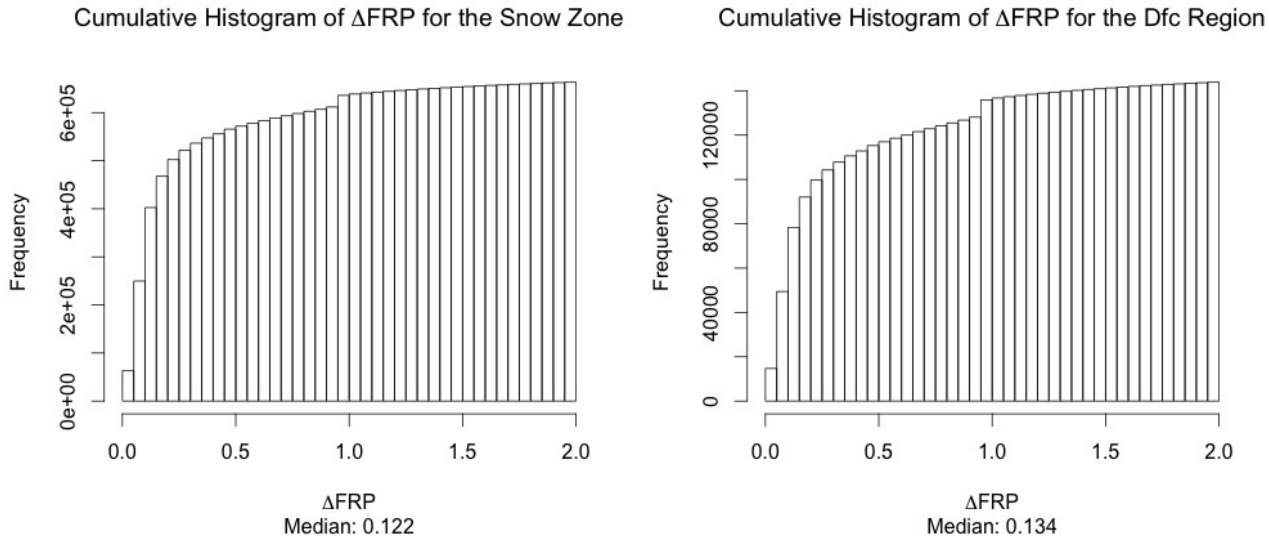

Figure 11: Cumulative histograms of the ΔFRP for the snow zone and Dfc region (Snow:Fully Humid:Cool Summer). With the Median for each distribution listed below, it is clear the distribution is significantly skewed towards ΔFRP values less than 0.5. Furthermore, the frequency of ΔFRP values of 1 raise questions about the satellite observations.

Box Plot Results

Box plots were prepared to evaluate the relationship of independent variables to the ΔFRP. For the evaluation, the independent variables were divided into the four quartiles and each corresponding box plot was generated from distributions of the ΔFRP of each quartiles. The outer whiskers of the box plots were calculated to be 1.5 x Interquartile Range (IQR) to identify potential outliers. Still, an overall trend could be seen through the behavior of the box plots, similar to the behavior of the scatterplots. In many cases, there were so many examples of potential outliers that the open circles used to mark their value appear as a solid line, as seen in Figure 12.

When evaluating the box plot of the FRP_0 (Figure 12) the observed trend showed an increase in ΔFRP as the FRP_0 increased, which was expected. Both the median value and interquartile range suggest that the larger FRP_0 values were more likely to lead to smaller decreases in FRP or even possibly a growth in FRP. The box plots for convective precipitation also displayed an expected trend. As the convective precipitation events increase in size, the ΔFRP values decrease. Larger precipitation events lead to larger decreases in FRP from one day to the next. This trend can be observed through the interquartile range, however a change between the median values is indistinguishable.

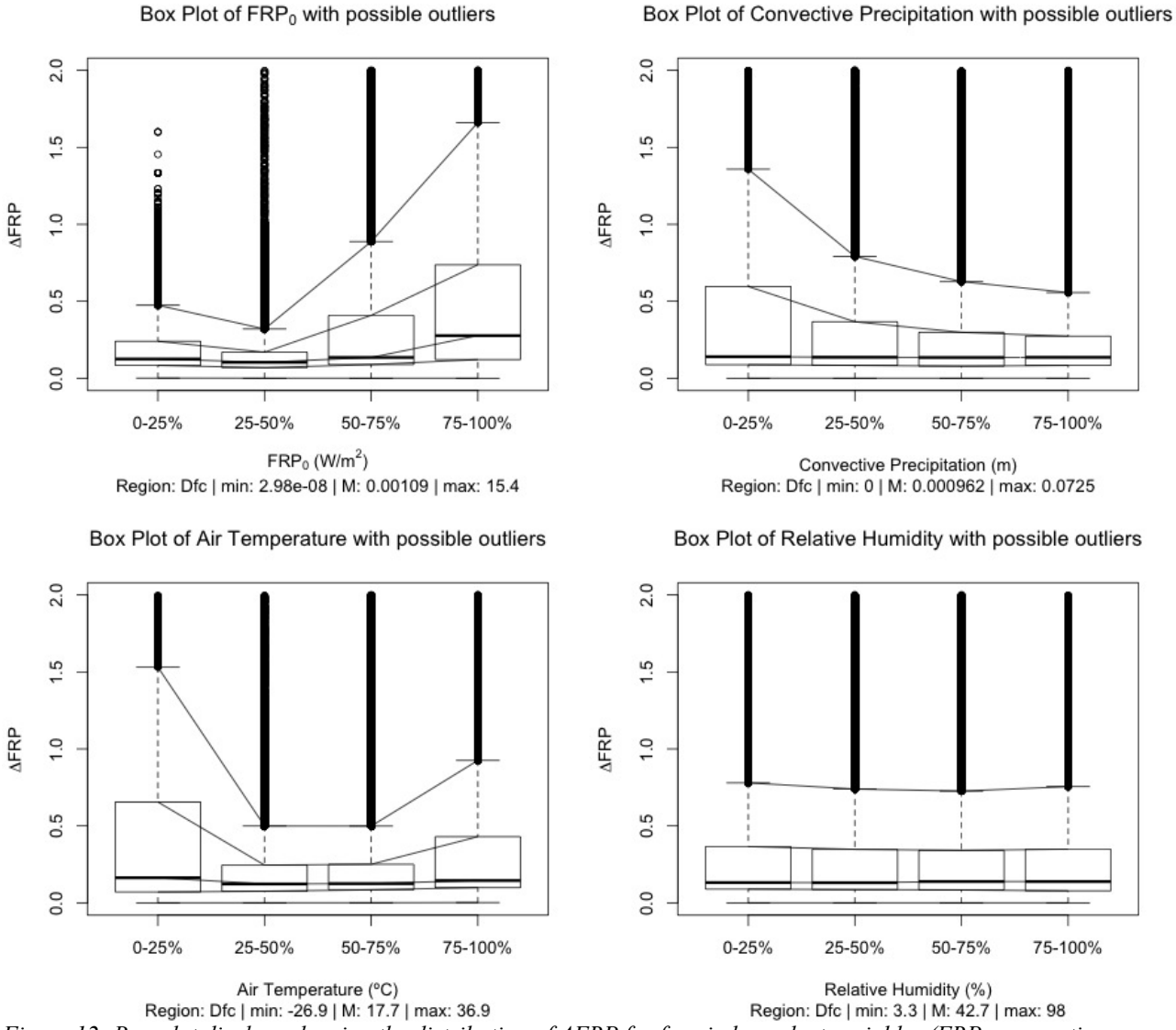

Figure 12: Box-plot displays showing the distribution of ΔFRP for four independent variables (FRP_0, convective precipitation, air temperature, and relative humidity) of the Dfc region (Snow:Fully Humid:Cool Summer), broken into quartiles. These box-plots help to highlight the trends of the median (black bar) and the IQR (the box) of ΔFRP in relation to each quartile of the variable. Possible outliers are represented by those values which fall beyond 1.5xIQR (whiskers), in many cases, the possible outliers number so many that it appears as a solid black line. Additionally, the median (M) is included along with the min and max values of each independent variable.

While some box plots showed expected relationships, other box plots were difficult to interpret. The box plot for air temperature (Figure 12) suggested that the 1st and 4th quartiles allow fire events to persist to a greater extent than the 2nd and 3rd quartiles. This behavior is clear in both the trend of

the median and the trend of the interquartile range. In particular, the behavior of the 1st quartile of air temperature, in regards to the ΔFRP, is puzzling. Furthermore, another relationship observed via the box plots was the existence of no relationship as shown with the relative humidity in Figure 12.

One observation common amongst all box plots generated for the analysis was the abundance of potential outliers. The suspected outliers were determined by setting the maximum and minimum whiskers at 1.5xIQR. The presence of outliers has been prevalent through modes of analysis. They present a problem in evaluation and can prevent a proper conclusion. While some box plots exhibited clearer trends than others, it was unclear whether or not the distributions of the quartiles were significantly different from one another, especially considering the number of potential outliers. This prompted further evaluation before modeling.

Mann-Whitney U Test Results

The Mann-Whitney U tests provided a unique way to evaluate the relationship between the ΔFRP and the independent variables. As the first step in model development and by determining statistically significant populations, Mann-Whitney U tests offered a way validate the trend of the median and to select the best regions. The suite of Mann-Whitney U tests were performed for each variable of each region and zone. If these tests were successful, the suspected trends observed would be validated and observations of the box plots would be corroborated. The percentage of unsuccessful U tests provided a means to identify the poorly associated variables and a criteria to eliminate regions from the modeling effort.

*Table 11: Mann-Whitney U test results for every independent variable of the equatorial zone. The * represents successful U tests showing statistically different groups. The +/- sign shows the trend of the median, from left to right. An X represents failed U tests where the two groups were not significantly different. The size of the each group is included in the table and for the equatorial zone 1.09% of U tests failed.*

variable	I:VII	I:II	II:III	III:IV	IV:V	V:VI	VI:VIII	region
FRP_0	* +	* -	* +	* +	* +	* -	* +	Equatorial
lsp	* -	* +	* -	* -	* +	* +	* +	Equatorial
lsp_0	* -	* +	* -	* -	* -	* -	* -	Equatorial
cp	* -	* +	* -	* -	* +	* +	* +	Equatorial
cp_0	* -	* +	* -	* -	* -	* -	* -	Equatorial
tp	* -	* +	* -	* -	* +	* +	* +	Equatorial
tp_0	* -	* +	* -	* -	* -	* -	* -	Equatorial
t	* +	* +	* +	* +	* +	* -	* -	Equatorial
d	* -	* -	* -	* -	* -	* +	* -	Equatorial
swc	* +	* +	* -	* -	* -	* +	* -	Equatorial
wind	* +	* +	* +	* +	* +	X	* +	Equatorial
rh	* -	* -	* -	* -	* +	* +	* +	Equatorial
ai	* -	* +	* -	* -	* +	* +	* -	Equatorial
size	I:178285	II:713152	III:891441	IV:891440	V:713152	VI:178291	VII:3387476	VIII:3387470

If the number of failed U tests were greater than 20% of the total tests, the regions were passed over for modeling. For some regions, such as the warm temperate zones, there were substantial amounts of failed U tests (Appendix 7: Mann-Whitney U Test Results:Error: Reference source not found). Additionally, particular attention was paid to the I:VII and VI:VIII U tests. Samples where 5% of the population was not statistically different than the remaining 95% immediately raised a red flag concerning the distinctness of the data and the observed trend. Applying the 20% failure, detailed in Table 13, left only seven regions and zones remaining for model development. Considering these results, equatorial zones (Table 11) showed the most statistically different population groups while the warm temperate zone had the most failed tests.

*Table 12: Mann-Whitney U test results for every independent variable of the Dfc region (Snow:Fully Humid:Cool Summer). The * represents successful U tests showing statistically different groups. The +/- sign shows the trend of the median, from left to right. An X represents failed U tests where the two groups were not significantly different. The size of the each group is included in the table and for the Dfc region 17.58% of U tests failed.*

variable	I:VII	I:II	II:III	III:IV	IV:V	V:VI	VI:VIII	region
FRP_0	* -	* -	* -	* +	* +	* +	* +	Dfc
lsp	* -	* -	* +	* -	* +	* +	* +	Dfc
lsp_0	* -	* -	* -	* -	* -	* -	* -	Dfc
cp	* +	X	* +	* -	X	X	* +	Dfc
cp_0	* -	X	* -	* -	* -	* -	* -	Dfc
tp	* +	* -	* +	* +	* +	* +	* +	Dfc
tp_0	* -	* -	* -	* -	* -	* -	* -	Dfc
t	* -	* -	* -	* +	* +	* +	* +	Dfc
d	* -	* -	* -	* +	* +	X	* -	Dfc
swc	* -	X	* -	* -	* +	* +	X	Dfc
wind	X	X	* +	X	X	X	X	Dfc
rh	* -	* -	X	X	* -	X	* +	Dfc
ai	* -	* -	* -	* +	* +	* +	* +	Dfc
size	I:7193	II:28776	III:35969	IV:35969	V:28776	VI:7195	VII:136685	VIII:136683

Comparing distributions of different percentages of data allowed for the trend of ΔFRP to be determined. Attention was paid to trends of the median, and their ability to replicate the trends observed in the box plots and preceding analysis. The U test results for the Dfc region (Snow:Fully Humid:Cool Summer) can be found in Table 12 and the trends correspond to the box plots trends presented in the results. Pertaining to air temperature, the Mann-Whitney U tests showed the same trends as the box plot (Figure 12). The Mann-Whitney U test corroborated the results from the box plots and showed the same trends for FRP_0. While the trend of relative humidity observed in the box plot (Figure 12) was easier to interpret with the Mann-Whitney U tests; the presence of failed tests warrant concern for inclusion. Similarly, the convective precipitation had failed U tests, raising a red flag, but the trends of the box plots and U tests were opposites. In cases where distributions are statistically significant from one another and there are limited failed U tests, the direction of the trend is validated. Avoiding the speculative nature of the box plots with potential outliers. The success of the Mann-Whitney U tests allowed for the selection of regions and variables to improve and streamline the results of modeling.

Table 13: Summary of the percentage of failed U-tests per region. Regions with failure percentage >20% were omitted from model development

Region/Zone	% Failed U-tests
Af	8.79
Am	3.3
Aw	3.29
Equatorial	1.09
Csa	41.76
Csb	47.25
Csc	98.9
Warm Temperate	35.16
Dfa	25.27
Dfb	16.48
Dfc	17.58
Snow	10.99

Model Results

Seven regions remained after a sorting of the U test results. All warm temperate regions were eliminated from model development, as well as the Dfa region (Snow:Fully Humid:Hot Summer). For each region, a full linear regression with a Bayesian Information Criteria was performed and initially evaluated with the model development data, before application to the evaluation dataset.

Table 14: Summary of the linear regression model via BIC for the Dfc region (Snow:Fully Humid:Cool Summer) with non-linear relationships between independent variables and ΔFRP considered (squared terms)

Region: Dfc	Estimate	Std. Error	t value	Pr(>|t|)
(Intercept)	0.2692	0.0014	195.23	0.0000
$(d)^2$	0.0006	0.0000	59.33	0.0000
cp	-11.0783	0.2016	-54.96	0.0000
lsp	8.7260	0.1719	50.76	0.0000
FRP_0	0.2930	0.0083	35.23	0.0000
$(FRP_0)^2$	-0.0365	0.0015	-24.84	0.0000

Through the use of linear modeling with BIC, a model for each zone and region was generated and evaluated. The Bayesian Information Criteria generated coefficients to yield the most appropriate linear model. A summary of the model results and the output of the BIC for the Dfc region (Snow:Fully Humid:Cool Summer) can be found in Table 14. For the Dfc region, the dew point temperature was the main explanatory variable, while the remaining four related were either FRP or moisture variables.

Table 15: Summary table of R^2 values of fitted ΔFRP vs. actual ΔFRP for the 7 regions that passed the Mann-Whitney U Test Selection. These R^2 values were from linear regression model development with BIC.

Region/Zone	R^2 of Fitted ΔFRP vs. Actual ΔFRP
Af	0.0162
Am	0.0312
Aw	0.0332
Equatorial	0.0345
Dfb	0.0318
Dfc	0.0508
Snow	0.0315

Table 16: Detailed summary of the best fit line of Fitted ΔFRP vs. Actual ΔFRP developed for the Dfc region (Snow:Fully Humid:Cool Summer) from the linear regression with BIC for years 2003-2007.

Region: Dfc	Estimate	Std. Error	t value	Pr(>|t|)
Intercept:	0.2931	0.0003	1034.95	0.0000
R-squared:	0.0508	0.0006	87.71	0.0000

After the BIC selection of coefficients from the 2003-2007 data and before model evaluation, the fitted values derived from the linear regression were evaluated with the development data. The R^2 value was calculated for the fitted vs actual values of the model development. The results are summarized for the Dfc region in Table 16 and for the six other regions and zones in Table 15. The BIC summary and Fitted ΔFRP vs. Actual ΔFRP best fit line summary for the remaining six regions can be found in Appendix 8: BIC and Modeling. The overall poor performance exhibited at this stage was discouraging, but modeling was performed for Dfc region (Snow:Fully Humid:Cool Summer).

With these selected coefficients determined from the 2003-2007 development data, modeled values were generated for the corresponding 2008-2010 evaluation data to check the model. The R^2 value comparing the modeled values and the observed data was evaluated. The evaluation of the model was only performed for one region, due to the poor results of model development. The R^2 comparing the Modeled vs. Actual ΔFRP values in the evaluation stage just as poor as the R^2 for the data from the development stage. The results of the model evaluation is summarized in Figure 13.

The scatterplot between modeled and actual values shows an R^2 value of 0.05462 confirming that it was not an effective model.

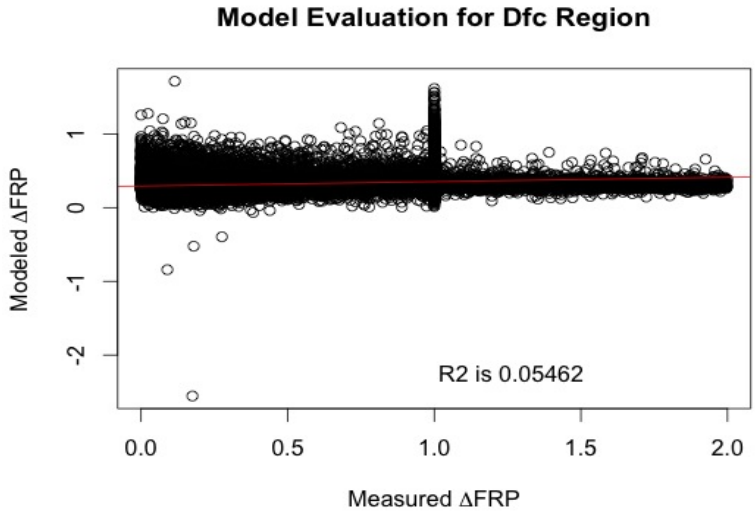

Figure 13: Evaluative scatterplot of Measured ΔFRP vs Modeled ΔFRP for the Dfc region (Snow:Fully Humid:Cool Summer) from years 2008-2010 using the linear model detailed in Table 14. The R^2 value of the best fit line is 0.05462.

Discussion

Overall, the results from the covariate analysis and model evaluation showed insignificant relationships between the independent variables and ΔFRP. The relationships typically showed trends that behaved with the expected relationship, but did not appropriately model ΔFRP. Furthermore, the relationships of independent variables differed across the zones and regions, thereby highlighting an inherent challenge in developing global models.

There is a lot of noise in the dataset. Individually, the independent variables only account for a fraction of that noise. But understanding the distribution of ΔFRP can partially explain poor correlation coefficients and low R^2 values observed in the early covariate analysis. For the snow zone, the cumulative histogram shows the median ΔFRP value is 0.134 (Figure 11). Considering that there are 663,000 ΔFRP values for the snow zone, half of these events represent at least an 86% decrease in FRP from one day to the next. Combined with the 3,566,000 ΔFRP values from the Equatorial zone (median: 0.136) and 221,000 ΔFRP values from the Warm Temperate zone (median: 0.108) there is a substantially large data set. While the size does not preclude the discovery of significant relationships, the impact of the meteorological variables on ΔFRP is more challenging to observe.

The impact of the data set size is clear in the scatterplots and box plots. Visual interpretation of the scatterplots is impossible without the help of box plots. By following the change of the median and IQR across the four quartiles of the independent variables, the box plots effectively provided a more robust explanation of the relationship to ΔFRP. Furthermore, box plots identified a substantial number of potential outliers for all independent variables, highlighting impact of the large dataset.

The overwhelming number of potential outliers necessitated an additional test to determine if the quartiles observed in the box plots were statistically different from one another. The Mann-Whitney

U test was successful in identifying statistically different populations; however, confusing trends were observed, which will be discussed later. Inclusion of the Bonferroni Correction was critically important in the analysis by correcting for the familywise error rate. Performing seven tests over the same population can skew the results of the U test. Whereby correcting the confidence interval from 0.5 to 0.007, the certainty of the statistical significance in preserved. This also insured that region selection done at this stage was fully warranted. By selecting regions that had greater than 80% successful U tests, the modeling process could be streamlined.

The five regions that passed the Mann-Whitney U test selection were the largest datasets, with the largest being the Aw (Equatorial:Winter Dry) at 2,613,908 entries. Of these five regions, three were from the tropical ecosystem and two were from the boreal ecosystem. The equatorial zone and snow zone, the two largest zones, also passed the Mann-Whitney U tests. The warm temperate ecosystem did not have any groups that passed through to modeling. Two possible conclusions can be made based on this observation. 1) Larger sample sizes yield more statistically significant trends and 2) Relationships between independent variables and ΔFRP are better suited to explain wildfire behavior in Boreal and Tropical ecosystems.

Regarding the first point, there is no doubt that the Mann-Whitney U tests offered the best understanding of the relationship between the independent variables and ΔFRP. However, the impact of population size on success is challenging to assess. Larger populations simply have more variables to differentiate themselves from one another. There will also be a greater distribution of both the independent variables and ΔFRP among larger populations. For the second point, the existence of stronger relationships between the independent variables and ΔFRP in different zones is a distinct possibility, this idea and the differences between zones will be discussed later.

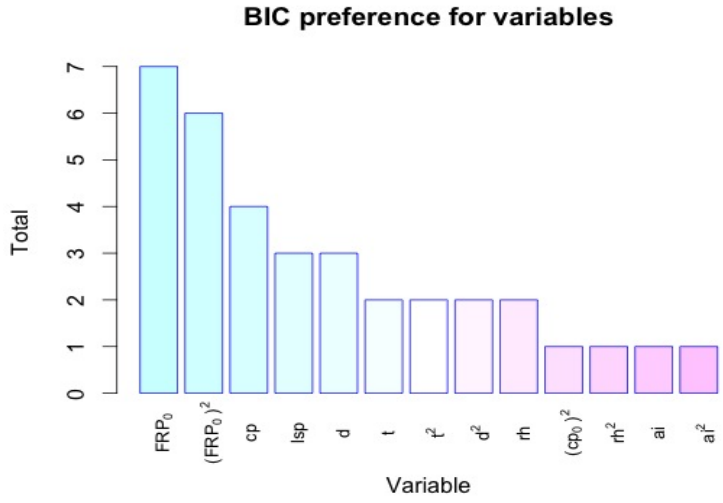

Figure 14: A bar graph summarizing the preferred explanatory values from the linear regression with BIC for the seven regions analyzed. FRP_0 was the most preferred followed by the $(FRP_0)^2$.

The Bayesian Information Criteria was impartial in variable selection. Following the region selection from the Mann-Whitney U tests, further selection could have been made to eliminate specific variables from the model development. Removing the independent variables where improper trends were observed or significant numbers of failed tests occurred can potentially improve the model. Not surprisingly, the FRP_0 was selected most often through BIC; appearing in the linear regression model of each zone. (Figure 14) Interestingly, variables with illogical trends observed in the Mann-Whitney U tests were selected through the BIC, which will be touched on

later.

This first attempt at modeling the relationship between FRP and meteorological variables encompassed the central scope of the project. There were other components of fire behavior that were not included due to time and the nominal improvement inclusion would have provided. Most notably, the spatial autocorrelation of ΔFRP was not calculated for these results. While spatial autocorrelation is a significant way to improve the model, the poor performance of that aspect of the models did not justify the inclusion of spatial autocorrelation in this project.

Variable Comparison & Performance

As highlighted in Figure 14, there were eight distinct variables selected for the linear regression model with BIC. FRP_0 was most often selected, followed by convective precipitation, large scale precipitation and dew point temperature. At the outset of the research, variables that were expected to impact ΔFRP were FRP_0, moisture variables, and movement variables; which is exactly what was seen. Furthermore, the relationships between the independent variables and ΔFRP were, whether positive or negative, expected to have a linear relationship. However, the variable selection by the linear regression model with BIC was both confirmed and confounded when referenced back to the Mann-Whitney U tests and covariate analysis. In addition to discussing the behavior of the BIC selected variables, the performance of the remaining variables will also be touched on.

FRP, FRP0 & ΔFRP

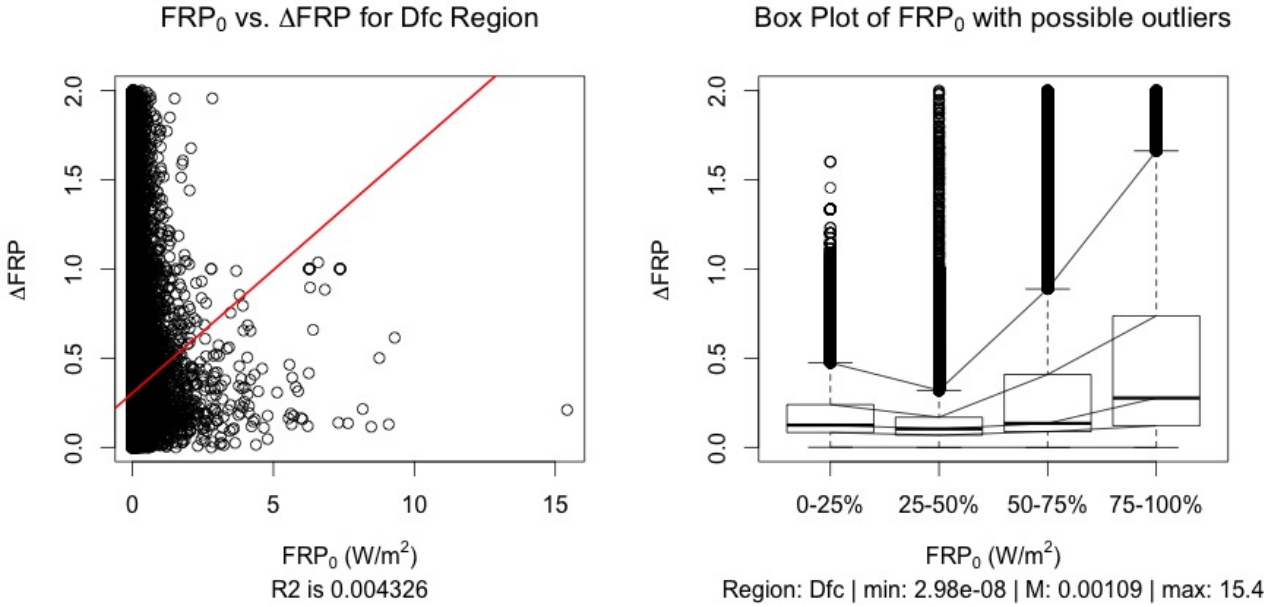

Figure 15: A side by side comparison, for ease of interpretation, of the scatterplot and box plot of the relationship between FRP_0 and ΔFRP for the Dfc region (Snow:Fully Humid:Cool Summer). The best fit line was included to show the predicted trend based on the scatter plot. Furthermore, it was at this stage where the curious behavior around the 2nd quartile was observed.

The data points of FRP_0 vs. ΔFRP reveal no visible trend in the scatterplot, and the corresponding fit line (R2 of 0.0043) showed no linear relationship. The box plot revealed a decrease from the first quartile to the second quartile which was puzzling, but the rest of the quartiles behaved logically as shown in Figure 15. The apparent, non-linear behavior of FRP_0 was confirmed through the evaluation of the Mann-Whitney U Tests. Table 17 displays the results of all Mann-Whitney U

tests for FRP_0, showing that the behavior observed in the Dfc box plot occurred in all regions and zones. This unexpected behavior could be explained by the duality of small FRP_0 values. The distribution of FRP_0 is heavily weighted towards values close to zero with the 50% of FRP_0 values less than $1.09e^{-3}$ W/m^2. The subsequent response of ΔFRP due to independent variables exhibit substantial variability. When considering the second quartile of FRP_0 for the Dfc region (Snow:Fully Humid:Cool Summer), the IQR of ΔFRP is less than 0.5, showing a majority of decreasing wildfire events. However, a substantial amount of potential outliers show increasing wildfire events.

Table 17: A concise summary of the Mann-Whitney U test results for the FRP_0 variable. The behavior of the median suggests the possibility of a threshold value of FRP_0 that exists in group III (25%-50%), or in the case of the Equatorial zone, group II (5%-25%).

variable	I:VII	I:II	II:III	III:IV	IV:V	V:VI	VI:VIII	region
FRP_0	* -	* -	* -	* +	* +	* +	* +	Af
FRP_0	* -	* -	* +	* +	* +	* +	* +	Am
FRP_0	* -	* -	* +	* +	* +	* +	* +	Aw
FRP_0	* +	* -	* +	* +	* +	* -	* +	Equatorial
FRP_0	* -	* -	* -	* +	* +	* +	* +	Csa
FRP_0	* -	* -	* -	* +	* +	* +	* +	Csb
FRP_0	X	X	X	X	X	X	X	Csc
FRP_0	* -	* -	* -	* +	* +	* +	* +	Warm Temperate
FRP_0	* -	* -	* -	* +	* +	* +	* +	Dfa
FRP_0	* -	* -	* -	* +	* +	* +	* +	Dfb
FRP_0	* -	* -	* -	* +	* +	* +	* +	Dfc
FRP_0	* -	* -	* -	* +	* +	* +	* +	snow

The two scenarios where small FRP_0 variables occur are either during the establishment of wildfire events or during the extinction of wildfire events. This ambiguity in small fire events has the ability to confound the trends expected. For theses small FRP_0 values in the first two quartiles, the corresponding ΔFRP primarily show deceasing fire events. However, for the second quartile, more potential outliers show an increase in wildfire size ($\Delta FRP > 1$). Increasing FRP_0 values suggest a more established fire capable of growth, but this behavior is not seen in the 1st quartile to the 2nd quartile.

It is unclear why wildfires, with FRP_0 in the smallest quartile, show smaller decreases (closer to 1) in ΔFRP than the larger FRP_0 values in the second quartile. All this is to say that the existence of the threshold for FRP_0 is likely because evaluating the 3rd and 4th quartiles of the distribution of FRP_0 where the expected behavior between FRP_0 and ΔFRP is shown. FRP_0 values below the threshold do not exhibit a clear trend. It is possible that FRP_0 values in the smallest two quartiles are confounded by other sources of thermal measurements or moved toward extinction through non-meteorological means such as total fuel consumption due to ecosystem type or geographic aspect; which leads to uncertain trends. An estimate of the threshold for the Dfc region would be in the 2nd quartile (same as group III from the Mann-Whitney U test) which is bounded at $3.64e^{-5}$ and $1.09e^{-3}$ W/m^2.

Another interesting behavior of the FRP data was the presence of ΔFRP values equal to 1. While the occurrence of identical FRP values on two sequential days is a distinct possibility, it is a small likelihood that this a common occurrence. Consider the cumulative histograms of ΔFRP for the Dfc region and Equatorial zone in Figure 11 on page 31; both graphs show a marked increase where ΔFRP is equal to 1. Values where $\Delta FRP = 1$ most likely arise from measurement error, where the subsequent satellite measurement is unavailable and rather than report the wildfire as extinct (FRP=0) the preceding day's FRP value is reported. The most likely explanation for an unavailable measurement is from overcast and cloudy days. Assuming there is only one day where ΔFRP=1, a

possible way to correct for this would be to calculate the average FRP value from the two FRP across the time step and use that value to calculate an ΔFRP closer to the truth.

Finally, the ΔFRP equation used for the analysis can be improved upon. The ratio ΔFRP used for this analysis is, in retrospect, too basic a representation of the change of FRP from one day to the next. The disregard of fire size significantly inhibits the ability to properly quantify the effect of meteorological variables. As it stands, the change between smaller FRP values can yield the same ΔFRP value as the change between larger FRP values. This is problematic because the impact of independent variables on ΔFRP is dependent on fire size. A significant large scale precipitation event (~0.001m) can completely extinguish a smaller fire event, while only partially impacting the ΔFRP of a larger fire event. To correct for this, a relative ΔFRP would be more effective by accounting for the size of FRP values. A more appropriate ΔFRP could appear as:

$$\Delta FRP = \frac{FRP}{FRP_0} \times \left(FRP - FRP_0 \right)$$

Equation 4: Possible improvement for the calculation of ΔFRP, factoring in the magnitude of ΔFRP.

This improved formula allows the size of wildfire events to be factored into the calculation. The subsequent interpretation is more straightforward because decreasing FRP will be less than zero and increasing FRP is greater than zero. Including the magnitude with the ratio can help the performance of the model, but a second option would be to look at the difference in magnitude.

Along these lines, the lack of fire extinction data inhibits the performance of the model and prevents a more robust understanding of the relationship between ΔFRP and the independent variables. Independent variables that have an inverse relationship with ΔFRP are particularly affected. Consider precipitation variables where large events lead to the immediate extinction of FRP; omitting the last phase of the fire event prevents pertinent information from being included in the overall evaluation of the relationship with ΔFRP. Furthermore, the predictive model is left without a conclusion as to what circumstances suggest complete extinction.

Moisture Variables

Convective precipitation, large scale precipitation, CP_0, relative humidity, and dew point temperature were all selected via BIC for inclusion in the linear regression modeling. As stated before, moisture plays a critical role in the behavior of fire by directly affecting the combustibility of fuel. Additionally, the absence of moisture can also increase the likelihood of wildfire events. Typically, the absence of moisture impacts wildfire potential over longer timescales (weeks and months) while the deposition of precipitation immediately inhibits wildfire events. The inclusion of a drought index is poised to improve the behavior of the linear regression model, but typically the drought index is consulted to determine ignition likelihood and fire severity. Drought indices follow timescales greater than those considered for the analysis, but variables measuring the presence of moisture have a direct impact.

Evaluation of the primary precipitation variables: large scale precipitation, convective precipitation, and total precipitation; exhibited peculiar relationships with ΔFRP. These variables are expected to show an inverse relationship with ΔFRP; however, the opposite relationship was observed. For large scale precipitation in the Dfc region (Snow:Fully Humid:Cool Summer), the incorrect relationship was immediately observed in the scatterplot. (Figure 16) The corresponding box plot revealed a more detailed relationship where the correct trend was observed in the first three quartiles but the

largest quartile of large scale precipitation showed an incorrect trend. This incorrect behavior is seen for all three precipitation variables. The impact of precipitation events can be significantly affected by the flaws of the ΔFRP equation discussed earlier, but there are other issues possibly confounding the observations.

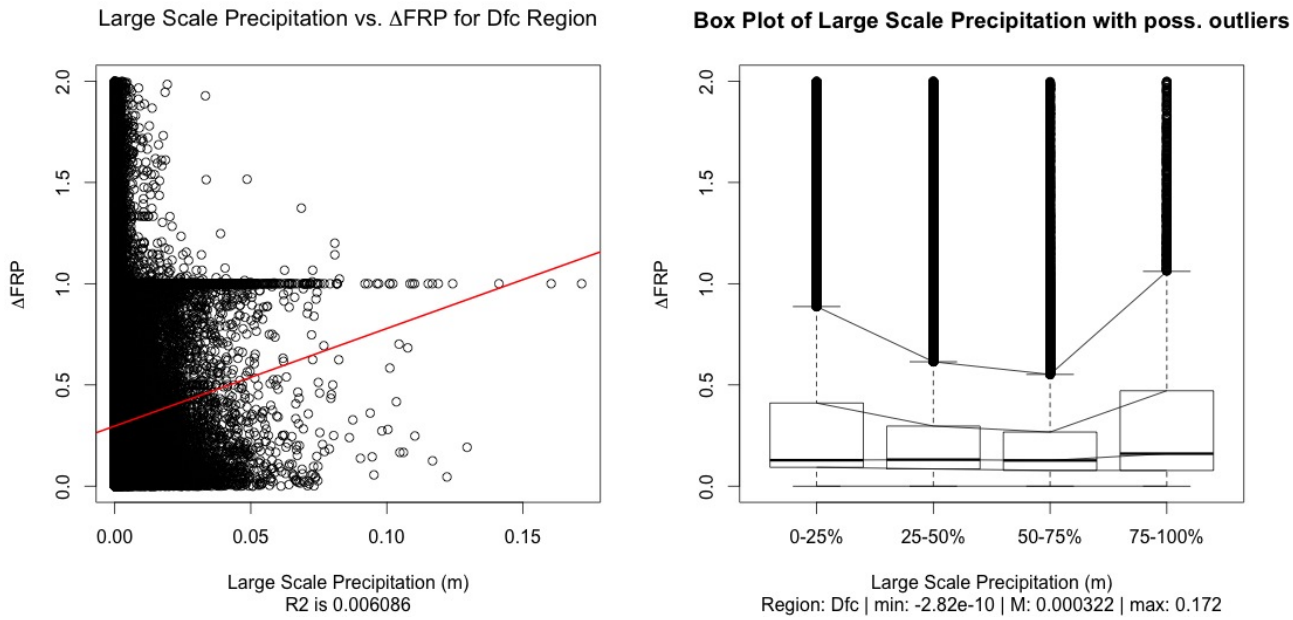

Figure 16: A side by side comparison, for ease of interpretation, of the scatterplot and box plot of the relationship between large scale precipitation and ΔFRP for the Dfc region (Snow:Fully Humid:Cool Summer). The best fit line was included to show the predicted trend based on the scatter plot. Furthermore, it was at this stage where the curious behavior at the 4th quartile was observed.

In particular, spatial issues come into play when evaluating the relationship with convective precipitation. As convective precipitation occurs on a smaller spatial scale, it does not have the capacity to impact the whole 0.5º grid cell. As a result, there is a distinct possibility that convective precipitation events do not occur over the wildfire events. Furthermore, thunderstorms are associated with convective precipitation events and, in the case of dry lightning associated with thunderstorms, can represent a natural wildfire ignition source. Large scale precipitation is poised to effect the whole grid cell, but illogical relationships are still observed. This may be due to the timing of observations. While there is no question that precipitation has an immediate effect on wildfire intensity, the timing of measurements can lead to discrepancies. The FRP measurements are made once daily, while the meteorological variables are composed of eight daily measurements. Regarding precipitation, the eight daily measurements were summated with no recording of in what time period the largest portion of the precipitation took place. This allows for the distinct possibility that precipitation values were taken after the FRP and do not effect the FRP value of that day.

This idea is corroborated when considering the time delayed precipitation values: LSP_0, CP_0, & TP_0. Table 18 displays the Mann-Whitney U tests for both convective precipitation and CP_0 for all regions and zones. Interestingly, the equatorial zone and corresponding regions show the correct trend for the smallest 50% of the distribution of convective precipitation. The remaining median trends show the incorrect relationship also found with large scale precipitation and total precipitation. Compared to the other zones, convective precipitation is most common in equatorial ecosystems due to the amount of moisture generated by the rainforests. The precipitation values showed statistically different populations, although incorrect trends, in the snow and equatorial zone; however, precipitation variables performed poorly in the warm temperate zone, which will be

touched on later.

When considering the CP_0, the expected inverse relationship is observed for nearly all regions and zones. This behavior was also found for LSP_0 and TP_0. Which suggests that the inclusion of the preceding day's precipitation values were warranted and also that the timing of measurements may be significantly off. This perceived timing issue may only be applicable to precipitation values, which are summations of the eight daily values. The other three variables selected the maximum (and in the case of soil water content, the minimum) values. For these independent variables their maximum and minimum values sync with daytime hours and peak fire time. Considering this behavior, it is surprising to see that the BIC for the linear regression model still selected convective precipitation and large scale precipitation rather than CP_0 and LSP_0.

Table 18: Summarization of the CP and CP_0 Mann-Whitney U tests, effectively showing the median trends across the regions and the marked difference between the relationships of CP_0 and CP to ΔFRP.

variable	I:VII	I:II	II:III	III:IV	IV:V	V:VI	VI:VIII	region
cp	* -	* -	* -	* +	* +	* +	* +	Af
cp	* -	* -	* -	* +	* +	* +	* +	Am
cp	* -	* -	* -	* -	* +	* +	X	Aw
cp	* -	* +	* -	* -	* +	* +	* +	Equatorial
cp	X	X	* +	X	* +	X	* +	Csa
cp	X	X	X	X	* +	X	* +	Csb
cp	X	X	X	X	X	X	X	Csc
cp	* +	X	X	X	* +	X	* +	Warm Temperate
cp	* +	* -	* +	* +	* +	* +	* +	Dfa
cp	* +	X	* +	X	* +	* +	* +	Dfb
cp	* +	X	* +	* -	X	X	* +	Dfc
cp	* +	* +	* +	X	* +	* +	* +	snow
cp_0	* -	* -	* -	* -	* -	X	* -	Af
cp_0	* -	* -	* -	X	* -	* -	* -	Am
cp_0	* -	* -	* -	* -	* -	* -	* -	Aw
cp_0	* -	* +	* -	* -	* -	* -	* -	Equatorial
cp_0	* -	* -	* +	X	* -	* -	* -	Csa
cp_0	* -	X	X	* -	* -	* -	* -	Csb
cp_0	X	X	X	* -	X	X	X	Csc
cp_0	* -	* -	* +	* -	* -	* -	* -	Warm Temperate
cp_0	* -	X	* -	* -	* -	* -	* -	Dfa
cp_0	* -	* +	* -	* -	* -	* -	* -	Dfb
cp_0	* -	X	* -	* -	* -	* -	* -	Dfc
cp_0	* -	* +	* -	* -	* -	* -	* -	snow

The secondary moisture variables, relative humidity and dew point temperature, were also selected through BIC. They both exhibited slightly negative trends in the scatterplots which was expected. However, the corresponding box plot revealed a flatter trend than expected for the relative humidity. In general, relative humidity showed statistically significant U tests for the equatorial zone and snow zone and the median trend showed the expected inverse relationship in the smallest two quartiles. Evaluation of the Mann-Whitney U tests for relative humidity (Table 19) suggests that there may be an upper threshold for relative humidity, above which an improper relationship exists. This behavior, and potential threshold, was observed only in the snow and equatorial zones and corresponding regions but it is unclear how this will affect the linear modeling. In the snow zone and corresponding regions, the failed Mann-Whitney U tests may be due to the flat trends similar to that observed for the Dfc region. The warm temperate zone and the corresponding regions contained many failed U tests that prohibited any firm conclusions from being made.

Similar to relative humidity, the dew point temperature also exhibited poor U test performance (Table 19) in the warm temperate zone. The behavior of the warm temperate zone will be discussed

later. Additionally, dew point temperature showed no statistical significance for the Dfa region. Beyond theses failed tests, the similar possibility of a threshold appears from the median trend behavior. It is not surprising that the two secondary moisture variables behave similarly. Both what they represent and the physical way in which they impact wildfire events are akin to one another.

Table 19: Summary of the relative humidity (rh) and dew point temperature (d) Mann-Whitney U tests, effectively showing the median trends across the regions and the differences between the relationships of rh and d to ΔFRP.

variable	I:VII	I:II	II:III	III:IV	IV:V	V:VI	VI:VIII	region
rh	* -	* -	* -	* +	* +	* +	* +	Af
rh	* -	* -	* -	* -	* +	* +	X	Am
rh	* -	* +	* -	* -	* +	* +	* +	Aw
rh	* -	* -	* -	* -	* +	* +	* +	Equatorial
rh	* +	X	* +	* -	* +	* +	* +	Csa
rh	* +	* -	X	X	X	X	X	Csb
rh	X	X	X	X	X	X	X	Csc
rh	* +	* +	* +	* +	* +	* +	* +	Warm Temperate
rh	* -	X	* -	* -	X	* +	* +	Dfa
rh	* -	* -	* -	* -	* +	* +	* +	Dfb
rh	* -	* -	X	X	* -	X	* +	Dfc
rh	* -	* -	* -	* -	* +	* +	* +	snow
d	* +	* +	X	X	* +	* +	* +	Af
d	* -	* -	* -	* -	* +	* +	* +	Am
d	* -	* +	* -	* -	* +	* +	* -	Aw
d	* -	* -	* -	* -	* -	* +	* -	Equatorial
d	X	X	* +	X	X	X	X	Csa
d	* +	X	X	* -	X	X	X	Csb
d	X	X	X	X	X	X	X	Csc
d	* +	X	* +	* -	X	X	X	Warm Temperate
d	X	X	X	X	X	X	* -	Dfa
d	* -	* -	* -	* -	X	* +	X	Dfb
d	* -	* -	* -	* +	* +	X	* -	Dfc
d	* -	* -	* -	* -	* -	X	* -	snow

In general, a more pronounced inverse relationship was expected to be visible for relative humidity and dew point temperature. The weak relationships observed could be emphasized by the flawed ΔFRP calculation mentioned earlier, which essentially weakened the signals of the impact of relative humidity and dew point temperature. Dew point temperature and relative humidity both relate to the water vapor in the air. The presence of water vapor has the same effect as precipitation on fuel, by lowering the combustibility. But unlike precipitation which is directly deposited on fuel, water vapor requires specific conditions to condense on the fuel, and thus lower the combustibility. As a result, the impact of changes in relative humidity and dew point temperature occur more slowly compared to precipitation, so the resulting trend will not be as pronounced.

Movement Variables

Air temperature, wind, and soil water content make up the movement variables in the analysis. Of these variables, only air temperature was selected through BIC for linear regression modeling. Where the water variables quantified the amount of moisture being added to the ecosystem, these movement variables represent the transition of moisture on the ecosystem level. Wind is capable of increasing the intensity of wildfire events by introducing more oxygen and spreading wildfire events by transporting embers to unlit areas increasing the size of the wildfire.

As a BIC selected variable, the incorrect behavior observed in the scatterplot for air temperature in the Dfc region was concerning. Air temperature effects on fuel combustibility have a direct

relationship, while the scatterplot suggest the possibility of an inverse relationship (Figure 17). Higher air temperatures increase evaporation and effectively dry out fuel, increasing the possibility of combustion. The box plot shows the expected direct relationship for the 3rd and 4th quartiles. But when evaluating the median trends for air temperature (Table 20), the behavior is inconsistent across the zones and regions.

The equatorial zone exhibits the best relationship with air temperature, both the median trend and statistical significance show the expected direct relationship. The warm temperate zone again shows many failed U tests suggesting a poor relationship. The snow zone shows expected behavior for the extreme variables, but shows inverse relationships for the smaller values. Extreme air temperature values are poised to have a pronounced effect on the snow zone due to them occurring in during the peak fire season for those regions.

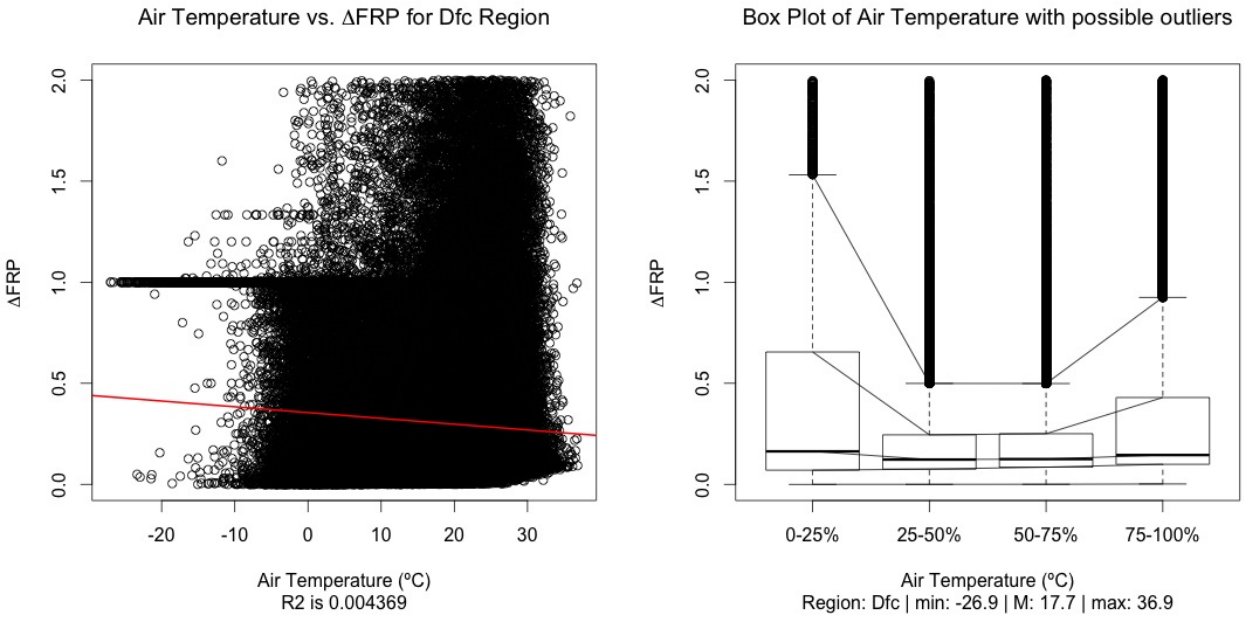

Figure 17: A side by side comparison, for ease of interpretation, of the scatterplot and box plot of the relationship between air temperature and ΔFRP for the Dfc region (Snow:Fully Humid:Cool Summer). The best fit line was added to show the predicted trend based on the scatter plot, which suggests the possibility of a non linear relationship.

Additional mechanisms that explain these temperature observation are similar to those of dew point temperature and relative humidity. The impacts of air temperature on wildfire behavior occur over a longer timescale than that of precipitation. Echoing the reasoning for weak observed relationships from dew point temperature; air temperature plays a large role in creating drought like conditions which occur over days and weeks. The immediate impact of small air temperature changes are uncertain. Extreme air temperature events are poised to have an immediate effect, with the corresponding increase in evaporation of fuel moisture. Additionally, the diurnal behavior of air temperature also limits the amount of time that increased temperatures can affect fuel combustibility with peak temperature values occurring in the middle of the day. Again, the observable relationship between air temperature and ΔFRP can be inhibited by the flawed ΔFRP calculation that disregards the magnitude of the wildfire.

Wind and soil water content were not selected for linear regression modeling. Soil water content is important in dictating fuel combustibility, but the timescale, mechanism and impact on fuel combustibility of soil water content does not correspond well to the daily behavior that was the focus of this study. The snow zone, and Dfa region in particular, was the only ecosystem that

exhibited the inverse relationship expected with soil water content which may correspond to the seasonality of wildfire events in the snow zone. In the equatorial zone there were statistically significant trends but for direct relationships, which is incorrect. Finally, the warm temperate zone suffered from failed U tests and incorrect relationships. Soil water content is important in determining drought conditions and may function better in predicting the occurrence of fire, but not the behavior of fire events.

Table 20: Summary of the air temperature (t) Mann-Whitney U tests, effectively showing the median trends across the regions and the relationship to ΔFRP.

variable	I:VII	I:II	II:III	III:IV	IV:V	V:VI	VI:VIII	region
t	X	* +	* -	* -	* +	* +	* +	Af
t	* +	* +	* -	* +	* +	* +	* +	Am
t	* +	* +	* +	* +	* +	* -	* -	Aw
t	* +	* +	* +	* +	* +	* -	* -	Equatorial
t	X	X	X	X	X	* +	* -	Csa
t	X	X	X	X	* -	* +	* +	Csb
t	X	X	X	X	X	X	X	Csc
t	X	X	X	X	* -	X	* -	Warm Temperate
t	X	X	* -	X	* +	* +	* +	Dfa
t	* -	* -	X	* -	* -	* +	* +	Dfb
t	* -	* -	* -	* +	* +	* +	* +	Dfc
t	* -	* -	* -	* -	* -	* +	* -	snow

When evaluating the effects of wind on ΔFRP, there were never strong trends observed in the scatterplots or box plots. This is puzzling, because wind increases wildfire in two distinct ways. Nevertheless, no relationship was evident. Unlike soil water content, wind will have an immediate impact on the spread of wildfire and on the intensity. Wind also exhibits diurnal behavior which confounds observations of the relationship when considering the timing for measurements (Mills, 2009). Wind introduces more oxygen to wildfire events, which enable the faster consumption of fuel. Once fuel is consumed the FRP will diminish, unless fire has spread to new areas. This intricate relationship can lead to weak relationships observed between wind and ΔFRP. The Mann-Whitney U tests confirmed this weak relationship with 8 of the 12 regions/zones failing at least four (of seven) U tests. Surprisingly, for the Am and Aw regions (Equatorial:Monsoon & Equatorial:Winter Dry), wind displayed a statistically significant and direct relationship. However, the box plot for the Am region conveys how minimal the direct relationship is between wind and ΔFRP (Figure 18).

Finally, the angstrom index is expected to show an inverse relationship with ΔFRP. The angstrom index is based on relative humidity and air temperature. This index was developed for Sweden, so it was not surprising to observe decent performance in the snow zone and corresponding regions. The box plot of angstrom index for the Dfc region (Snow:Fully Humid:Cool Summer) (Appendix 6: Box Plots) showed the expected inverse relationship for the 1st and 2nd quartiles. For the Dfc region, the median angstrom index value was 3.15 covering the favorable conditions of wildfire ignition. For the remaining values greater than four, a direct relationship was observed which was counterintuitive. This behavior was seen in the Mann-Whitney U tests for the snow zone and equatorial zone. Surprisingly, the angstrom index was selected for linear regression modeling in the Am region (Equatorial:Monsoon). Like the snow regions, the equatorial regions displayed the correct inverse relationship for the 1st and 2nd quartiles, but a direct relationship in the 3rd 4th. It is unclear why the angstrom index displayed a significant and correct relationship to ΔFRP in the equatorial zone, especially when considering the poor performance of angstrom index in the warm temperate regions. As mentioned earlier, the angstrom index takes into account relative humidity and air temperature. Explanations of the insignificance of the angstrom index in linear regression

modeling follow the same reasons that impact the two independent variables composing it. Furthermore, it is likely that the flawed ΔFRP calculation also contributes to the weak relationship.

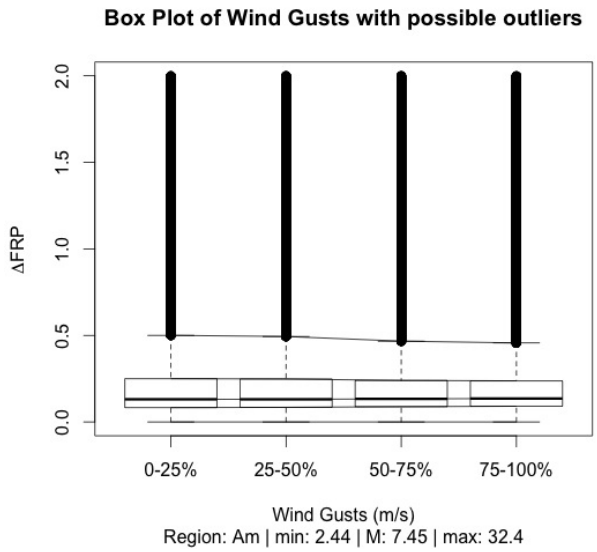

Figure 18: The box plot of ΔFRP and wind for the Am region (Equatorial:Fully Humid), where the Mann-Whitney U tests confirmed a statistically significant positive trend.

Ecosystem Impacts

Each zone was selected to represent a significantly different ecosystem where wildfire was present. Differentiating between these zones allowed for more specific models to be developed for each area and, consequently, a better understanding of the differences could be gained from the BIC selections. As expected, there were substantial differences between all three zones. The equatorial and snow zones both produced regions with sufficient trends for modeling. The warm temperate zone did not have any regions appropriate for modeling and generally exhibited relationships that were neither statistically significant nor logical. As a result, three parameters were evaluated in an effort to explain the differences among the zones; meteorological variables, ecosystem structure, and anthropogenic influences.

Before evaluating the different meteorological variables that were selected with BIC for linear regression modeling, an understanding of the seasonal occurrence of FRP events aids in the differentiation between zones. (Figure 19) From 2003 through 2007, the equatorial zone had the most cases of FRP activity among all three zones. Spatially, the equatorial zone covers the most area too. FRP events in the equatorial zone remain consistent throughout the year showing at least 1000 events per day, with peaks occurring in the late summer. The snow zone is second to the equatorial zone in both number of FRP events and the size of the zone. However, the snow zone exhibits the most seasonal behavior. There are almost no FRP events in the winter months, followed by substantial FRP events throughout the spring and late summer. For the warm temperate zone, FRP events occurring throughout the year and there is a substantial increase during the summer months. Of the three zones, warm temperate covers the smallest area and subsequently has the lowest amount of FRP events.

The BIC selection for the equatorial zone determined relative humidity, FRP_0 and CP_0 as the three primary variables necessary for linear regression modeling. In the case of the snow zone, large scale

precipitation, dew point temperature, and FRP_0 were selected. Although the warm temperate zone did not pass the Mann-Whitney U tests selection, BIC was still performed for purposes of comparison. Large scale precipitation, FRP_0, and dew point temperature were selected for linear regression modeling in the warm temperate zone. The meteorological variables fell into the same categories for all three zones. Each contained FRP_0, common among all BIC selections. Immediate precipitation events were also reflected in the BIC selection along with secondary moisture variables. There was no distinct variation in BIC variable selection among the zones, further highlighting the significance of these variable in fire modeling.

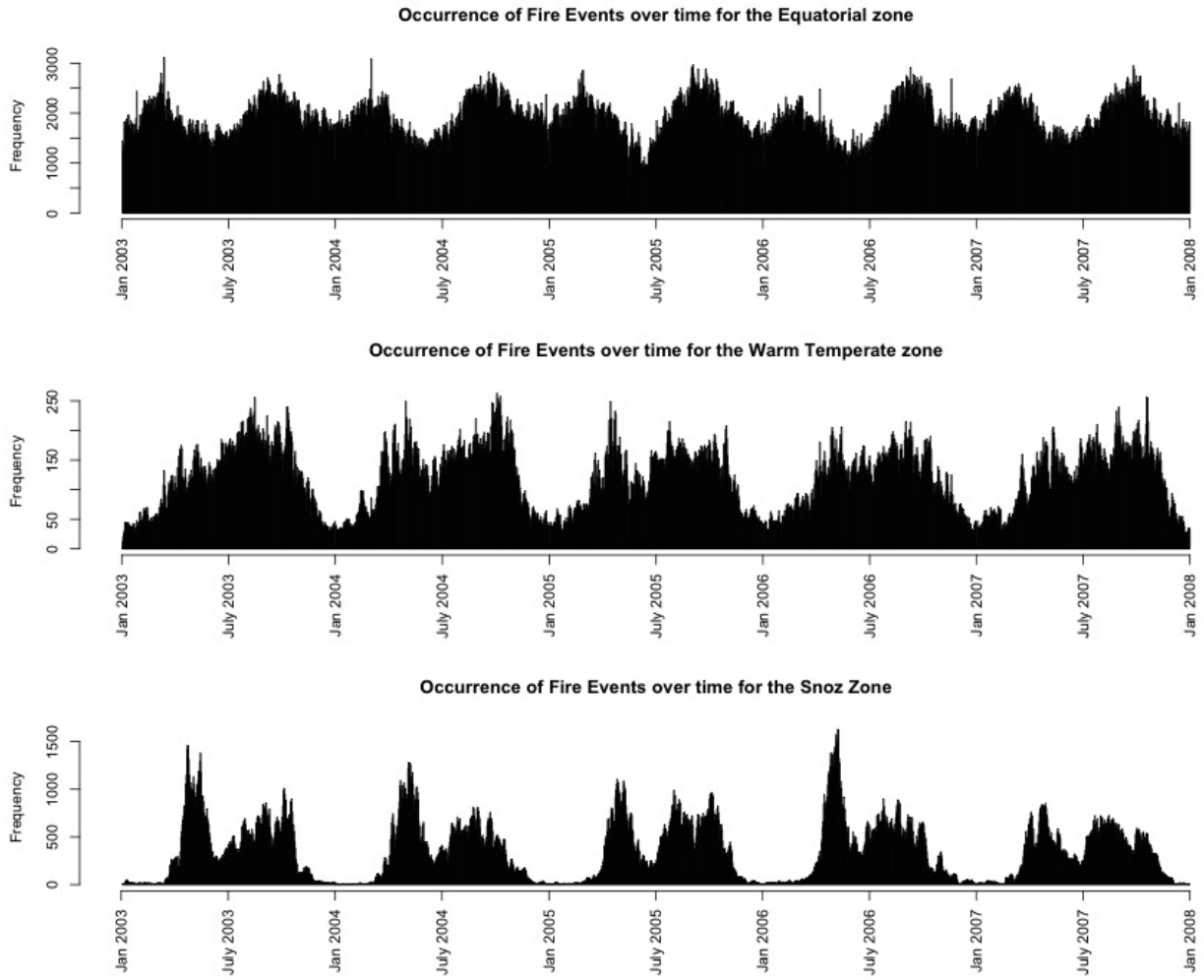

Figure 19: The seasonal occurrence of FRP events from 2003 to 2008 for the three zones considered in the analysis.

The ecosystem structure varied across each zone, which can explain some of the varied behavior observed. The snow zone is composed primarily of boreal forests. These ecosystems tend to have a substantial fuel load from downed trees and lack of disturbance (Peterson et al. 2013). The seasonality of FRP events suggests a limited influence of anthropogenic ignitions and stronger reliance on natural ignition and favorable fire conditions. The snow zone is a homogeneous ecosystem, all contained in the Northern hemisphere. The homogeneity allows for large meteorological trends to effect the wildfire likelihood across significant portions of the zone. Like the snow zone, larger meteorological events affect wildfire likelihood in the equatorial zone. The equatorial zone is mostly homogeneous in its ecosystem structure. The two primary ecosystems covered in the equatorial zone are rainforests and savannahs. Savannahs are ecosystems where

wildfire is inherent to the maintenance of the ecosystem structure. There are undoubted anthropogenic influences as these are accessible farmlands. But these two primary ecosystems are vastly different in regards to fuel load and vegetation structure. Unlike the boreal forests, rainforests are subject to more fragmentation. Slash and burn practices are used to clear much of the land for anthropogenic uses. The influence of anthropogenic uses is more prevalent in the equatorial zone because of it's proximity to population centers. While anthropogenic influences are common in the equatorial zones, and to a lesser extent the snow zone, the vast size of these two zones lessen the impact of anthropogenic use and disruption.

Unlike the snow and equatorial zone, the warm temperate zone exhibits more heterogeneity in the ecosystem structure. Throughout the analysis, the warm temperate zone and corresponding regions (Csa, Csb, & Csc) exhibited poor performance in the Mann-Whitney U tests. This was also the smallest zone, both in FRP events and in area. Due to smaller sample sizes, the sources of heterogeneity among the regions can have a greater impact on the results. The warm temperate zone was selected to represent Mediterranean ecosystems which, in addition to the Mediterranean Basin, are found in central Chile, California, south west Australia, and western South Africa. This heavily populated, subtropical ecosystem is the only zone considered with non-contiguous locations in the Northern and Southern hemisphere.

Naturally occurring fires are an active part of the ecosystem due to the dry summers that characterize the regions but there are diverse responses to wildfires across this ecosystem (Lucas, Hennessy, Mills, & Bathols, 2007). In the paper by Montenegro et al. (2004) they highlight three factors differentiating the five Mediterranean climates: natural ignition sources, anthropogenic influences and successional regeneration schemes. According to the paper, there is no indication of wildfire ignition by lightning in Chile, while this is a common ignition sources for the other Mediterranean ecosystems. The ignition of wildfire events in Chile are all anthropogenic. The lack of natural wildfire ignition has inhibited the establishment of fire-dependent flora in Chile. As a result, post-fire regeneration occurs on a slower time scale than in other Mediterranean ecosystems altering the fuel load and ignition likelihood. This created a significant variation in biomass and potential fuel loads across the Mediterranean ecosystems. Anthropogenic ignition is found across all five areas. The anthropogenic influence is also seen in landscape fragmentation due to agriculture, grazing, and wood gathering for charcoal. More effective fire suppression is found due to increased population growth and development, further altering fuel loads.

Anthropogenic influences are factors in all zones. However, the remoteness of the snow zone and the vastness of the equatorial zone limit the impact of anthropogenic disturbances across the ecosystems. In effect, the influence of anthropogenic habits on wildfire persistence (ΔFRP) is not as noticeable for these two zones. The size and location of the warm temperate zone suggest the strongest influence of anthropogenic habits on ΔFRP. Whether it's wildfire ignition or effective wildfire sequestration, anthropogenic influence in the warm temperate zone can explain the poor relationships observed between meteorological variables and ΔFRP.

Impacts of the Köppen-Geiger Climate Classification

The Köppen-Geiger climate classification is based on the climatological observations of precipitation and temperature, rather than what is actually on the ground, representing an atmospheric approach to classification. However, temperature and precipitation are only two components that dictate the expected fuel loads of ecosystems. The dependence on temperature and precipitation observations to determine the Köppen-Geiger climate classification can lead to potential discrepancies between predicted and actual land types. In light of these improvements,

discrepancies exist between predicted and actual ecosystems. There is a distinct possibility that the Köppen-Geiger classifications do not fully represent the actual ecosystems present at specific locations. This can misrepresent the behavior of fire and provide false signals in the data used for model development.

Consider for example the great plains of North America, occupying the center of the continent; this region is renowned for agricultural production. Not only is there a significant anthropogenic impact on the ecosystem, but the natural environment is not properly modeled by Köppen-Geiger. Similarly this can be seen in the Boreal forests of Canada, that in reality only enter the United States near the northernmost Great Lake (Lake Superior), however the Köppen-Geiger classification shows boreal forest reaching as far south as Chicago, IL on Lake Michigan. Along these lines, the impact of human activities on ecosystem type have not been accommodated in the Köppen-Geiger classification, while this is not specified goal of the classification, the impact of humans and their ability to change ecosystem type through fire suppression, agricultural and industrial motivations can further the discrepancy between the predicted classifications and actual ecosystems.

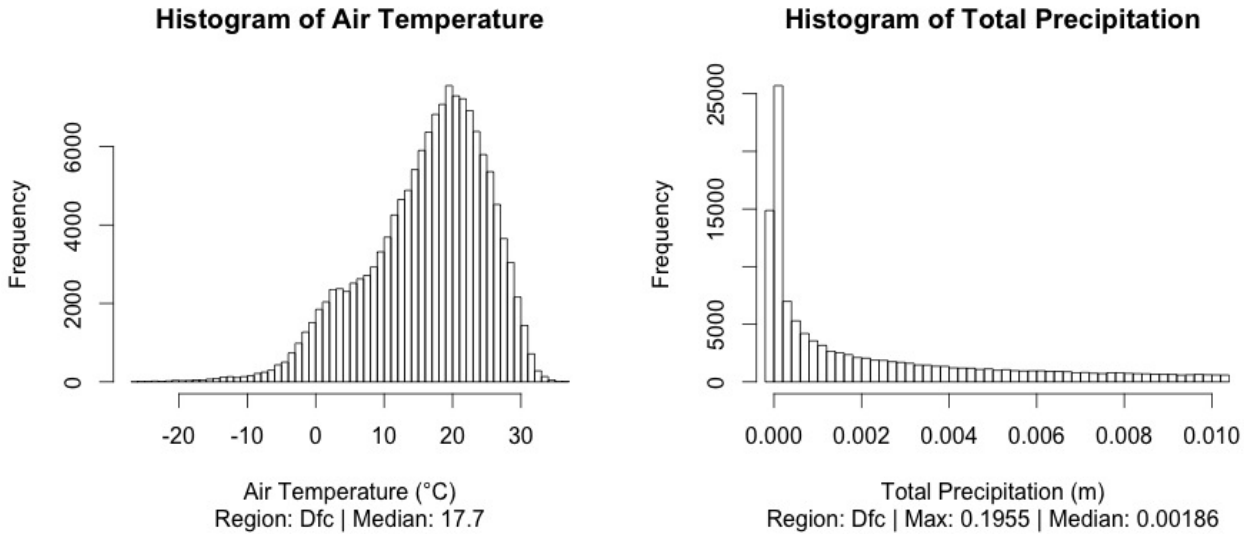

Figure 20: Histograms of two independent variables (air temperature & total precipitation) for the Dfc region (Snow:Fully Humid:Cool Summer). The Median of each variable is included in the histograms.

Cross-examining the histograms of precipitation and air temperature (Figure 20) for the Dfc region (Snow:Fully Humid:Cool Summer) with the corresponding Köppen-Geiger criteria, detailed in Table 3, small discrepancies can be seen. Data for these histograms represent meteorological variables during FRP events only, the behavior of precipitation and temperature for non-fire events in the Dfc region were not assessed. Still, the precipitation values fall inline with Köppen-Geiger criteria. The histogram for precipitation shows the majority of daily values measure less 2 mm per day. Furthermore, the majority of fire events occur in the summer months (Figure 21) for the Dfc region, furthering the possibility of fulfilling the precipitation criteria.

The temperature histogram for the Dfc region exhibits some discrepancies with the corresponding Köppen-Geiger criteria. The temperature values for the Dfc region satisfy the first criterium of Tmin ≤ -3 ºC. However, there are many values greater than 22 ºC which violate the criteria for both the Dfc and Dfb regions and suggest a climate classification more akin to the Dfa region (Kottek et al., 2006).

In addition to the potential discrepancies between predicted and actual ecosystems, the selection of

climate regions may have precluded the opportunity for successful modeling. The motivation for selection of the nine regions was based on finding significantly different ecosystems where fire would be expected. While it is my opinion that the inclusion of the boreal region, equatorial, and warm temperate zones provided a significant and distinct scale over which to develop and evaluate a model, there is a possibility that other regions could have performed better. The addition of a steppe region or broadleaf forest region where fire played a significant land management role, could have possibly improved the performance of the model, or exhibited stronger relationships between the variables.

Simply stated, the use of actual, on the ground, land types rather than a climate based classification system, have the potential to show more significant relationships amongst the variables leading to a better model. However, working on a large global scale, finding a map detailing the actual land types is a significant challenge.

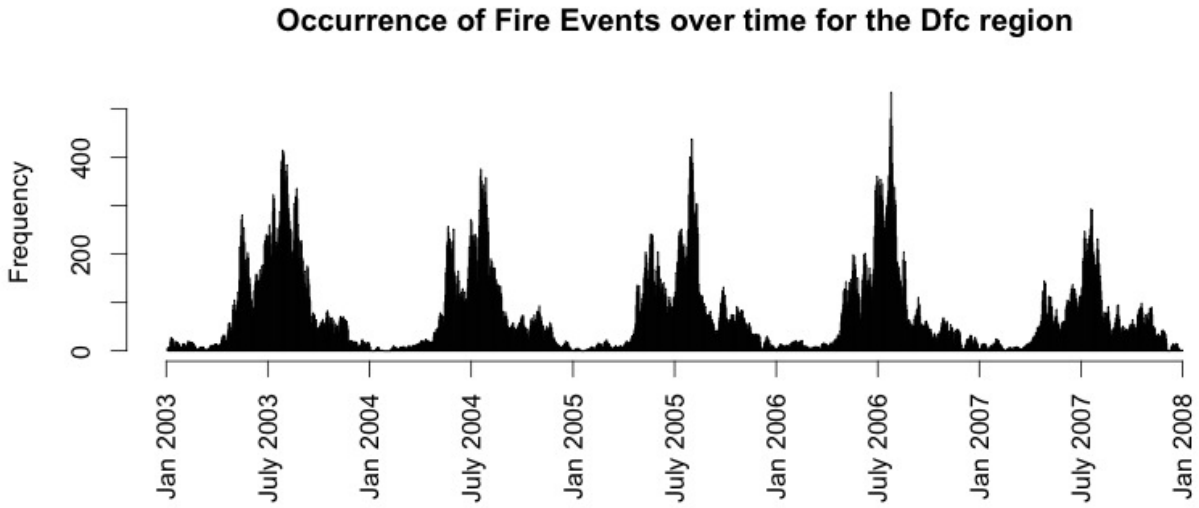

Figure 21: Graph showing the temporal trends of fire events in the Dfc region (Snow:Fully Humid:Cool Summer). Generated for the model development data, where each bar represents the number of grid cells with FRP measurements.

Conclusion

The result of this analysis and model development did not yield any linear model appropriate for predicting the behavior of FRP. It is clear from this work that modeling the evolution of wildfire is a complex and challenging undertaking. The impact of meteorological variables is undoubtedly a significant driver, but the inclusion of other parameters are necessary. Expected relationships were observed in the Mann-Whitney U tests however the majority of regions and zones were not suitable for modeling. This disproves the first hypothesis, and highlights some issues with the methodology. The Bayesian Information Criteria applied to the eligible regions and zones showed a preference to FRP_0 and moisture variables which confirms the second hypothesis. For the zones, theses two variable types were predominant, while regions showed similar preferences that also included air temperature and angstrom index. The prevalence of FRP_0 and moisture variables was not a surprise, rather the absence of movement variables such as wind and air temperature was more surprising as these were expected to have a significant impact of wildfire behavior (Golding & Caesar, 2011). However, there was important information gained regarding the interrelationships between meteorological variables and their subsequent relationship to FRP.

The performance of different regions highlighted interesting behaviors. After the Mann-Whitney U

test selection, there were no remaining regions from the warm temperate ecosystem. Most of the regions were selected for the snow ecosystem, and all regions included for the equatorial ecosystem. This suggests the significance of the size of the dataset as the remaining regions were also the largest. The equally worse linear model generated during the analysis was for the Dfc region (Snow:Fully Humid:Cool Summer) in the snow zone with an R^2 value of 0.055.

It is clear that this approach to modeling is flawed. The prevalence of insignificant relationships is confusing. The physical processes and improperly gridded data are not to blame for this observation. Rather, analytical approaches are responsible for the insignificance observed. Namely, the ΔFRP calculation that disregards the magnitude of the fire events. The incorrect ΔFRP calculation used in the analysis accounts for a significant amount of the uncertainty surrounding the results of the model. Appropriately considering the magnitude of the decrease in FRP from one day to the next would ideally enable the meteorological variables to better explain the response. Using either the proposed ΔFRP calculation (Equation 4) or simple the difference in FRP could correct for the insignificant relationships observed.

Furthermore, the scale of the model is too large. Attempts to model the wildfire evolution on a global scale introduces too much noise and inhibits the effectiveness of BIC and linear regression modeling. This is primarily tied to ecosystem representation, to account for fuel load and ecosystem type. Working on smaller scales and using actual observations of landscape type would allow for more homogeneous ecosystems and more appropriate fuel loads.

Better results could be obtained if future researchers accounted for the magnitude of the change in FRP. Furthermore, by focusing on smaller areas, with on-the-ground records of ecosystem type, the model will presumably perform better. A better understanding and accommodation for the anthropogenic ignition and sequestration habits are poised improved the model and eliminate uncertainty. In summary, possible variables to incorporate into predictive models include: natural fire extinction (over night behavior), burned area calculations (Giglio, Loboda, Roy, Quayle, & Justice, 2009), ecosystem fuel loads (Coen et al., 2013), fire propagation models (Beezley & Chakraborty, 2008; Mandel et al., 2007), anthropogenic mitigation, drought indices, and topographic aspect. All of which are poised to increase the model performance.

In addition to the added variables that can improve the model and eliminate uncertainty, the development of indices and thresholds for meteorological values would be an appropriate focus for future research. Threshold behaviors were discussed earlier for FRP_0, dew point temperature, and relative humidity. Determining what exactly these are, and how they differ across ecosystems is important to understand before application. Furthermore, proper thresholds and indices would need to be determined from year round data for each ecosystem while the data used for this research only contained variables from the active fire events. This could be achieved through the comparison of time series for precipitation and temperature, similar to those seen for FRP in Figure 19. This can show to possibility of similar temporal patterns between the dependent and independent variables, or if a lagged relationship exists.

Assuming that an eventual model is developed to effectively predict FRP behavior, the logical next step would be to incorporate this information into existing weather models. One application would allow for the calculation of black carbon content and ozone particulates expected from the fire events. Secondly, accounting for the existing wind models, the potential impact on human health from smoke and particulates could provide a greater reaction time to urban areas. Understanding the evolution of fire events is a challenge; however, with a changing climate and increasing population, the benefits of predictive modeling are significant.

Bibliography

Akaike, H. (1974). A new look at the statistical model identification. Automatic Control, IEEE Transactions on, 19(6), 716-723.

Barker, T. (2007). Climate Change 2007 : An Assessment of the Intergovernmental Panel on Climate Change, (November), 12-17.

Beezley, J., & Chakraborty, S. (2008). Real-time data driven wildland fire modeling. … *Science–ICCS 2008*, 46-53. Retrieved from http://link.springer.com/chapter/10.1007/978-3-540-69389-5_7

Bowman, D., Balch, J., & Artaxo, P. (2009). Fire in the Earth system. *science*, *16*(April), 481-484. Retrieved from http://www.sciencemag.org/content/324/5926/481.short

Carmona, M, Armesto, J, Aravena, J, & Pérez, C 2002, 'Coarse woody debris biomass in successional and primary temperate forests in Chiloé Island, Chile', Forest Ecology & Management, 164, 1-3, p. 265, GreenFILE, EBSCOhost, viewed 14 August 2013.

Chandler, C., Cheney, P., Thomas, P., Traubard, L., and Williams, D. (1983), Fire in Forestry (Vol. 1: forest fire behavior and effects), Wiley-Interscience Publication.

Coen, J. L., Cameron, M., Michalakes, J., Patton, E. G., Riggan, P. J., & Yedinak, K. M. (2013). WRF-Fire: Coupled Weather–Wildland Fire Modeling with the Weather Research and Forecasting Model. *Journal of Applied Meteorology and Climatology*, *52*(1), 16-38. doi:10.1175/JAMC-D-12-023.1

Crozier, L., & Dwyer, G. (2006). Combining population‐dynamic and ecophysiological models to predict climate‐induced insect range shifts. The American Naturalist, 167(6), 853-866.

Csiszar, I. A., Arino, O., Geraci, R., Giglio, L., & Sessa, R. (2009). Fire: Fire Disturbance. Terrestrial Essential Climate Variables, 13.

Dunn, O. J. (1961). Multiple comparisons among means. Journal of the American Statistical Association, 56(293), 52-64.

Easterling, W., Aggarwal, P., & Batima, P. (2007). –Food, Fibre, and Forest Products 3, 273-313. Retrieved from http://ipcc-wg2.gov/AR4/SOD/Ch05.pdf

European Centre for Medium-Range Weather Forecasts, 2012. IFS Documentation - Cy37r2 [online] Available at: <http://www.ecmwf.int/research/ifsdocs/CY37r2/>

Flannigan, M. D., Logan, K. A., Amiro, B. D., Skinner, W. R., & Stocks, B. J. (2005). Future area burned in Canada. Climatic change, 72(1-2), 1-16.

Freeborn, P. H., Wooster, M. J., & Roberts, G. (2011). Addressing the spatiotemporal sampling design of MODIS to provide estimates of the fire radiative energy emitted from Africa. *Remote Sensing of Environment*, *115*(2), 475-489. doi:10.1016/j.rse.2010.09.017

Giglio, L. (2010). MODIS collection 5 active fire product user's guide version 2.4. *University of Maryland: College Park, MD*, (February). Retrieved from http://198.118.255.205/sites/default/files/field/document/MODIS_Fire_users_Guide_2.4.pdf

Giglio, L., Loboda, T., Roy, D. P., Quayle, B., & Justice, C. O. (2009). An active-fire based burned area mapping algorithm for the MODIS sensor. *Remote Sensing of Environment*, *113*(2), 408-420. doi:10.1016/j.rse.2008.10.006

Giglio, L., Descloitres, J., Justice, C.O., Kaufman, Y. 2003. An enhanced contextual fire detection algorithm for MODIS. Remote Sensing of Environment, 87:273-282.

Golding, N., & Caesar, J. (2011). *Meteorological factors influencing forest fire risk under climate change mitigation*. Met Office Hadley Centre (p. 30).

Gonzalez, M, Veblen, T, & Sibold, J n.d., 'Influence of fire severity on stand development of Araucaria araucana-Nothofagus pumilio stands in the Andean cordillera of south-central Chile', Austral Ecology, 35, 6, pp. 597-615, Science Citation Index, EBSCOhost, viewed 14 August 2013.

Ichoku, C., & Kaufman, Y. (2005). A method to derive smoke emission rates from MODIS fire radiative energy measurements. *Geoscience and Remote Sensing, ...*, *43*(11), 2636-2649. Retrieved from http://ieeexplore.ieee.org/xpls/abs_all.jsp?arnumber=1522624

Justice, C. O., Giglio, L., Korontzi, S., Owens, J., Morisette, J. T., Roy, D., ... & Kaufman, Y. (2002). The MODIS fire products. Remote Sensing of Environment, 83(1), 244-262.

Kaiser, J., Suttie, M., & Flemming, J. (2009). Global real‐time fire emission estimates based on space‐borne fire radiative power observations. *AIP conference ...*, (Irs 2008), 25-28. Retrieved from http://link.aip.org/link/?APCPCS/1100/645/1

Kaiser, J. W., Heil, a., Andreae, M. O., Benedetti, a., Chubarova, N., Jones, L., Morcrette, J.-J., et al. (2012). Biomass burning emissions estimated with a global fire assimilation system based on observed fire radiative power. *Biogeosciences*, *9*(1), 527-554. doi:10.5194/bg-9-527-2012

Kinney, P. L. (2008). Climate change, air quality, and human health. *American journal of preventive medicine*, *35*(5), 459-67. doi:10.1016/j.amepre.2008.08.025

Konovalov, I. B., Beekmann, M., Kuznetsova, I. N., Yurova, a., & Zvyagintsev, a. M. (2011). Atmospheric impacts of the 2010 Russian wildfires: integrating modelling and measurements of the extreme air pollution episode in the Moscow megacity region. *Atmospheric Chemistry and Physics Discussions*, *11*(4), 12141-12205. doi:10.5194/acpd-11-12141-2011

Kottek, M., Grieser, J., Beck, C., Rudolf, B., & Rubel, F. (2006). World Map of the Köppen-Geiger climate classification updated. *Meteorologische Zeitschrift*, *15*(3), 259-263. doi:10.1127/0941-2948/2006/0130

Lawrence, M. G. (2005). The Relationship between Relative Humidity and the Dewpoint Temperature in Moist Air: A Simple Conversion and Applications. *Bulletin of the American Meteorological Society*, *86*(2), 225-233. doi:10.1175/BAMS-86-2-225

Lehsten, V., Harmand, P., Palumbo, I., & Arneth, a. (2010). Modelling burned area in Africa. *Biogeosciences*, *7*(10), 3199-3214. doi:10.5194/bg-7-3199-2010

Lucas, C., Hennessy, K., Mills, G., & Bathols, J. (2007). Bushfire Weather in Southeast Australia : Recent Trends and Projected Climate Change Impacts Bushfire CRC and Australian Bureau of Meteorology * CSIRO Marine and Atmospheric Research September 2007 Consultancy Report prepared for The Climate Institute of, (September).

Mandel, J., Beezley, J. D., Bennethum, L. S., Chakraborty, S., Coen, J. L., Douglas, C. C., Hatcher, J., et al. (2007). *A dynamic data driven wildland fire model* (Vol. 2007, pp. 1042-1049). Retrieved from http://link.springer.com/chapter/10.1007/978-3-540-72584-8_137

Mann, H. B., & Whitney, D. R. (1947). On a test of whether one of two random variables is stochastically larger than the other. The annals of mathematical statistics, 18(1), 50-60.

Mills, G. (2009). Meteorological drivers of extreme bushfire events in southern Australia, (January 1997). Retrieved from http://www.cawcr.gov.au/events/modelling_workshops/workshop_2009/presentations/MILLS_1Dec.pdf

Montenegro, G. L. O. R. I. A., Ginocchio, R. O. S. A. N. N. A., Segura, A. L. E. J. A. N. D. R. O., Keely, J. E., & Gómez, M. (2004). Fire regimes and vegetation responses in two Mediterranean-climate regions. Revista chilena de historia natural, 77(3), 455-464.

Mölders, N. (2008). Suitability of the Weather Research and Forecasting (WRF) model to predict the June 2005 fire weather for Interior Alaska. Weather and Forecasting, 23(5), 953-973.

Peterson, D., Hyer, E., & Wang, J. (2013). A short-term predictor of satellite-observed fire activity in the North American boreal forest: Toward improving the prediction of smoke emissions. Atmospheric Environment.

Ramanathan, V., & Carmichael, G. (2008). Global and regional climate changes due to black carbon. *Nature geoscience*, 221-227. Retrieved from http://www.nature.com/ngeo/journal/vaop/ncurrent/full/ngeo156.html

Rubel, F., & Kottek, M. (2010). Observed and projected climate shifts 1901–2100 depicted by world maps of the Köppen-Geiger climate classification. *Meteorologische Zeitschrift*, *19*(2), 135-141. doi:10.1127/0941-2948/2010/0430

Schlegel, B, & Donoso, P n.d., 'Effects of forest type and stand structure on coarse woody debris in old-growth rainforests in the Valdivian Andes, south-central Chile', Forest Ecology And Management, 255, 5-6, pp. 1906-1914, Science Citation Index, EBSCOhost, viewed 14 August 2013.

Schwarz, G. (1978). Estimating the dimension of a model. The annals of statistics, 6(2), 461-464.

Stambaugh, Michael C., et al. "Spatial patterning of fuels and fire hazard across a central US deciduous forest region." Landscape ecology 26.7 (2011): 923-935.

Vermote, E., Ellicott, E., Dubovik, O., Lapyonok, T., Chin, M., Giglio, L., & Roberts, G. J. (2009). An approach to estimate global biomass burning emissions of organic and black carbon from MODIS fire radiative power. *Journal of Geophysical Research*, *114*(D18), 1-22. doi:10.1029/2008JD011188

Werf, G. R. V. D., Randerson, J. T., Collatz, G. J., Giglio, L., Kasibhatla, P. S., Jr, A. F. A., Olsen, S. C., et al. (2004). Continental-scale partitioning of fire emissions during the 1997 to 2001 El Niño/La Niña period. *Science (New York, N.Y.)*, *303*(5654), 73-6. doi:10.1126/science.1090753

Westerling, A. L., Hidalgo, H. G., Cayan, D. R., & Swetnam, T. W. (2006). Western. *Science (New York, N.Y.)*, *313*.

Wooster, M. J., Roberts, G., Perry, G. L. W., & Kaufman, Y. J. (2005). Retrieval of biomass combustion rates and totals from fire radiative power observations: FRP derivation and calibration relationships between biomass consumption and fire radiative energy release. *Journal of Geophysical Research*, *110*(D24), 1-24. doi:10.1029/2005JD006318

Appendix 1: Köppen-Geiger Climate Map

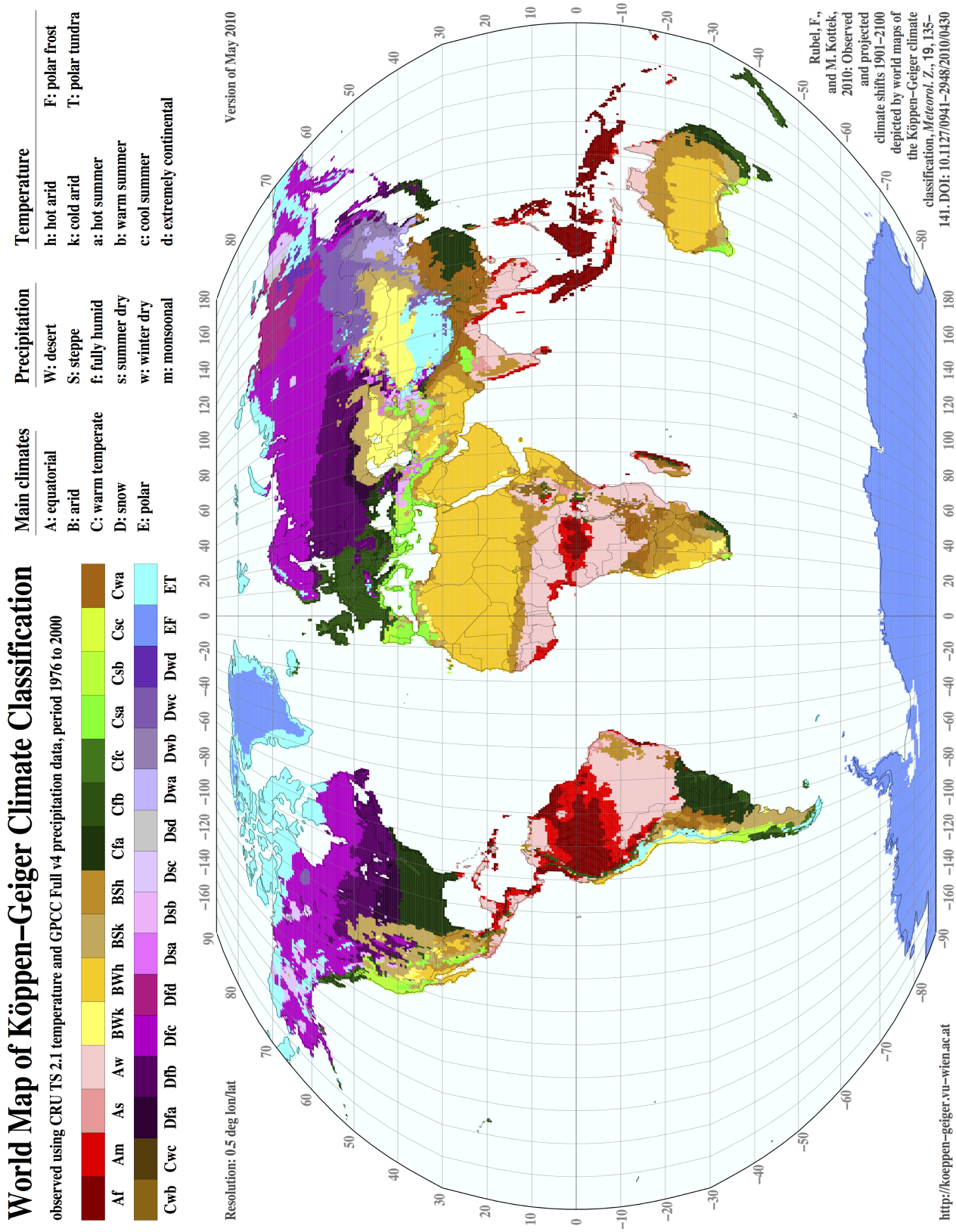

Figure 22: Global Map of the Köppen-Geiger Climate Classifications for 1976-2000 with a resolution of 0.5° lat/lon. 9 regions were selected for the analysis. Af, Am & Aw (red gradients) occur along the equator and include tropical forests. Csa, Csb & Csc (light green gradient) occur in both the Northern and Southern hemispheres, typically along the western coasts and Mediterranean Sea. Dfa, Dfb & Dfc (purple gradient) occur in the Northern hemisphere and include boreal forests. (Kottek et al. 2010; [online] http://koeppen-geiger.vu-wein.ac.at)

Appendix 2: Mapped Variables

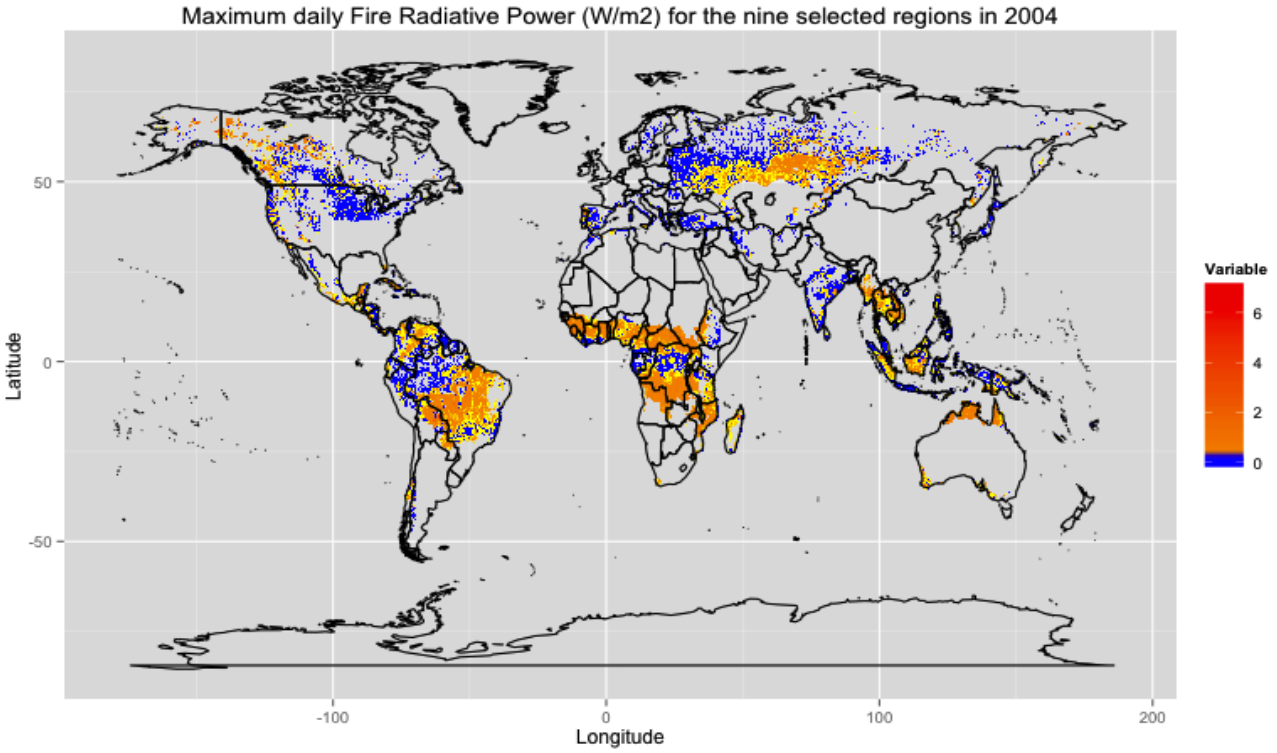

Figure 23: Map of maximum daily FRP values for the year 2004. Maximum daily FRP value 7.169 W/m^2. Resolution of the map is 0.5° lat/lon.

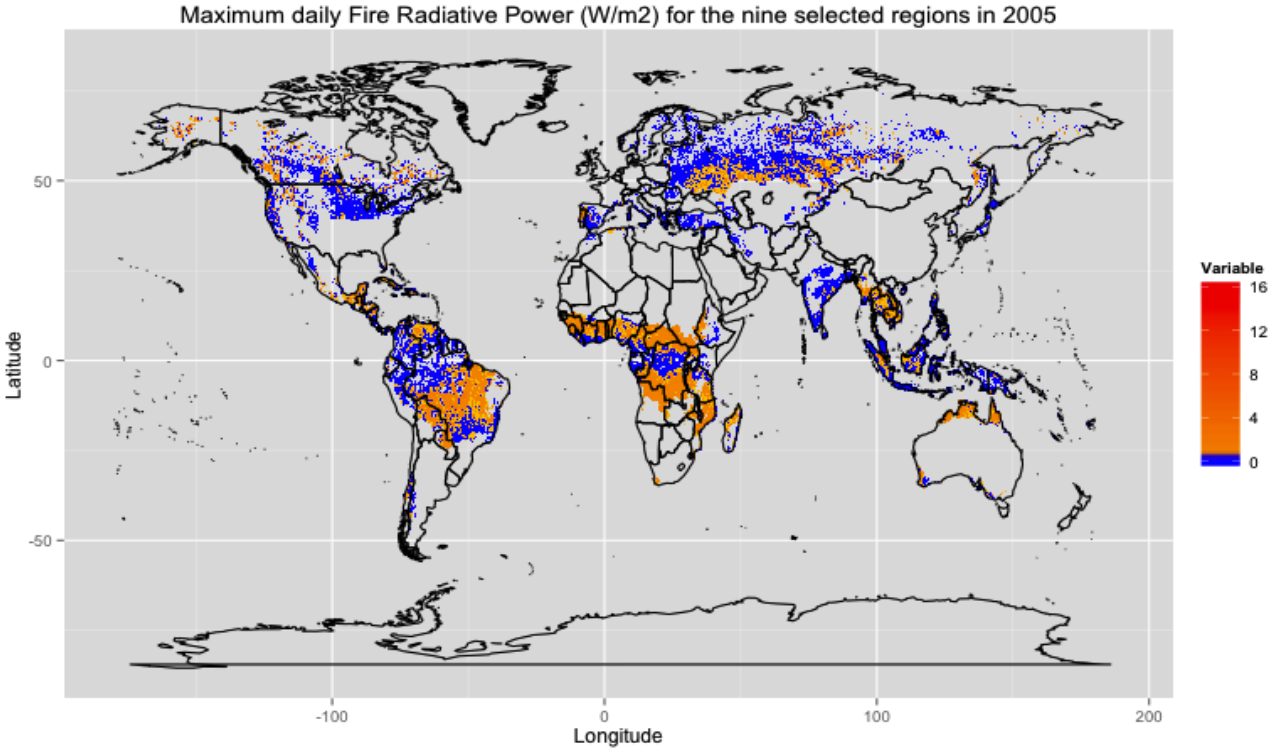

Figure 24: Map of maximum daily FRP values for the year 2005. Maximum daily FRP value is 16.76 W/m^2. Resolution of the map is 0.5° lat/lon.

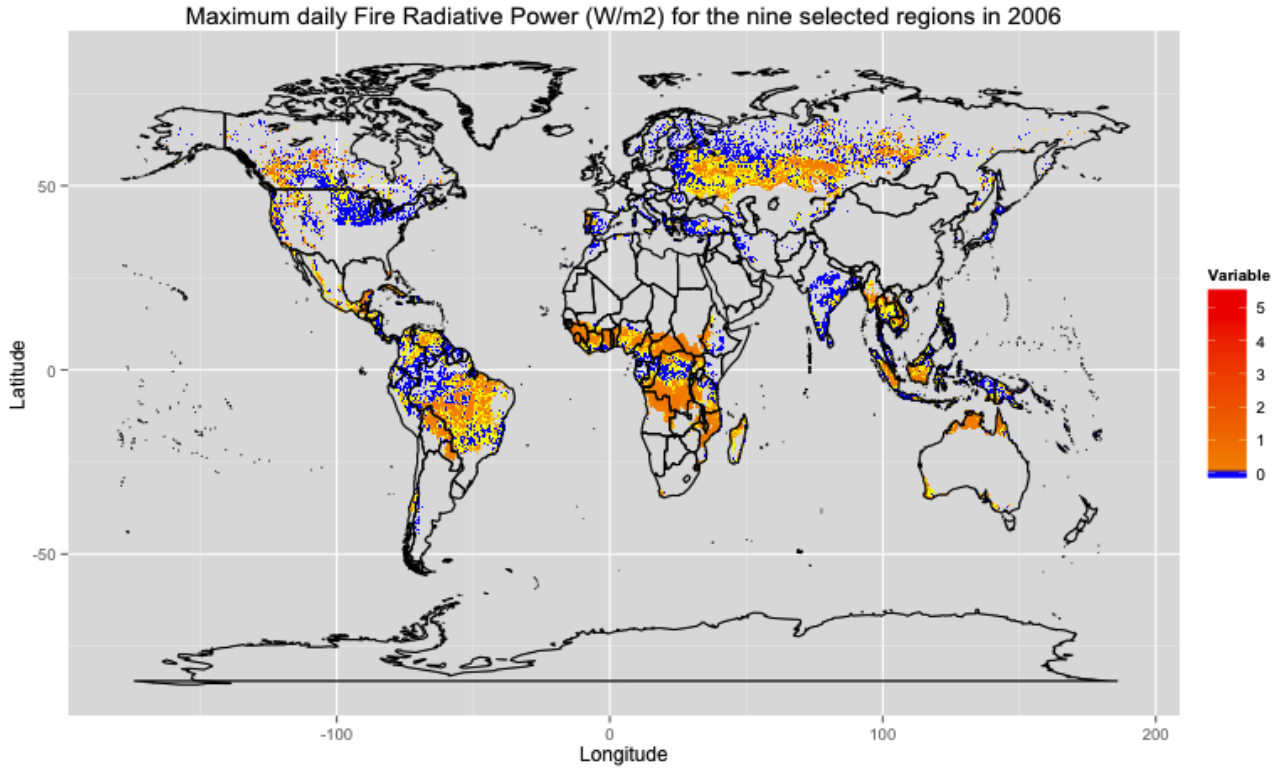

Figure 25: Map of maximum daily FRP values for the year 2006. Maximum daily FRP value is 5.54 W/m^2. Resolution of the map is 0.5° lat/lon.

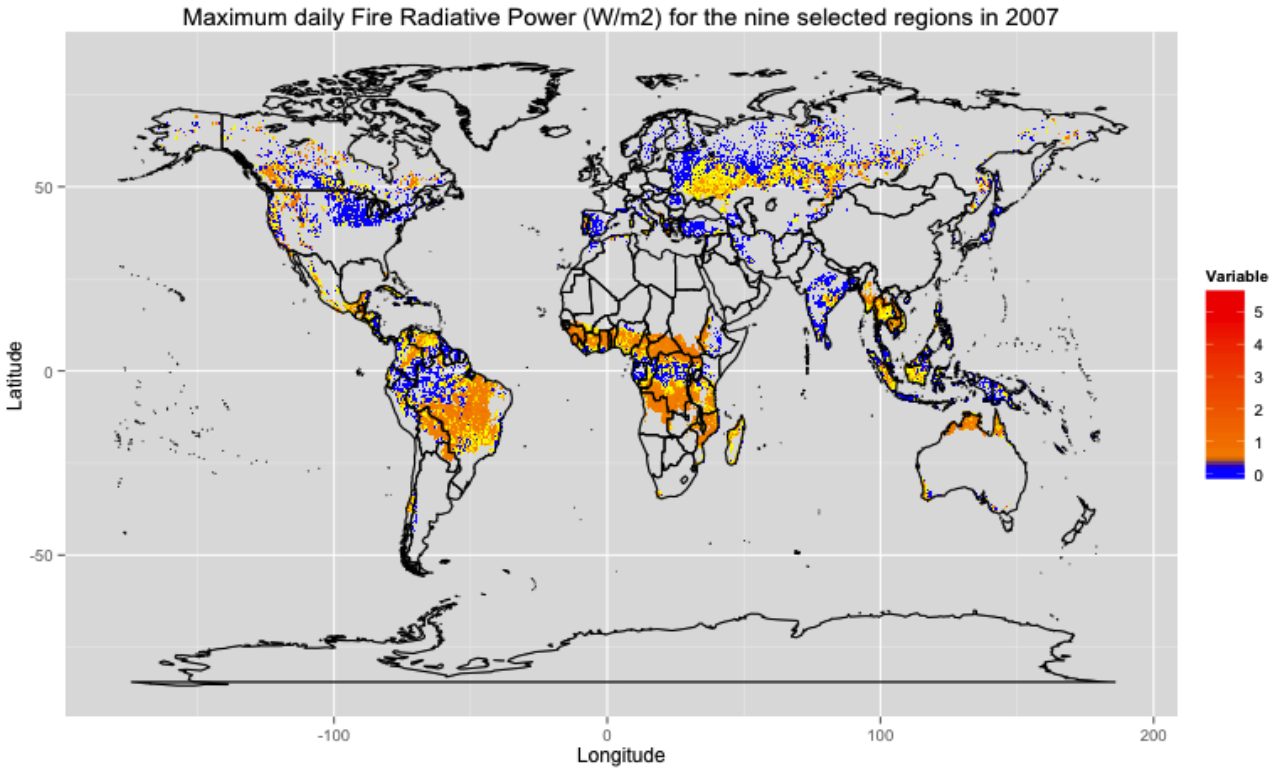

Figure 26: Map of maximum daily FRP values for the year 2007. Maximum daily FRP value is 5.644 W/m^2. Resolution of the map is 0.5° lat/lon.

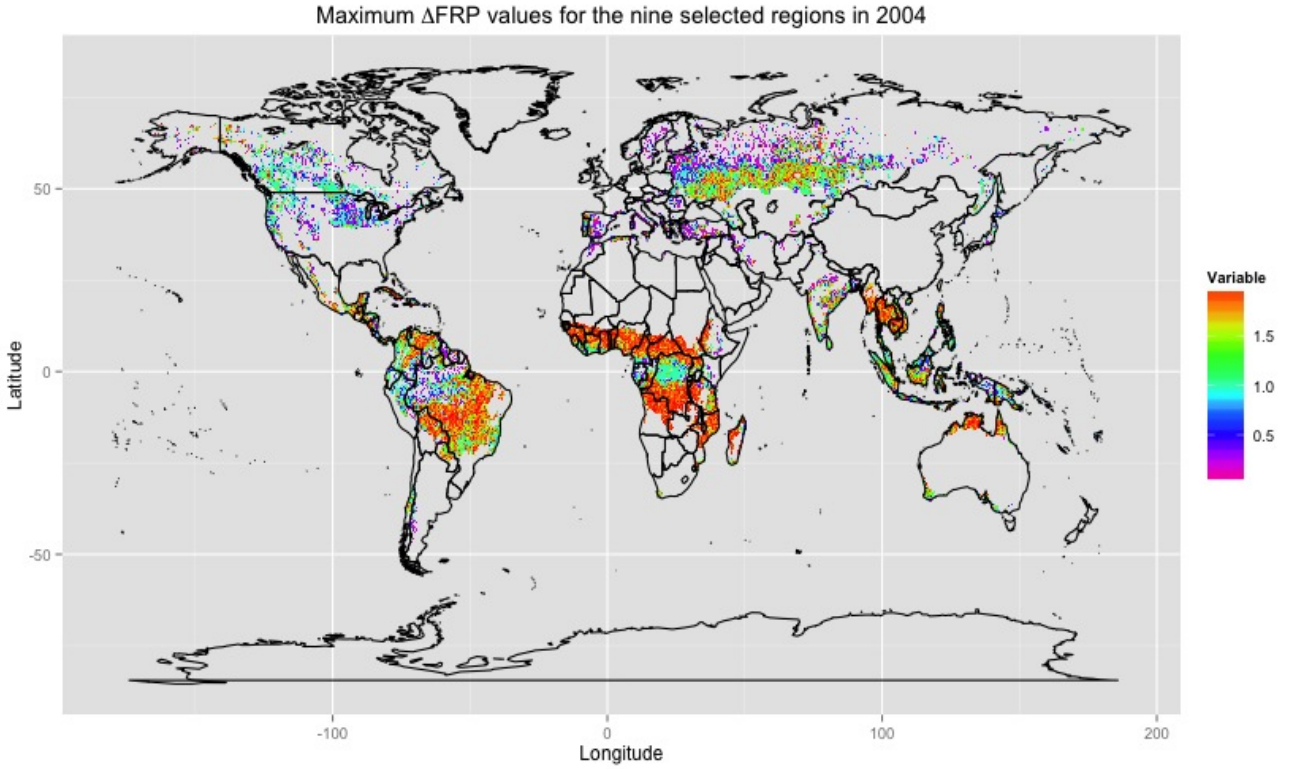

Figure 27: Map of maximum daily ΔFRP values for the year 2004. Maximum daily ΔFRP values occur around the Equator. Resolution of the map is 0.5° lat/lon.

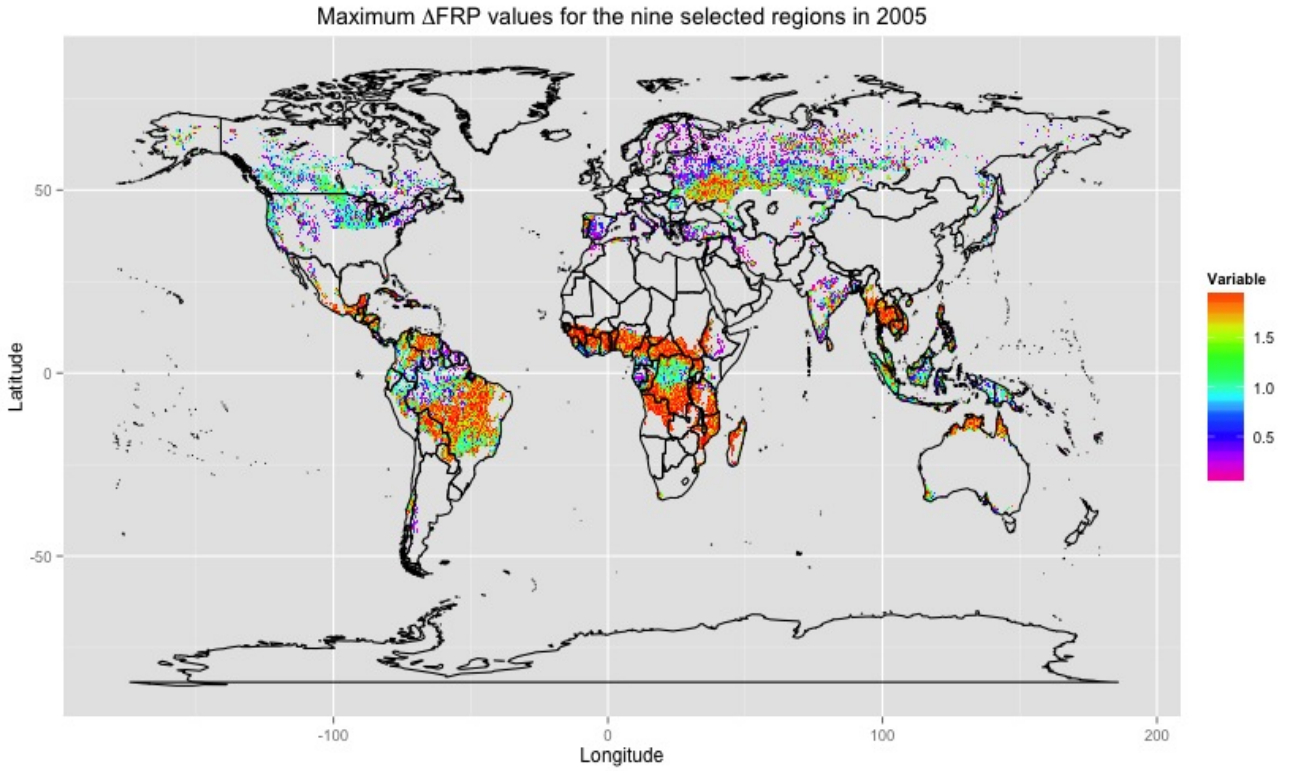

Figure 28: Map of maximum daily ΔFRP values for the year 2005. Maximum daily ΔFRP values occur around the Equator. Resolution of the map is 0.5° lat/lon.

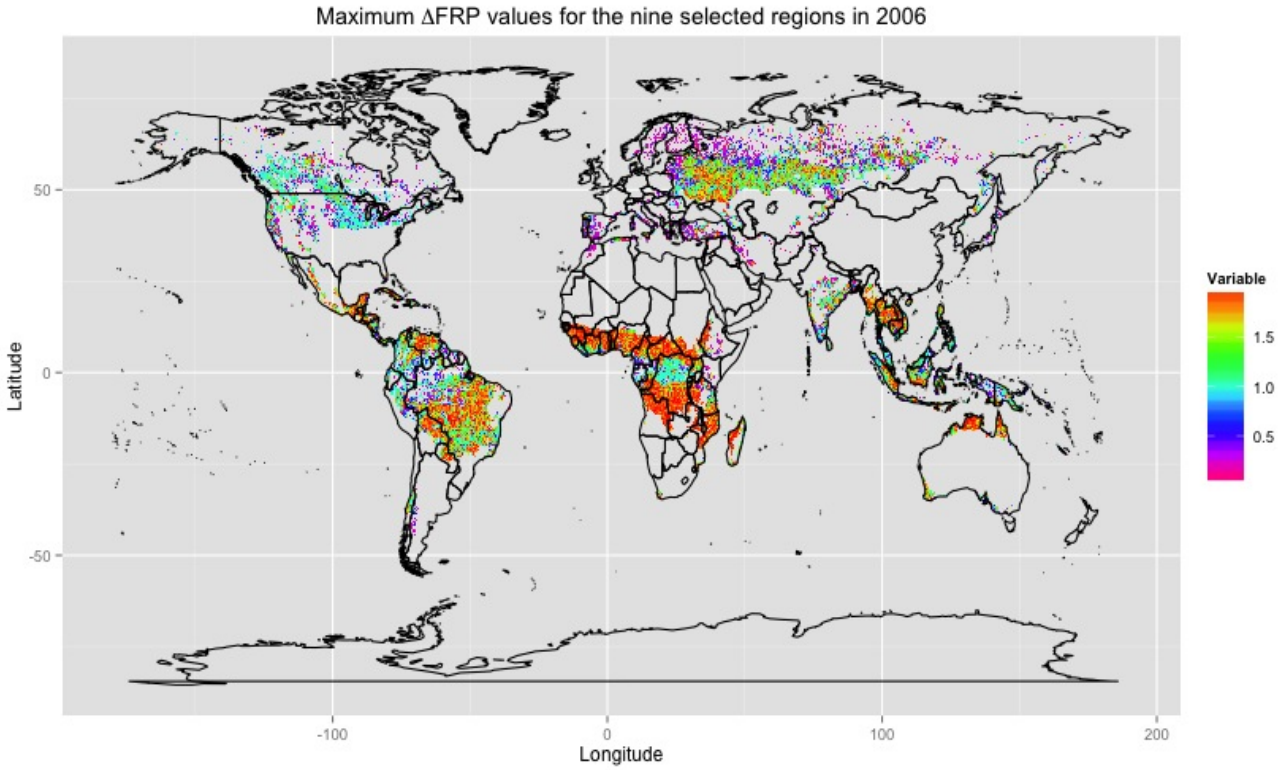

Figure 29: Map of maximum daily ΔFRP values for the year 2006. Maximum daily ΔFRP values occur around the Equator. Resolution of the map is 0.5° lat/lon.

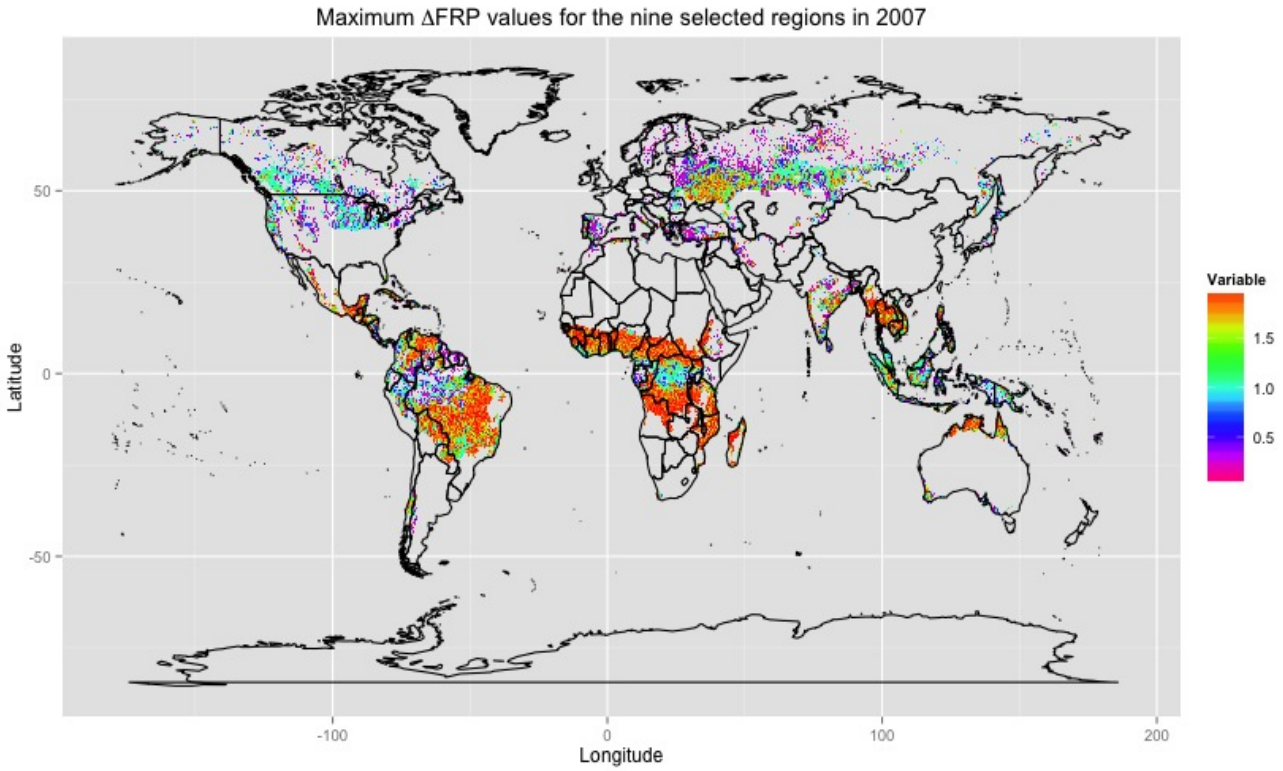

Figure 30: Map of maximum daily ΔFRP values for the year 2007. Maximum daily ΔFRP values occur around the Equator. Resolution of the map is 0.5° lat/lon.

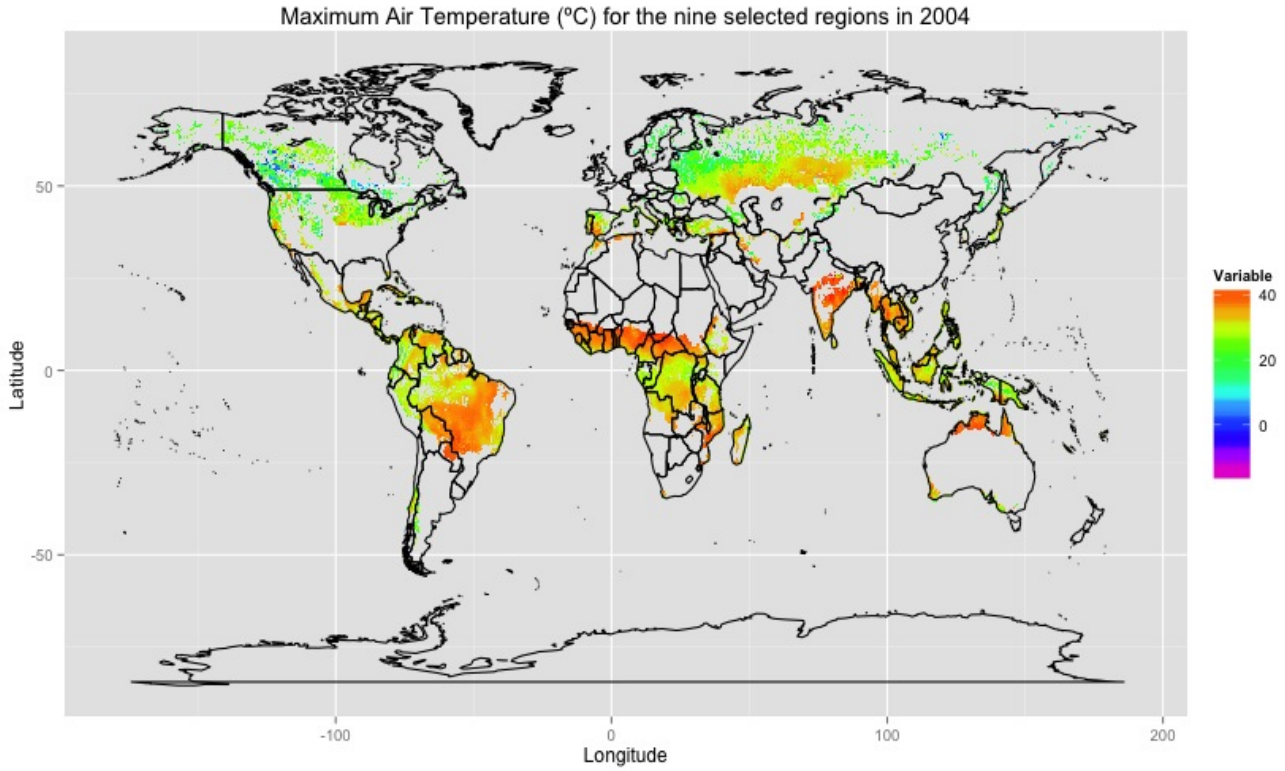

Figure 31: Map of maximum daily Air Temperature values for the year 2004. Maximum daily Air Temperature is 44.35 ºC. Resolution of the map is 0.5º lat/lon.

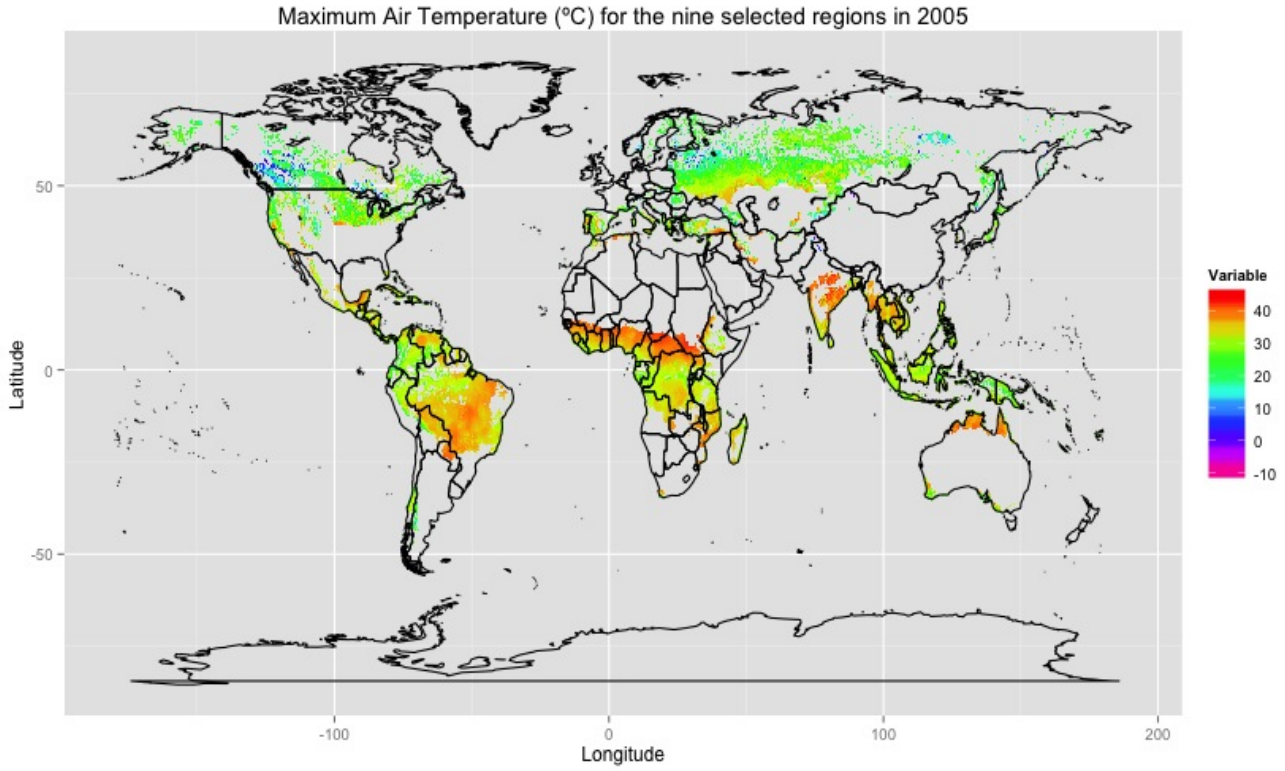

Figure 32: Map of maximum daily Air Temperature values for the year 2005. Maximum daily Air Temperature is 45.15 ºC. Resolution of the map is 0.5º lat/lon.

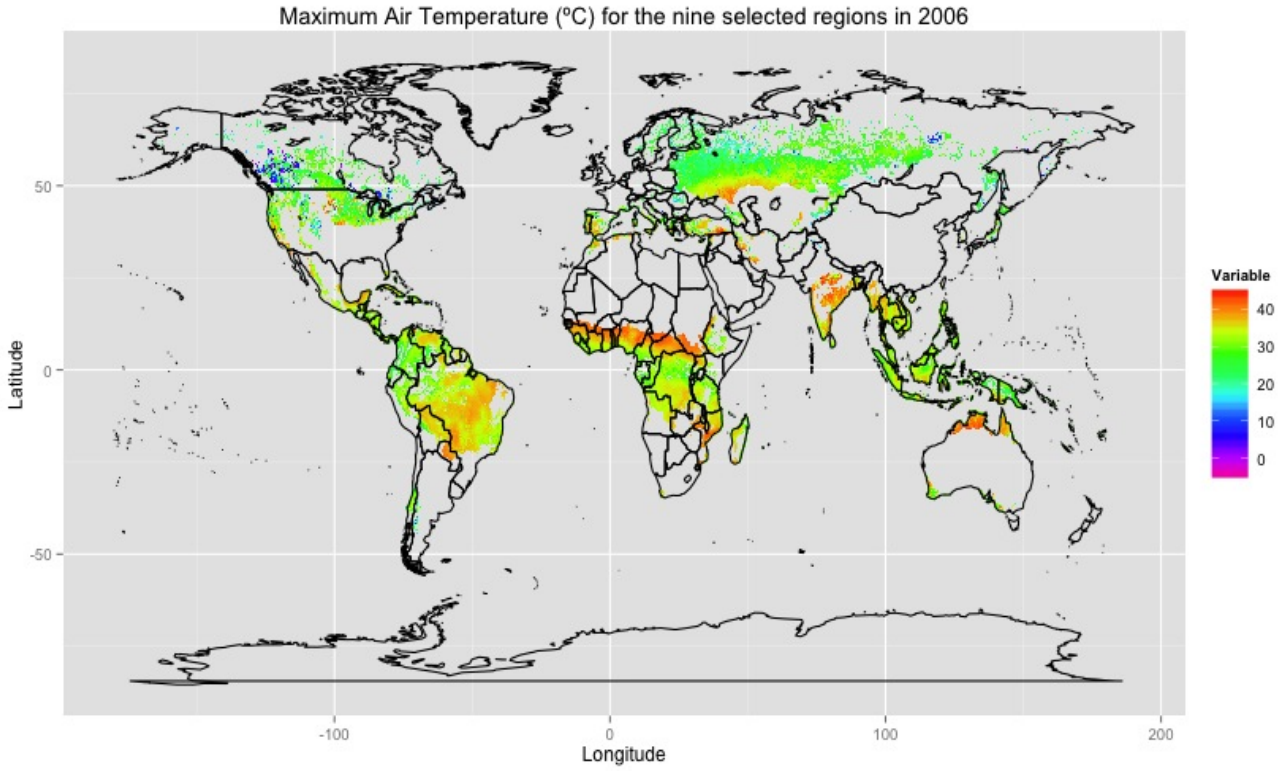

Figure 33: Map of maximum daily Air Temperature values for the year 2006. Maximum daily Air Temperature is 44.05 ºC. Resolution of the map is 0.5º lat/lon.

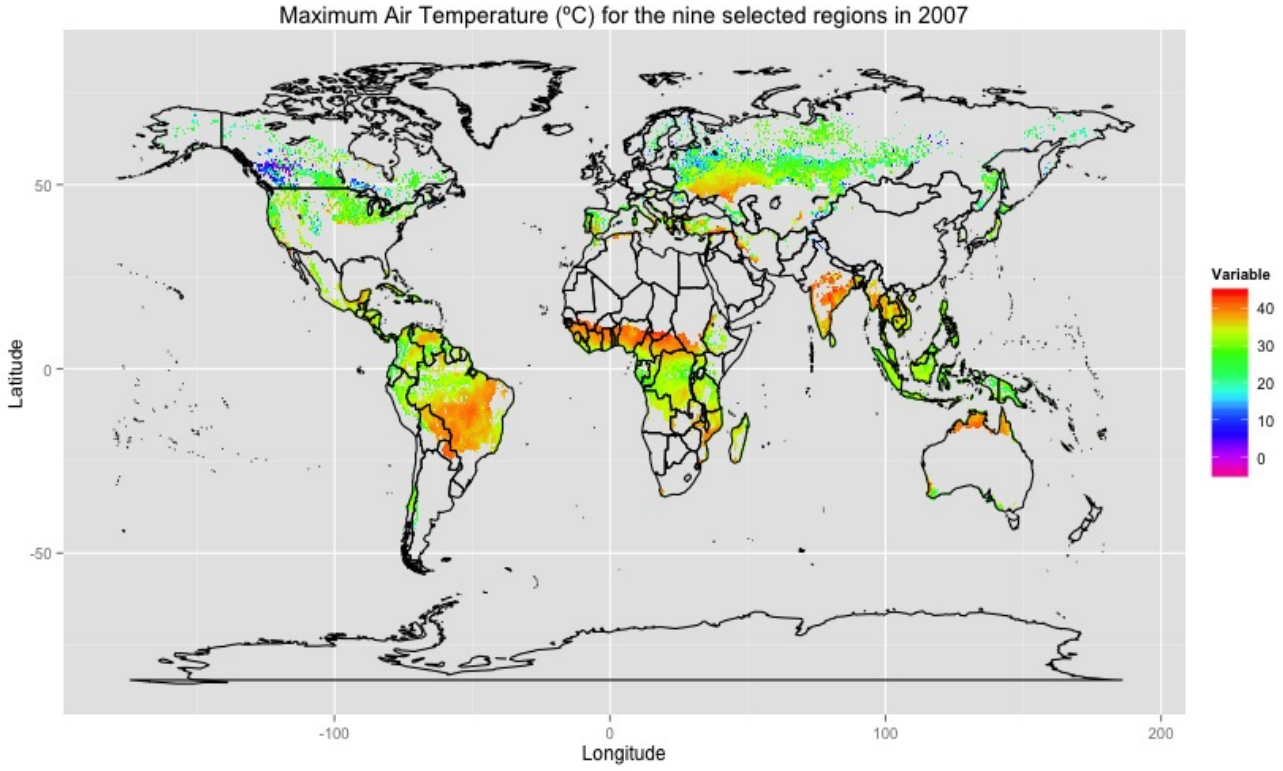

Figure 34: Map of maximum daily Air Temperature values for the year 2007. Maximum daily Air Temperature is 44.45 ºC. Resolution of the map is 0.5º lat/lon.

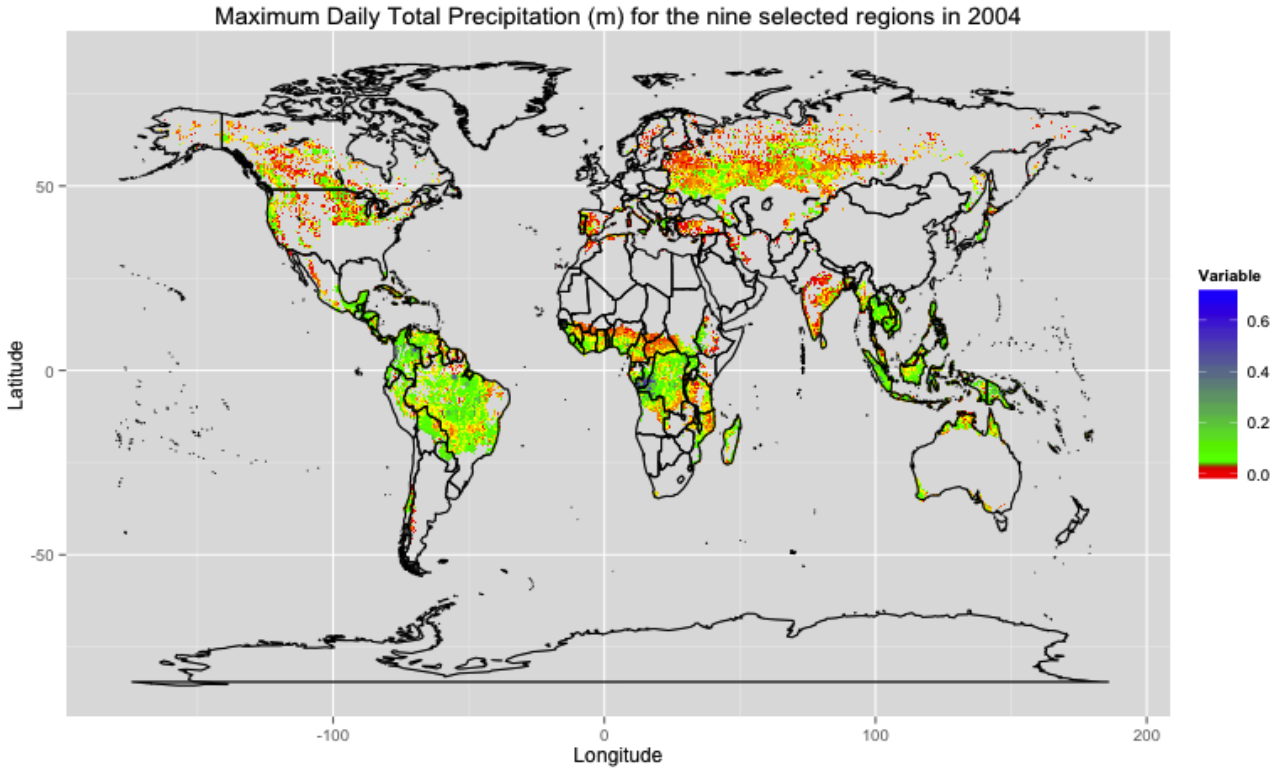

Figure 35: Map of maximum daily Total Precipitation values for the year 2004. Maximum daily Total Precipitation is 0.7317 m. Resolution of the map is 0.5° lat/lon.

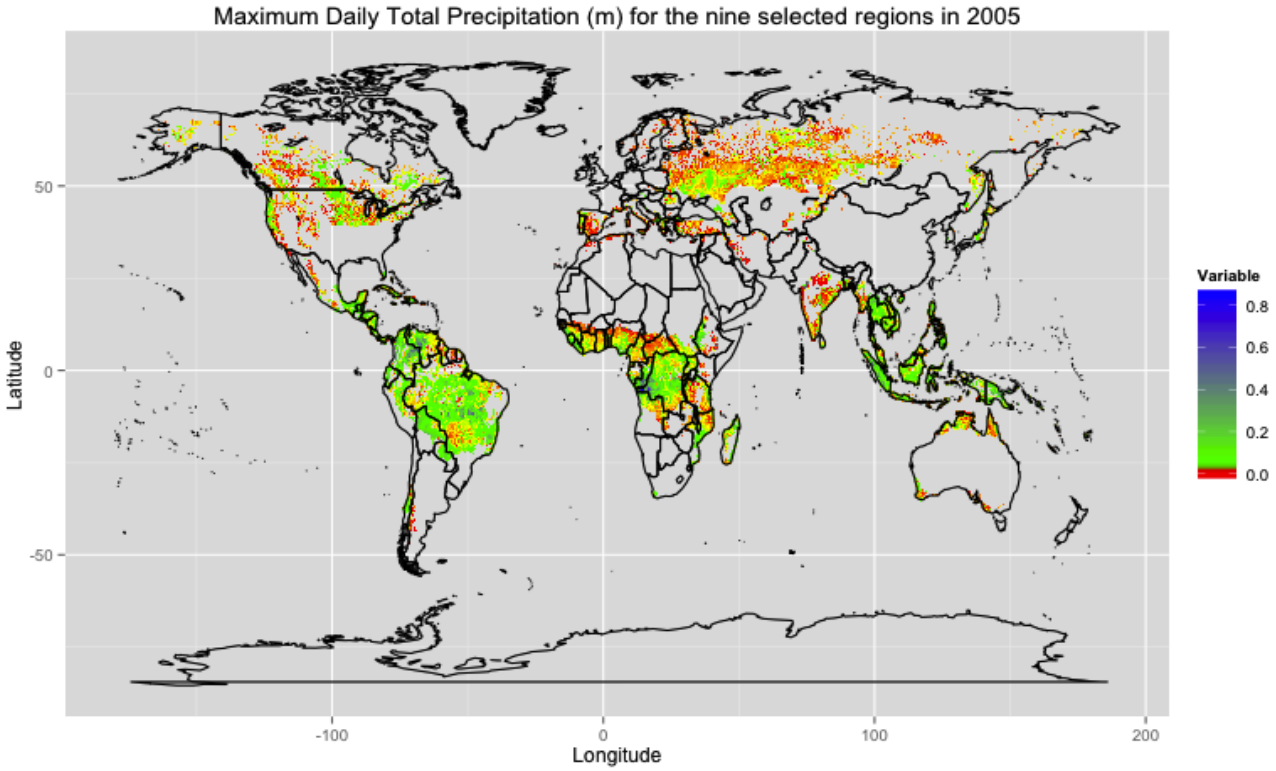

Figure 36: Map of maximum daily Total Precipitation values for the year 2005. Maximum daily Total Precipitation is 0.8605 m. Resolution of the map is 0.5° lat/lon.

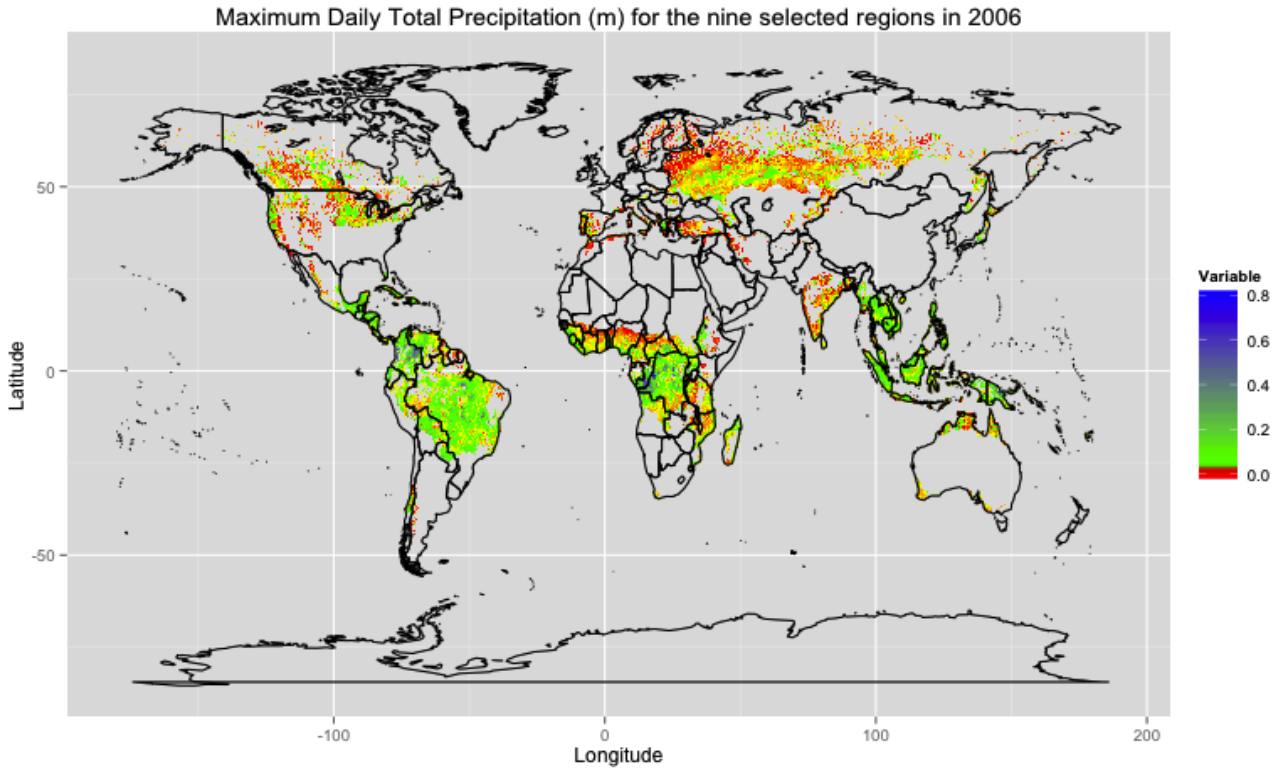

Figure 37: Map of maximum daily Total Precipitation values for the year 2006. Maximum daily Total Precipitation is 0.8224 m. Resolution of the map is 0.5° lat/lon.

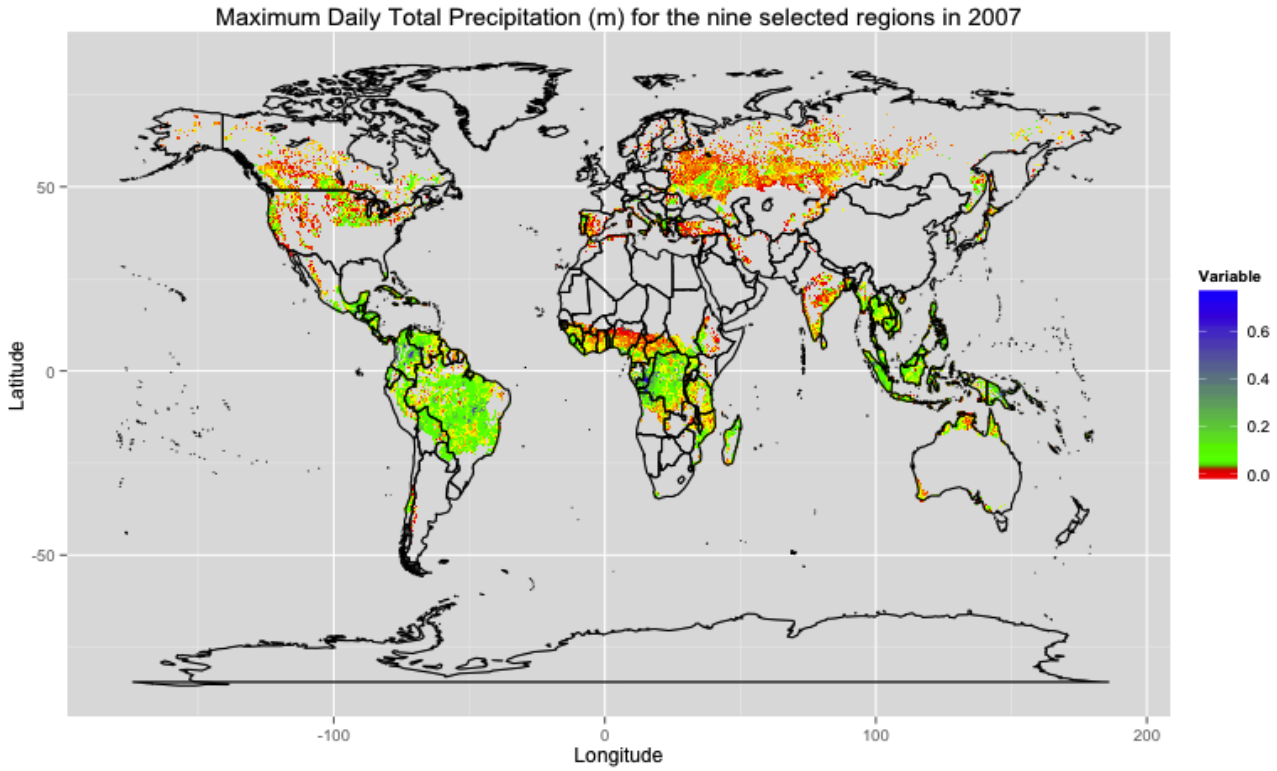

Figure 38: Map of maximum daily Total Precipitation values for the year 2007. Maximum daily Total Precipitation is 0.7798 m. Resolution of the map is 0.5° lat/lon.

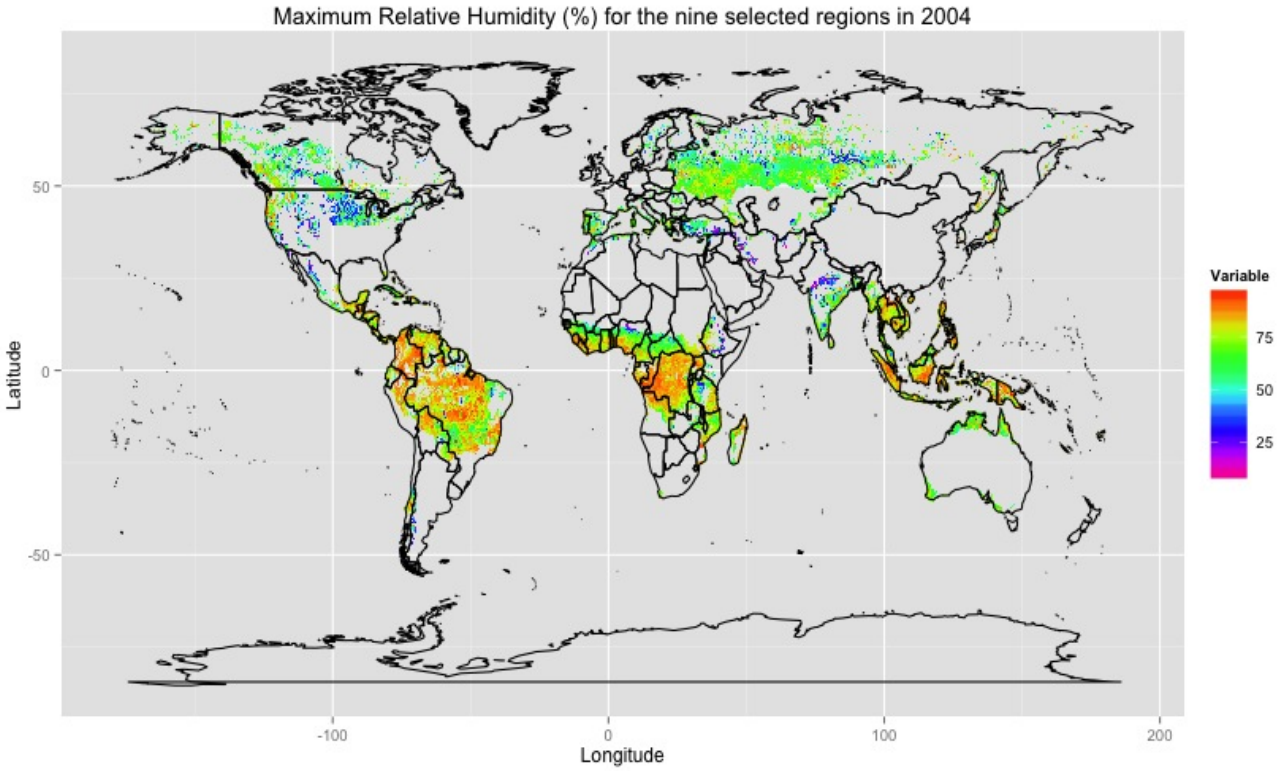

Figure 39: Map of maximum daily Relative Humidity values for the year 2004. Maximum daily Relative Humidity is 97.49%. Resolution of the map is 0.5° lat/lon.

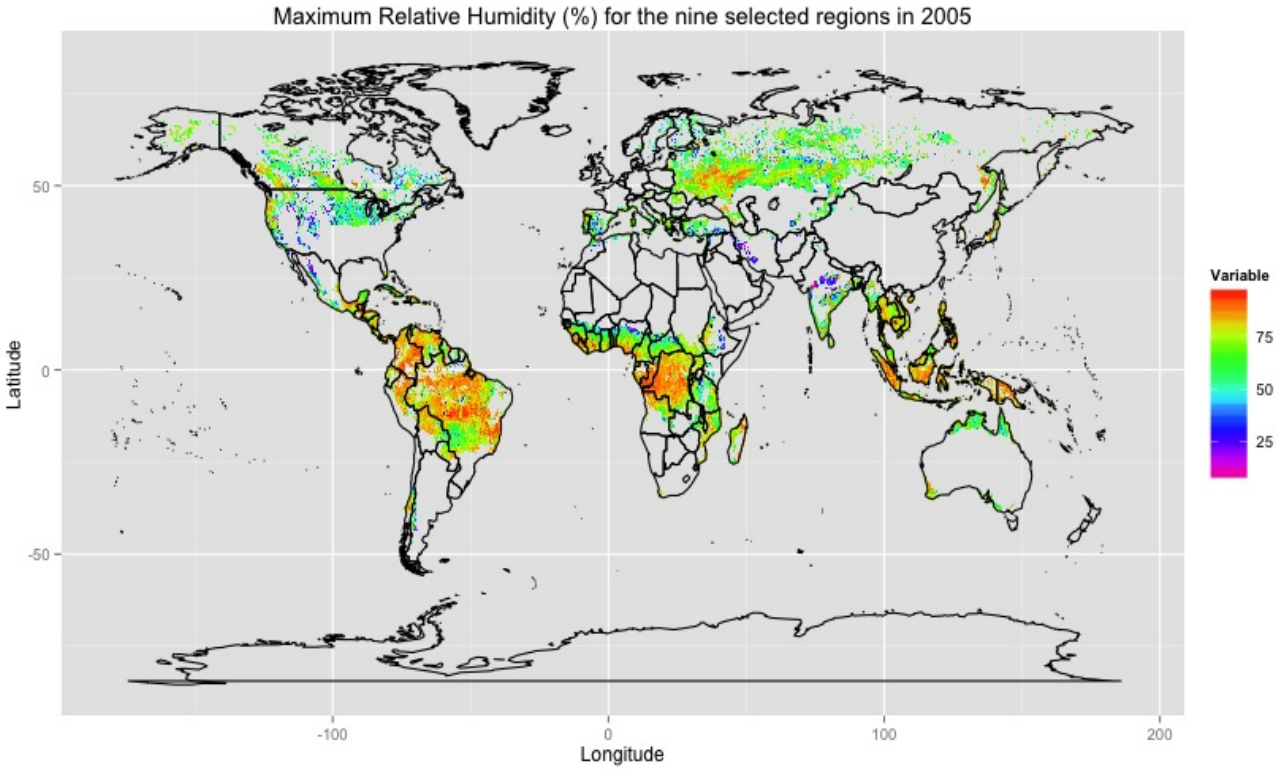

Figure 40: Map of maximum daily Relative Humidity values for the year 2005. Maximum daily Relative Humidity is 97.00%. Resolution of the map is 0.5° lat/lon.

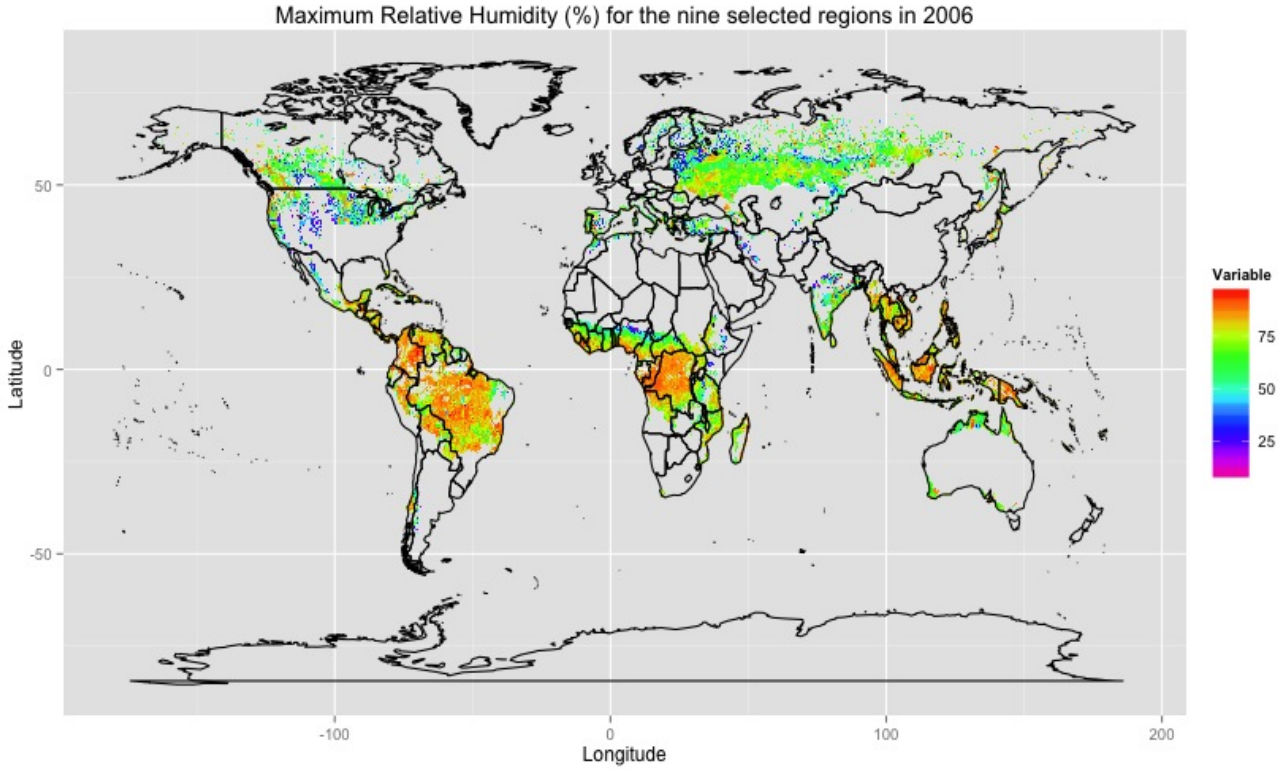

Figure 41: Map of maximum daily Relative Humidity values for the year 2006. Maximum daily Relative Humidity is 96.43%. Resolution of the map is 0.5° lat/lon.

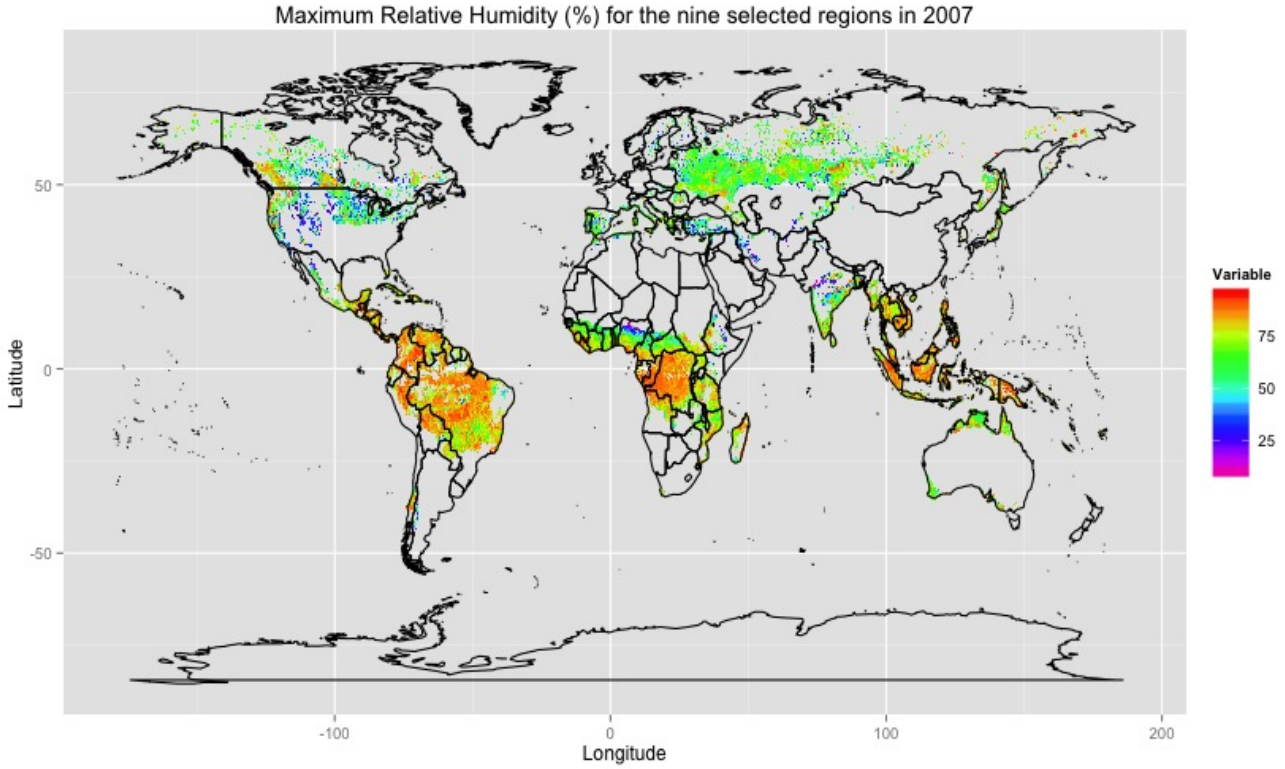

Figure 42: Map of maximum daily Relative Humidity values for the year 2007. Maximum daily Relative Humidity is 95.85%. Resolution of the map is 0.5° lat/lon.

Appendix 2: Autocorrelation Tables

Fire Radiative Power Autocorrelation Tables:

Table 21: Summary of the autocorrelation of FRP values for the equatorial zone and corresponding regions.

Lag (days)	Af	Am	Aw	Equatorial
0	1.00	1.00	1.00	1.00
1	0.57	0.58	0.58	0.58
2	0.35	0.41	0.41	0.41
3	0.28	0.33	0.33	0.33
4	0.23	0.28	0.30	0.29

Table 22: Summary of the autocorrelation of FRP values for the warm temperate zone and corresponding regions.

Lag (days)	Csa	Csb	Csc	Warm Temperate
0	1.00	1.00	1.00	1.00
1	0.45	0.59	0.15	0.52
2	0.29	0.41	-0.09	0.36
3	0.10	0.30	-0.11	0.21
4	0.03	0.25	-0.09	0.15

Large Scale Precipitation Autocorrelation Tables:

Table 23: Summary of the autocorrelation of large scale precipitation values for the equatorial zone and corresponding regions.

Lag (days)	Af	Am	Aw	Equatorial
0	1.00	1.00	1.00	1.00
1	0.31	0.24	0.23	0.27
2	0.16	0.12	0.13	0.15
3	0.14	0.10	0.11	0.13
4	0.13	0.10	0.10	0.13

Table 24: Summary of the autocorrelation of large scale precipitation values for the warm temperate zone and corresponding regions.

Lag (days)	Csa	Csb	Csc	Warm Temperate
0	1.00	1.00	1.00	1.00
1	0.31	0.36	0.44	0.35
2	0.10	0.18	0.12	0.17
3	0.07	0.13	0.00	0.13
4	0.06	0.11	-0.05	0.11

Convective Precipitation Autocorrelation Tables:

Table 25: Summary of the autocorrelation of convective precipitation values for the equatorial zone and corresponding regions.

Lag (days)	Af	Am	Aw	Equatorial
0	1.00	1.00	1.00	1.00
1	0.52	0.58	0.65	0.65
2	0.35	0.44	0.52	0.52
3	0.30	0.39	0.47	0.47
4	0.28	0.36	0.44	0.45

Table 26: Summarization of the autocorrelation of convective precipitation values for the warm temperate zone and corresponding regions.

Lag (days)	Csa	Csb	Csc	Warm Temperate
0	1.00	1.00	1.00	1.00
1	0.45	0.41	0.30	0.44
2	0.21	0.16	0.38	0.19
3	0.13	0.10	0.24	0.12
4	0.10	0.07	0.13	0.09

Appendix 3: Independent Variable Correlations

Table 27: Summary of the correlation coefficients for the independent variables produced from the equatorial zone. For variables directly provided by ECMWF, the highest correlation and most significant relationship observed was between convective precipitation (cp) and dew point temperature (d) in the equatorial zone.

Variable	FRP_0	lsp	lsp_0	cp	cp_0	tp	tp_0	t	d	swc	wind	rh	ai
FRP_0	1.00	-0.04	-0.04	-0.10	-0.11	-0.08	-0.09	0.12	-0.16	-0.08	0.07	-0.18	-0.17
lsp	-0.04	1.00	0.30	0.48	0.34	0.88	0.37	-0.23	0.18	0.24	-0.12	0.29	0.30
lsp_0	-0.04	0.30	1.00	0.28	0.48	0.34	0.87	-0.19	0.17	0.24	-0.12	0.25	0.25
cp	-0.10	0.48	0.28	1.00	0.71	0.84	0.56	-0.44	0.54	0.52	-0.36	0.70	0.67
cp_0	-0.11	0.34	0.48	0.71	1.00	0.60	0.85	-0.38	0.49	0.54	-0.32	0.62	0.60
tp	-0.08	0.88	0.34	0.84	0.60	1.00	0.54	-0.38	0.41	0.43	-0.27	0.57	0.55
tp_0	-0.09	0.37	0.87	0.56	0.85	0.54	1.00	-0.33	0.38	0.45	-0.25	0.50	0.48
t	0.12	-0.23	-0.19	-0.44	-0.38	-0.38	-0.33	1.00	-0.33	-0.33	0.19	-0.68	-0.82
d	-0.16	0.18	0.17	0.54	0.49	0.41	0.38	-0.33	1.00	0.39	-0.33	0.87	0.77
swc	-0.08	0.24	0.24	0.52	0.54	0.43	0.45	-0.33	0.39	1.00	-0.35	0.48	0.47
wind	0.07	-0.12	-0.12	-0.36	-0.32	-0.27	-0.25	0.19	-0.33	-0.35	1.00	-0.38	-0.35
rh	-0.18	0.29	0.25	0.70	0.62	0.57	0.50	-0.68	0.87	0.48	-0.38	1.00	0.98
ai	-0.17	0.30	0.25	0.67	0.60	0.55	0.48	-0.82	0.77	0.47	-0.35	0.98	1.00

Table 28: Summary of the correlation coefficients for the independent variables produced from the warm temperate zone. For variables directly provided by ECMWF, the highest correlation and most significant relationship observed was between large scale precipitation (lsp) and convective precipitation (cp) in the warm temperate zone.

Variable	FRP_0	lsp	lsp_0	cp	cp_0	tp	tp_0	t	d	swc	wind	rh	ai
FRP_0	1.00	-0.01	-0.01	-0.02	-0.02	-0.01	-0.01	0.03	-0.00	-0.03	0.02	-0.03	-0.03
lsp	-0.01	1.00	0.43	0.52	0.30	0.93	0.43	-0.28	0.01	0.24	0.24	0.33	0.35
lsp_0	-0.01	0.43	1.00	0.27	0.53	0.42	0.92	-0.26	-0.02	0.24	0.11	0.26	0.30
cp	-0.02	0.52	0.27	1.00	0.53	0.81	0.43	-0.26	0.15	0.23	0.16	0.43	0.40
cp_0	-0.02	0.30	0.53	0.53	1.00	0.44	0.82	-0.23	0.10	0.25	0.07	0.34	0.33
tp	-0.01	0.93	0.42	0.81	0.44	1.00	0.49	-0.31	0.08	0.26	0.24	0.42	0.42
tp_0	-0.01	0.43	0.92	0.43	0.82	0.49	1.00	-0.29	0.03	0.28	0.11	0.33	0.35
t	0.03	-0.28	-0.26	-0.26	-0.23	-0.31	-0.29	1.00	0.32	-0.35	-0.13	-0.55	-0.86
d	-0.00	0.01	-0.02	0.15	0.10	0.08	0.03	0.32	1.00	-0.42	-0.15	0.57	0.18
swc	-0.03	0.24	0.24	0.23	0.25	0.26	0.28	-0.35	-0.42	1.00	0.04	-0.10	0.12
wind	0.02	0.24	0.11	0.16	0.07	0.24	0.11	-0.13	-0.15	0.04	1.00	0.01	0.08
rh	-0.03	0.33	0.26	0.43	0.34	0.42	0.33	-0.55	0.57	-0.10	0.01	1.00	0.90
ai	-0.03	0.35	0.30	0.40	0.33	0.42	0.35	-0.86	0.18	0.12	0.08	0.90	1.00

Appendix 4: Scatterplots

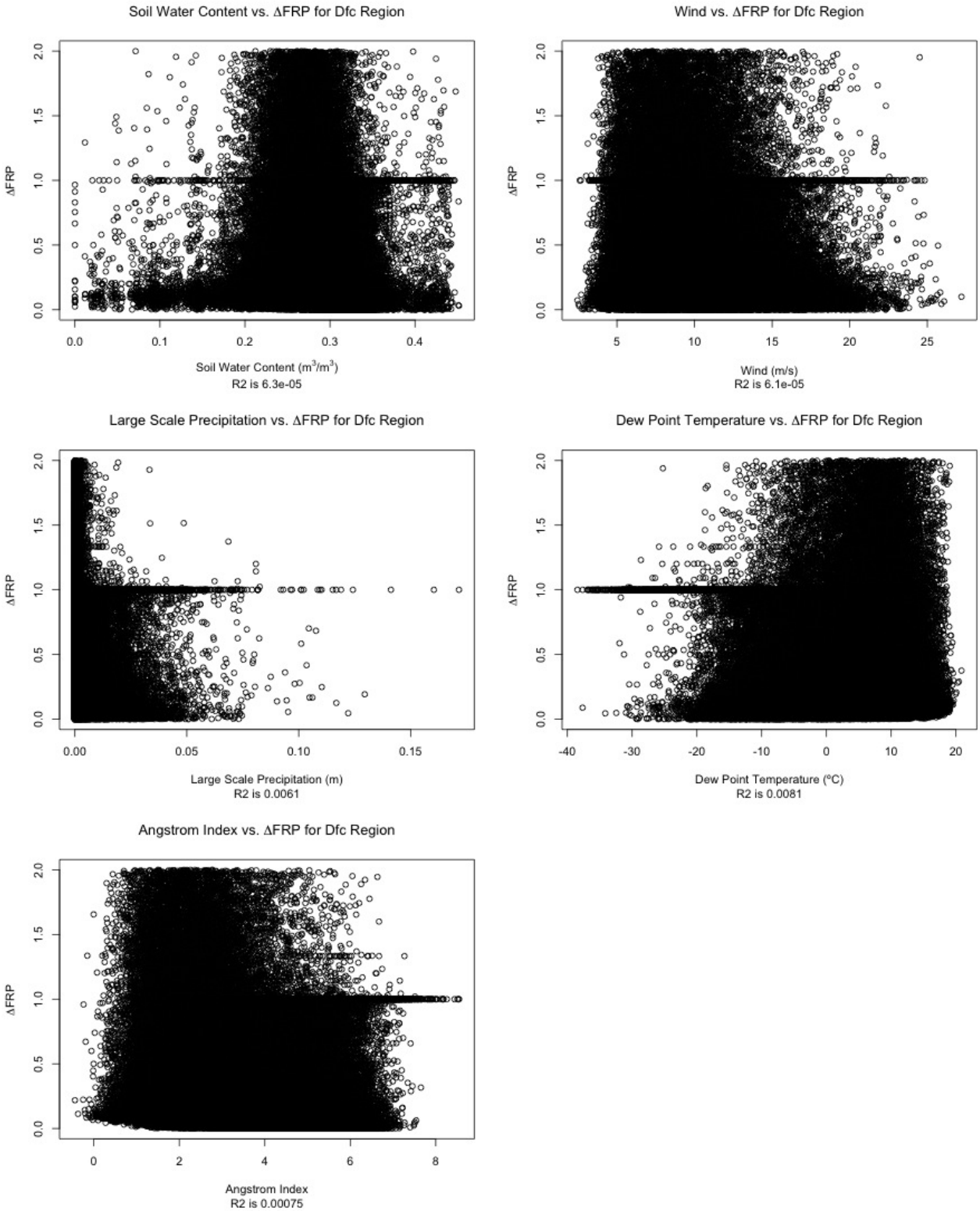

Figure 43: Scatterplots of the five remaining independent variables (soil water content, wind, large scale precipitation, dew point temperature, and angstrom index) and their relation to ΔFRP for the Dfc region (Snow:Fully Humid:Cool Summer). The R^2 is reported below each scatterplot, and in all cases R^2 is miniscule.

Appendix 5: Histograms

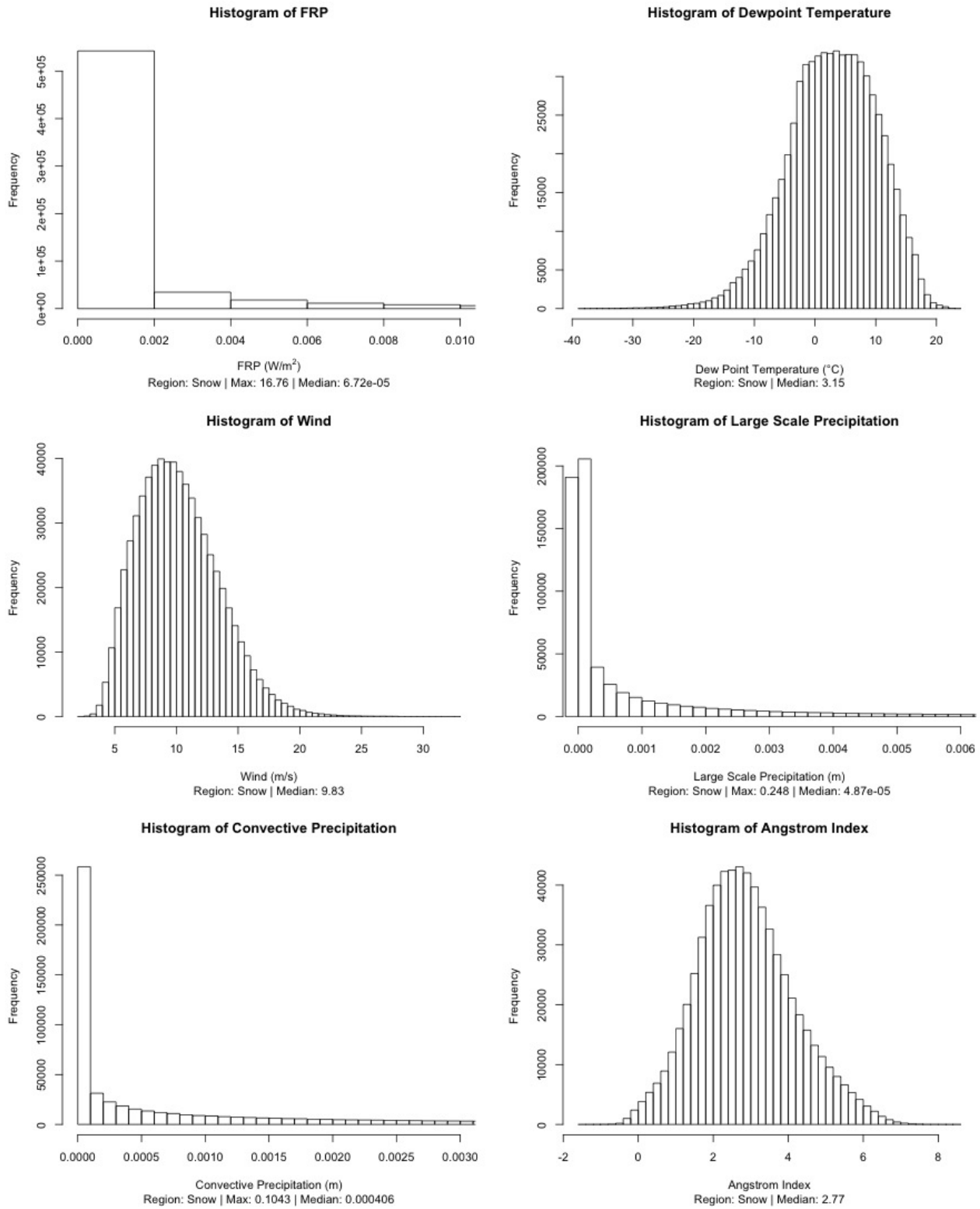

Figure 44: Histograms of the six remaining independent variables (FRP, dew point temperature, wind, large scale precipitation, convective precipitation & angstrom index) for the snow zone. The Median of each variable is included in the histograms. The FRP and precipitation variables exhibit a skewed distribution, while the other variables exhibit characteristic normal distributions.

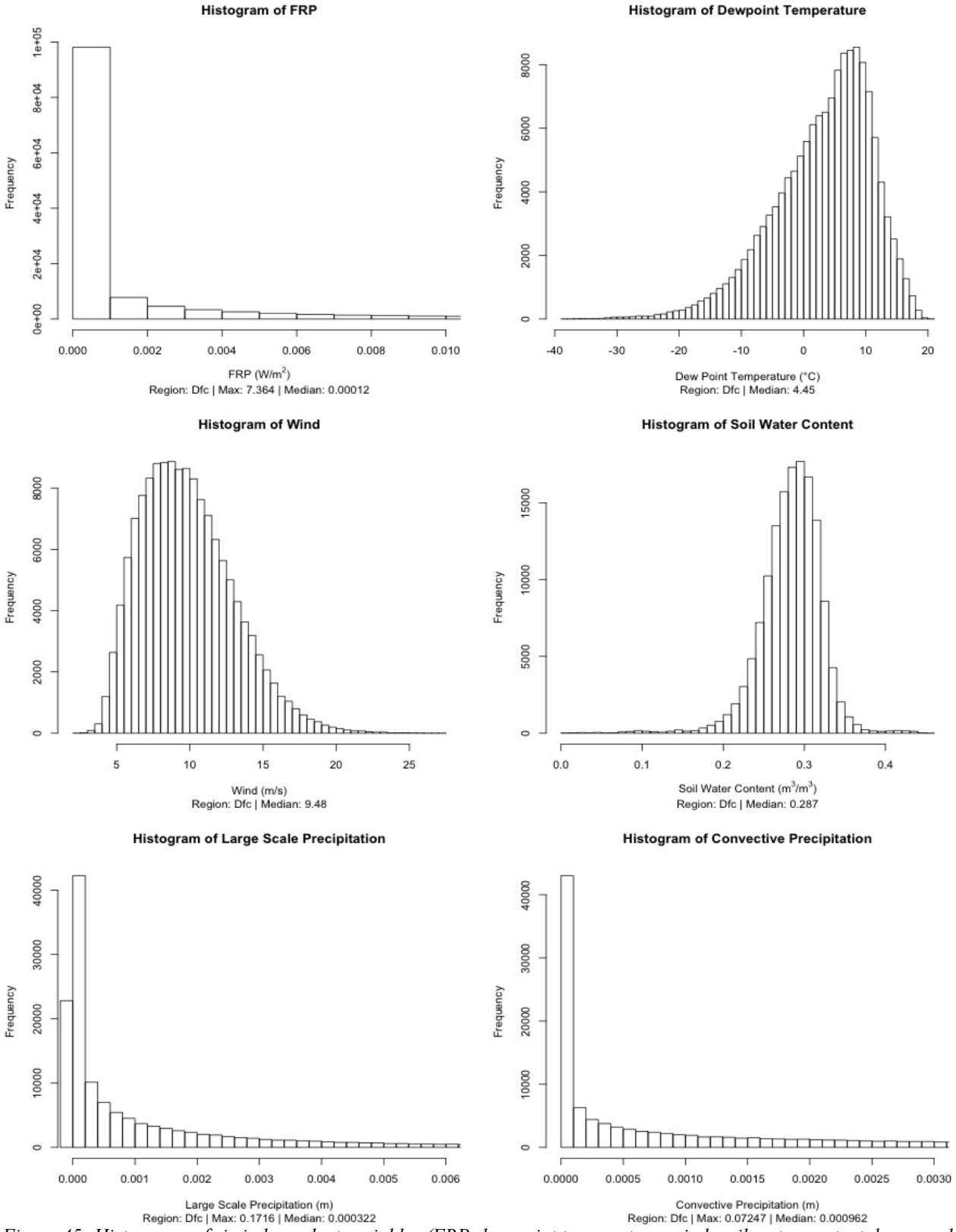

Figure 45: Histograms of six independent variables (FRP, dew point temperature, wind, soil water content, large scale precipitation, convective precipitation) for the Dfc region (Snow:Fully Humid:Cool Summer). The Median of each variable is included in the histograms. The FRP and precipitation variables exhibit a skewed distribution, while the other variables exhibit characteristic normal distributions.

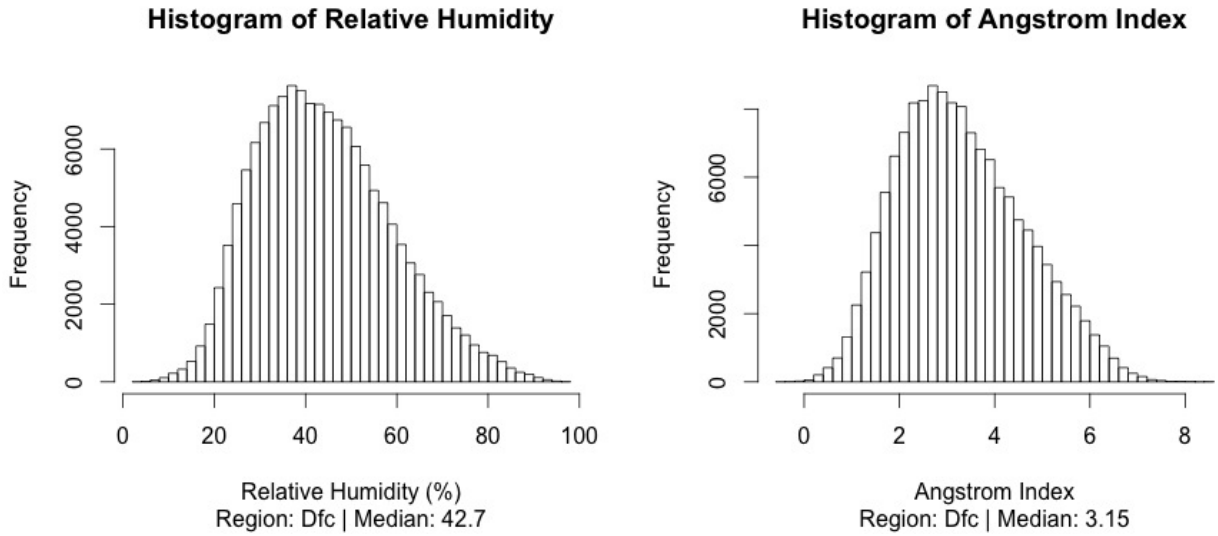

Figure 46: Histograms of two remaining independent variables (relative humidity and angstrom index) for the Dfc region (Snow:Fully Humid:Cool Summer). The Median of each variable is included in the histograms. The both variables exhibit a characteristic normal distribution.

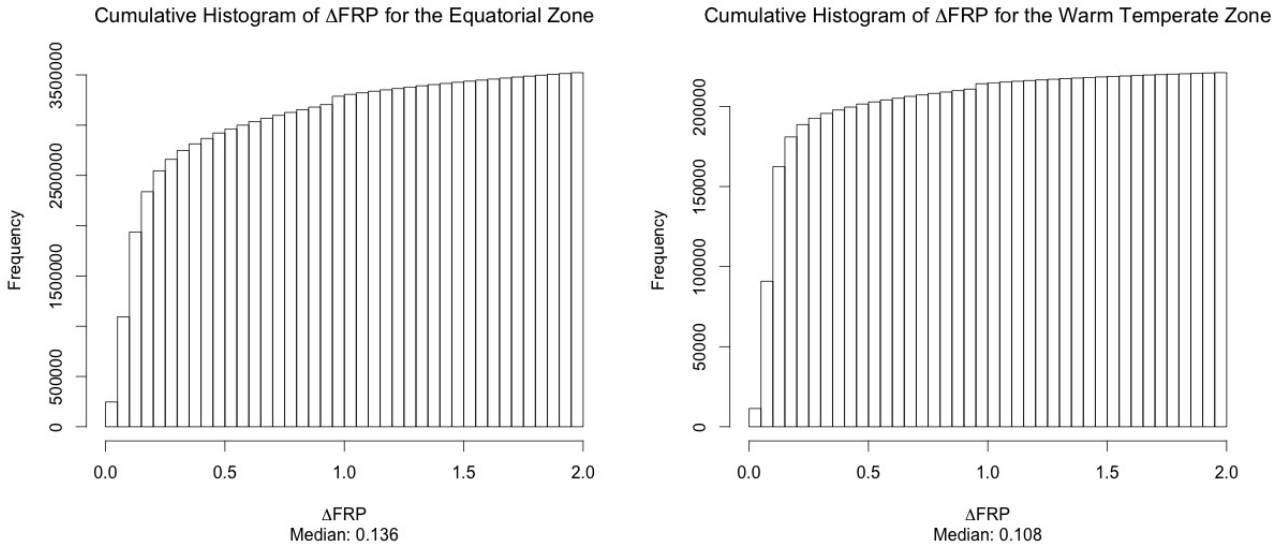

Figure 47: Cumulative histograms of ΔFRP for the Equatorial and Warm Temperate zones with the Median listed. Illustrating the skewed distribution of ΔFRP and the majority of values less than 0.2.

Appendix 6: Box Plots

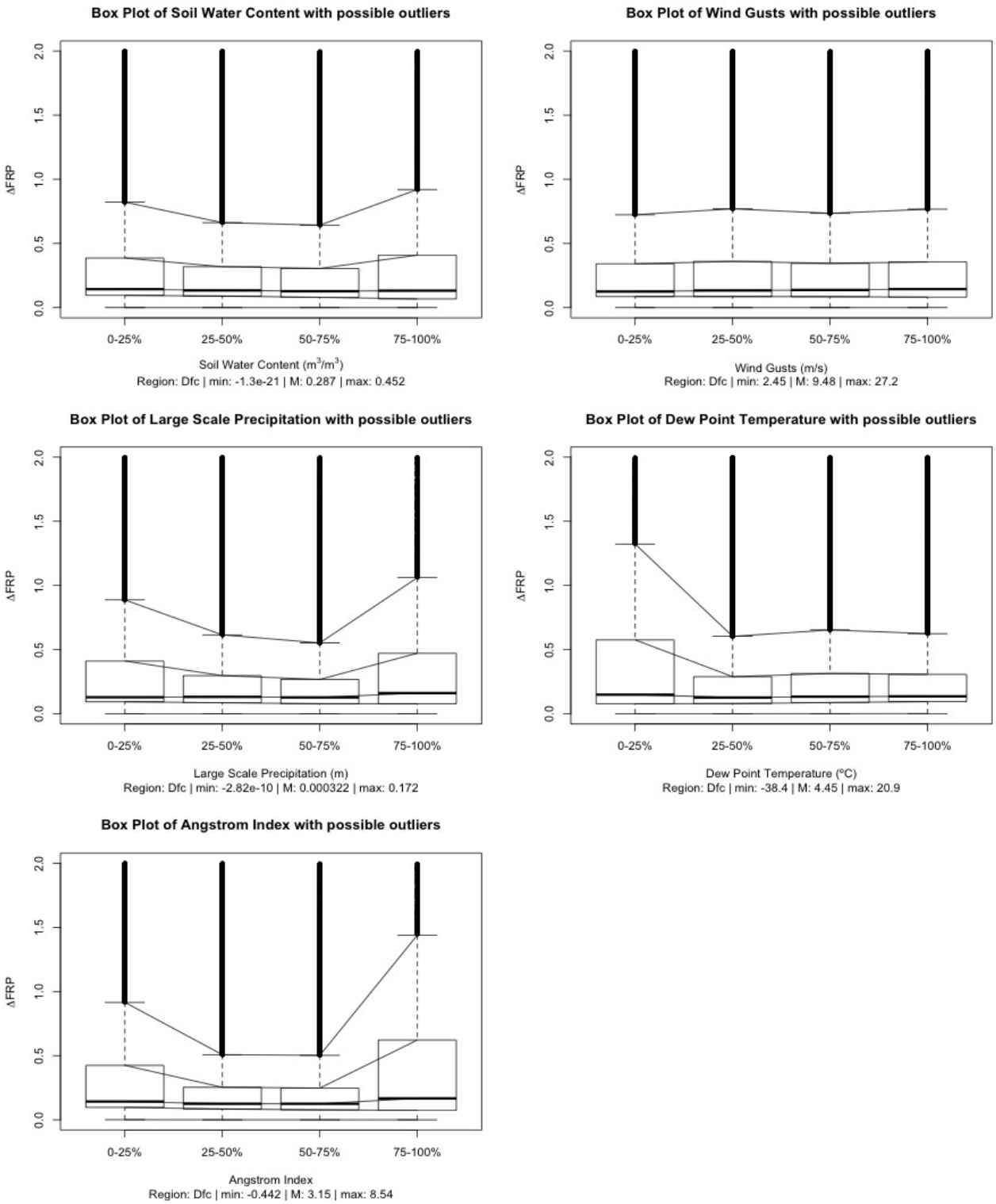

Figure 48: Box-plot displays showing the distribution of ΔFRP for five remaining independent variables (soil water content, wind, large scale precipitation, dew point temperature, angstrom index) of the Dfc region (Snow:Fully Humid:Cool Summer), broken into quartiles. These box-plots help to highlight the trends of the median (black bar) and the IQR (the box) of ΔFRP in relation to each quartile of the variable. Possible outliers are represented by those values which fall beyond 1.5xIQR (whiskers). In many cases, the possible outliers number so many that it appears as a solid black line. Additionally, the median (M) is included along with the min and max values of each independent variable.

Appendix 7: Mann-Whitney U Test Results

*Table 29: Mann-Whitney U test results for every independent variable of the Af region (Equatorial:Fully Humid). The * represents successful U tests showing statistically different groups. The +/- sign shows the trend of the median, from left to right. An X represents failed U tests where the two groups were not significantly different. The size of the each group is included in the table and for the Af region 8.79% of U tests failed.*

variable	I:VII	I:II	II:III	III:IV	IV:V	V:VI	VI:VIII	region
FRP_0	* -	* -	* -	* +	* +	* +	* +	Af
lsp	* -	* -	* -	* +	* +	* +	* +	Af
lsp_0	* -	* -	* -	* -	* -	* -	* -	Af
cp	* -	* -	* -	* +	* +	* +	* +	Af
cp_0	* -	* -	* -	* -	* -	X	* -	Af
tp	* -	* -	* -	* +	* +	* +	* +	Af
tp_0	* -	* -	* -	* -	* -	* -	* -	Af
t	X	* +	* -	* -	* +	* +	* +	Af
d	* +	* +	X	X	* +	* +	* +	Af
swc	* +	* +	* +	* -	* -	* +	* +	Af
wind	* -	* -	X	X	* -	X	X	Af
rh	* -	* -	* -	* +	* +	* +	* +	Af
ai	* -	* -	* -	* +	* +	* +	* +	Af
size	I:20519	II:82079	III:102599	IV:102598	V:82079	VI:20521	VII:389876	VIII:389874

*Table 30: Mann-Whitney U test results for every independent variable of the Am region (Equatorial:Monsoon). The * represents successful U tests showing statistically different groups. The +/- sign shows the trend of the median, from left to right. An X represents failed U tests where the two groups were not significantly different. The size of the each group is included in the table and for the Am region 3.29% of U tests failed.*

variable	I:VII	I:II	II:III	III:IV	IV:V	V:VI	VI:VIII	region
FRP_0	* -	* -	* +	* +	* +	* +	* +	Am
lsp	* -	* -	* -	* -	* +	* +	X	Am
lsp_0	* -	* -	* -	* -	* -	* -	* -	Am
cp	* -	* -	* -	* +	* +	* +	* +	Am
cp_0	* -	* -	* -	X	* -	* -	* -	Am
tp	* -	* -	* -	* +	* +	* +	* +	Am
tp_0	* -	* -	* -	* -	* -	* -	* -	Am
t	* +	* +	* -	* +	* +	* +	* +	Am
d	* -	* -	* -	* -	* +	* +	* +	Am
swc	* +	* +	* +	* -	* -	* +	* -	Am
wind	* +	* +	* +	* +	* +	* +	* +	Am
rh	* -	* -	* -	* -	* +	* +	X	Am
ai	* -	* -	* -	* -	* +	* +	* +	Am
size	I:27072	II:108291	III:135365	IV:135365	V:108291	VI:27074	VII:514386	VIII:514384

*Table 31: Mann-Whitney U test results for every independent variable of the Aw Region (Equatorial:Winter Dry). The * represents successful U tests showing statistically different groups. The +/- sign shows the trend of the median, from left to right. An X represents failed U tests where the two groups were not significantly different. The size of the each group is included in the table and for the Aw region 3.3% of U tests failed.*

variable	I:VII	I:II	II:III	III:IV	IV:V	V:VI	VI:VIII	region
FRP_0	* -	* -	* +	* +	* +	* +	* +	Aw
lsp	* -	* +	* -	* -	* +	* +	X	Aw
lsp_0	* -	* +	* -	* -	* -	* -	* -	Aw
cp	* -	* -	* -	* -	* +	* +	X	Aw
cp_0	* -	* -	* -	* -	* -	* -	* -	Aw
tp	* -	* +	* -	* -	X	* +	* +	Aw
tp_0	* -	* +	* -	* -	* -	* -	* -	Aw
t	* +	* +	* +	* +	* +	* -	* -	Aw
d	* -	* +	* -	* -	* +	* +	* -	Aw
swc	* +	* +	* -	* -	* -	* +	* -	Aw
wind	* +	* +	* +	* +	* +	* +	* +	Aw
rh	* -	* +	* -	* -	* +	* +	* +	Aw
ai	* +	* +	* -	* -	* +	* +	* +	Aw
size	I:130694	II:522782	III:653477	IV:653477	V:522782	VI:130696	VII:2483214	VIII:2483212

*Table 32: Mann-Whitney U test results for every independent variable of the Csa region (Warm Temperate:Summer Dry:Hot Summer). The * represents successful U tests showing statistically different groups. The +/- sign shows the trend of the median, from left to right. An X represents failed U tests where the two groups were not significantly different. The size of the each group is included in the table and for the Csa region 41.76% of U tests failed.*

variable	I:VII	I:II	II:III	III:IV	IV:V	V:VI	VI:VIII	region
FRP_0	* -	* -	* -	* +	* +	* +	* +	Csa
lsp	X	X	X	* +	* +	* +	* +	Csa
lsp_0	X	* +	X	* +	* -	* -	* -	Csa
cp	X	X	* +	X	* +	X	* +	Csa
cp_0	* -	* -	* +	X	* -	* -	* -	Csa
tp	X	X	X	X	* +	* +	* +	Csa
tp_0	X	* +	X	* +	* -	* -	* -	Csa
t	X	X	X	X	X	* +	* -	Csa
d	X	X	* +	X	X	X	X	Csa
swc	* -	X	* -	X	* +	X	* +	Csa
wind	X	X	X	* +	* +	X	* +	Csa
rh	* +	X	* +	* -	* +	* +	* +	Csa
ai	* +	X	X	* +	X	* +	* +	Csa
size:	I:6805	II:27226	III:34032	IV:34033	V:27226	VI:6807	VII:129324	VIII:129322

*Table 33: Mann-Whitney U test results for every independent variable of the Csb region (Warm Temperate:Summer Dry:Warm Summer). The * represents successful U tests showing statistically different groups. The +/- sign shows the trend of the median, from left to right. An X represents failed U tests where the two groups were not significantly different. The size of the each group is included in the table and for the Csb region 47.25% of U tests failed.*

variable	I:VII	I:II	II:III	III:IV	IV:V	V:VI	VI:VIII	region
FRP_0	* -	* -	* -	* +	* +	* +	* +	Csb
lsp	X	X	* -	* +	* +	* +	* +	Csb
lsp_0	* -	X	X	* -	* -	* -	* -	Csb
cp	X	X	X	X	* +	X	* +	Csb
cp_0	* -	X	X	* -	* -	* -	* -	Csb
tp	X	X	* +	X	* +	* +	* +	Csb
tp_0	* -	X	X	* -	* -	* -	* -	Csb
t	X	X	X	X	* -	* +	* +	Csb
d	* +	X	X	* -	X	X	X	Csb
swc	X	X	* +	* -	X	X	X	Csb
wind	X	X	X	X	X	* +	* +	Csb
rh	* +	* -	X	X	X	X	X	Csb
ai	* -	* -	* +	X	X	* +	X	Csb
size	I:4241	II:16970	III:21212	IV:21212	V:16970	VI:4243	VII:80607	VIII:80605

*Table 34: Mann-Whitney U test results for every independent variable of the Csc region (Warm Temperate:Summer Dry:Cool Summer). The * represents successful U tests showing statistically different groups. The +/- sign shows the trend of the median, from left to right. An X represents failed U tests where the two groups were not significantly different. The size of the each group is included in the table and for the Csc region 98.9% of U tests failed.*

variable	I:VII	I:II	II:III	III:IV	IV:V	V:VI	VI:VIII	region
FRP_0	X	X	X	X	X	X	X	Csc
lsp	X	X	X	X	X	X	X	Csc
lsp_0	X	X	X	X	X	X	X	Csc
cp	X	X	X	X	X	X	X	Csc
cp_0	X	X	X	* -	X	X	X	Csc
tp	X	X	X	X	X	X	X	Csc
tp_0	X	X	X	X	X	X	X	Csc
t	X	X	X	X	X	X	X	Csc
d	X	X	X	X	X	X	X	Csc
swc	X	X	X	X	X	X	X	Csc
wind	X	X	X	X	X	X	X	Csc
rh	X	X	X	X	X	X	X	Csc
ai	X	X	X	X	X	X	X	Csc
size	I:6	II:27	III:33	IV:33	V:27	VI:8	VII:128	VIII:126

*Table 35: Mann-Whitney U test results for every independent variable of the warm temperate zone. The * represents successful U tests showing statistically different groups. The +/- sign shows the trend of the median, from left to right. An X represents failed U tests where the two groups were not significantly different. The size of the each group is included in the table and for the warm temperate zone 35.16% of U tests failed.*

variable	I:VII	I:II	II:III	III:IV	IV:V	V:VI	VI:VIII	region
FRP_0	* -	* -	* -	* +	* +	* +	* +	Warm Temperate
lsp	X	X	X	* -	X	* +	* +	Warm Temperate
lsp_0	* -	* +	X	* +	* -	* -	* -	Warm Temperate
cp	* +	X	X	X	* +	X	* +	Warm Temperate
cp_0	* -	* -	* +	* -	* -	* -	* -	Warm Temperate
tp	X	X	X	X	* +	* +	* +	Warm Temperate
tp_0	* -	* +	X	* -	* -	* -	* -	Warm Temperate
t	X	X	X	X	* -	X	* -	Warm Temperate
d	* +	X	* +	* -	X	X	X	Warm Temperate
swc	X	X	* -	* +	* +	X	X	Warm Temperate
wind	X	* -	X	* +	* +	* +	* +	Warm Temperate
rh	* +	* +	* +	* +	* +	* +	* +	Warm Temperate
ai	* +	X	* -	X	X	* +	* +	Warm Temperate
Size	I:11055	II:44222	III:55278	IV:55277	V:44222	VI:11057	VII:210056	VIII:210054

*Table 36: Mann-Whitney U test results for every independent variable of the Dfa region (Snow:Fully Humid:Hot Summer). The * represents successful U tests showing statistically different groups. The +/- sign shows the trend of the median, from left to right. An X represents failed U tests where the two groups were not significantly different. The size of the each group is included in the table and for the Dfa region 25.27% of U tests failed.*

variable	I:VII	I:II	II:III	III:IV	IV:V	V:VI	VI:VIII	region
FRP_0	* -	* -	* -	* +	* +	* +	* +	Dfa
lsp	* -	* -	X	* -	* +	* +	* +	Dfa
lsp_0	* -	X	X	* -	* -	* -	* -	Dfa
cp	* +	* -	* +	* +	* +	* +	* +	Dfa
cp_0	* -	X	* -	* -	* -	* -	* -	Dfa
tp	X	X	* +	* +	* +	* +	* +	Dfa
tp_0	* -	X	* -	* -	* -	* -	* -	Dfa
t	X	X	* -	X	* +	* +	* +	Dfa
d	X	X	X	X	X	X	* -	Dfa
swc	* -	* -	* -	* -	* +	* -	* -	Dfa
wind	X	X	X	X	* +	* +	* +	Dfa
rh	* -	X	* -	* -	X	* +	* +	Dfa
ai	* -	* -	* -	X	* -	* +	* +	Dfa
size	I:4948	II:19797	III:24747	IV:24747	V:19797	VI:4950	VII:94038	VIII:94036

*Table 37: Mann-Whitney U test results for every independent variable of the Dfb region (Snow:Fully Humid:Warm Summer). The * represents successful U tests showing statistically different groups. The +/- sign shows the trend of the median, from left to right. An X represents failed U tests where the two groups were not significantly different. The size of the each group is included in the table and for the Dfb region 16.48% of U tests failed.*

variable	I:VII	I:II	II:III	III:IV	IV:V	V:VI	VI:VIII	region
FRP_0	* -	* -	* -	* +	* +	* +	* +	Dfb
lsp	* +	X	* -	* -	* +	* +	* +	Dfb
lsp_0	* -	X	* -	* -	* -	* -	* -	Dfb
cp	* +	X	* +	X	* +	* +	* +	Dfb
cp_0	* -	* +	* -	* -	* -	* -	* -	Dfb
tp	* +	* -	* +	* +	* +	* +	* +	Dfb
tp_0	* -	* -	* -	* -	* -	* -	* -	Dfb
t	* -	* -	X	* -	* -	* +	* +	Dfb
d	* -	* -	* -	* -	X	* +	X	Dfb
swc	* -	X	* -	X	X	* -	* -	Dfb
wind	* +	* +	X	X	X	X	X	Dfb
rh	* -	* -	* -	* -	* +	* +	* +	Dfb
ai	* -	* -	* -	* +	* +	* +	* +	Dfb
size	I:21025	II:84103	III:105129	IV:105130	V:84103	VI:21027	VII:399492	VIII:399490

*Table 38: Mann-Whitney U test results for every independent variable of the snow zone. The * represents successful U tests showing statistically different groups. The +/- sign shows the trend of the median, from left to right. An X represents failed U tests where the two groups were not significantly different. The size of the each group is included in the table and for the snow zone 10.99% of U tests failed.*

variable	I:VII	I:II	II:III	III:IV	IV:V	V:VI	VI:VIII	region
FRP_0	* -	* -	* -	* +	* +	* +	* +	snow
lsp	* +	* -	* -	* +	* +	* +	* +	snow
lsp_0	* -	X	* -	* -	* -	* -	* -	snow
cp	* +	* +	* +	X	* +	* +	* +	snow
cp_0	* -	* +	* -	* -	* -	* -	* -	snow
tp	* +	* -	* +	* +	* +	* +	* +	snow
tp_0	* -	* -	* -	* -	* -	* -	* -	snow
t	* -	* -	* -	* -	* -	* +	* -	snow
d	* -	* -	* -	* -	* -	X	* -	snow
swc	* +	* -	X	* +	X	X	* +	snow
wind	* +	X	* +	X	* +	X	X	snow
rh	* -	* -	* -	* -	* +	* +	* +	snow
ai	* +	* -	* -	* +	* +	* +	* +	snow
size	I:33168	II:132676	III:165845	IV:165846	V:132676	VI:33170	VII:630213	VIII:630211

Appendix 8: BIC and Modeling

Table 39: Summary of the linear regression model via BIC for the Af region (Equatorial:Fully Humid).

Region: Af	Estimate	Std. Error	t value	Pr(>|t|)
(Intercept)	0.9106	0.0300	30.38	0.0000
FRP_0	1.0460	0.0195	53.68	0.0000
cp	2.7371	0.0503	54.44	0.0000
$(FRP_0)^2$	-0.3359	0.0095	-35.48	0.0000
$(t)^2$	0.0012	0.0000	29.25	0.0000
t	-0.0579	0.0022	-26.59	0.0000

Table 40: Detailed summary of the best fit line of Fitted ΔFRP vs. Actual ΔFRP developed for the Af region from the linear regression with BIC for years 2003-2007.

Region: Af	Estimate	Std. Error	t value	Pr(>|t|)
Intercept:	0.2328	0.0001	3128.91	0.0000
R-squared:	0.0162	0.0002	82.26	0.0000

Table 41: Summary of the linear regression model via BIC for the Am region (Equatorial:Monsoon).

Region: Am	Estimate	Std. Error	t value	Pr(>|t|)
(Intercept)	0.2522	0.0016	159.21	0.0000
FRP_0	0.7943	0.0093	85.18	0.0000
$(FRP_0)^2$	-0.5017	0.0082	-61.09	0.0000
cp	2.3364	0.0418	55.95	0.0000
ai	-0.0597	0.0012	-47.97	0.0000
$(ai)^2$	0.0087	0.0002	36.21	0.0000

Table 42: Detailed summary of the best fit line of Fitted ΔFRP vs. Actual ΔFRP developed for the Am region from the linear regression with BIC for years 2003-2007.

Region: Am	Estimate	Std. Error	t value	Pr(>|t|)
Intercept:	0.1830	0.0001	2698.18	0.0000
R-squared:	0.0312	0.0003	122.38	0.0000

Table 43: Summary of the linear regression model via BIC for the Aw region (Equatorial:Winter Dry).

Region: Aw	Estimate	Std. Error	t value	Pr(>|t|)
(Intercept)	0.4420	0.0007	635.53	0.0000
d	-0.0036	0.0001	-48.70	0.0000
FRP_0	0.8499	0.0060	140.62	0.0000
$(FRP_0)^2$	-0.4646	0.0050	-93.44	0.0000
rh	-0.0025	0.0000	-83.67	0.0000
cp	3.4046	0.0481	70.79	0.0000

Table 44: Detailed summary of the best fit line of Fitted ΔFRP vs. Actual ΔFRP developed for the Aw region from the linear regression with BIC for years 2003-2007.

Region: Aw	Estimate	Std. Error	t value	Pr(>|t|)
Intercept:	0.3025	0.0001	5390.38	0.0000
R-squared:	0.0332	0.0001	299.40	0.0000

Table 45: Summary of the linear regression model via BIC for the Equatorial zone.

Equatorial Zone	Estimate	Std. Error	t value	Pr(>|t|)
(Intercept)	1.6463	0.0041	405.52	0.0000
rh	-0.0236	0.0002	-124.08	0.0000
FRP_0	-2.2139	0.0219	-101.08	0.0000
$(FRP_0)^2$	0.8318	0.0174	47.72	0.0000
$(rh)^2$	0.0001	0.0000	53.30	0.0000
cp_0	-5.8690	0.1371	-42.81	0.0000

Table 46: Detailed summary of the best fit line of Fitted ΔFRP vs. Actual ΔFRP developed for the Equatorial Zone from the linear regression with BIC for years 2003-2007.

Equatorial Zone	Estimate	Std. Error	t value	Pr(>|t|)
Intercept:	0.7580	0.0002	4629.79	0.0000
R-squared:	0.0345	0.0001	376.06	0.0000

Table 47: Summary of the linear regression model via BIC for the Dfb region (Snow:Fully Humid:Warm Summer).

Region: Dfb	Estimate	Std. Error	t value	Pr(>|t|)
(Intercept)	0.2985	0.0022	134.99	0.0000
lsp	7.6713	0.1038	73.87	0.0000
d	-0.0052	0.0001	-48.48	0.0000
$(t)^2$	0.0004	0.0000	59.20	0.0000
t	-0.0104	0.0002	-44.64	0.0000
FRP_0	0.1705	0.0063	27.12	0.0000

Table 48: Detailed summary of the best fit line of Fitted ΔFRP vs. Actual ΔFRP developed for the Dfb region from the linear regression with BIC for years 2003-2007.

Region: Dfb	Estimate	Std. Error	t value	Pr(>|t|)
Intercept:	0.2422	0.0001	2166.73	0.0000
R-squared:	0.0318	0.0003	117.57	0.0000

Table 49: Summary of the linear regression model via BIC for the snow zone.

Snow Zone	Estimate	Std. Error	t value	Pr(>|t|)
(Intercept)	0.2380	0.0005	437.45	0.0000
lsp	7.0459	0.0762	92.48	0.0000
d	-0.0051	0.0001	-87.75	0.0000
$(d)^2$	0.0003	0.0000	58.43	0.0000
FRP_0	0.3711	0.0057	64.79	0.0000
$(FRP_0)^2$	-0.0323	0.0007	-44.68	0.0000

Table 50: Detailed summary of the best fit line of Fitted ΔFRP vs. Actual ΔFRP developed for the snow zone from the linear regression with BIC for years 2003-2007.

Snow Zone	Estimate	Std. Error	t value	Pr(>|t|)
Intercept:	0.2514	0.0001	2751.33	0.0000
R-squared:	0.0315	0.0002	146.81	0.0000

Table 52: Summary of the linear regression model via BIC for the warm temperate zone.

Warm Temperate	Estimate	Std. Error	t value	Pr(>|t|)
(Intercept)	0.2022	0.0008	245.71	0.0000
lsp	6.0094	0.1909	31.49	0.0000
FRP_0	0.4492	0.0116	38.83	0.0000
$(FRP_0)^2$	-0.0633	0.0023	-27.69	0.0000
d	-0.0015	0.0001	-17.94	0.0000
$(tp)^2$	-22.7291	1.5494	-14.67	0.0000

Table 51: Detailed summary of the best fit line of Fitted ΔFRP vs. Actual ΔFRP developed for the warm temperate zone from the linear regression with BIC for years 2003-2007.

WT zone	Estimate	Std. Error	t value	Pr(>|t|)
Intercept:	0.1988	0.0001	2173.23	0.0000
R-squared:	0.0154	0.0003	58.83	0.0000

Appendix 9: Computer Script

The R script was responsible for analyzing the data, running the model, and generating the figures and tables.

A copy the script used in the analysis can be found online at the Lund University Publication Database at [https://lup.lub.lu.se/luur/download?func=downloadFile&recordOId=4286230&fileOId=4286232]

Alternatively, a version will be hosted on my personal Dropbox at [https://www.dropbox.com/s/fau028tp2kthrhx/Demet_2013_NGEM01_Script.R]

Institutionen för naturgeografi och ekosystemvetenskap, Lunds Universitet.

Student examensarbete (Seminarieuppsatser). Uppsatserna finns tillgängliga på institutionens geobibliotek, Sölvegatan 12, 223 62 LUND. Serien startade 1985. Hela listan och själva uppsatserna är även tillgängliga på LUP student papers (www.nateko.lu.se/masterthesis) och via Geobiblioteket (www.geobib.lu.se)

The student thesis reports are available at the Geo-Library, Department of Physical Geography and Ecosystem Science, University of Lund, Sölvegatan 12, S-223 62 Lund, Sweden. Report series started 1985. The complete list and electronic versions are also electronic available at the LUP student papers (www.nateko.lu.se/masterthesis) and through the Geo-library (www.geobib.lu.se)

245 Linnea Jonsson (2012). Impacts of climate change on Pedunculate oak and Phytophthora activity in north and central Europe
246 Ulrika Belsing (2012) Arktis och Antarktis föränderliga havsistäcken
247 Anna Lindstein (2012) Riskområden för erosion och näringsläckage i Segeåns avrinningsområde
248 Bodil Englund (2012) Klimatanpassningsarbete kring stigande havsnivåer i Kalmar läns kustkommuner
249 Alexandra Dicander (2012) GIS-baserad översvämningskartering i Segeåns avrinningsområde
250 Johannes Jonsson (2012) Defining phenology events with digital repeat photography
251 Joel Lilljebjörn (2012) Flygbildsbaserad skyddszonsinventering vid Segeå
252 Camilla Persson (2012) Beräkning av glaciärers massbalans – En metodanalys med fjärranalys och jämviktslinjehöjd över Storglaciären
253 Rebecka Nilsson (2012) Torkan i Australien 2002-2010 Analys av möjliga orsaker och effekter
254 Ning Zhang (2012) Automated plane detection and extraction from airborne laser scanning data of dense urban areas
255 Bawar Tahir (2012) Comparison of the water balance of two forest stands using the BROOK90 model
256 Shubhangi Lamba (2012) Estimating contemporary methane emissions from tropical wetlands using multiple modelling approaches
257 Mohammed S. Alwesabi (2012) MODIS NDVI satellite data for assessing drought in Somalia during the period 2000-2011
258 Christine Walsh (2012) Aerosol light absorption measurement techniques: A comparison of methods from field data and laboratory experimentation
259 Jole Forsmoo (2012) Desertification in China, causes and preventive actions in modern time
260 Min Wang (2012) Seasonal and inter-annual variability of soil respiration at Skyttorp, a Swedish boreal forest
261 Erica Perming (2012) Nitrogen Footprint vs. Life Cycle Impact Assessment methods – A comparison of the methods in a case study.
262 Sarah Loudin (2012) The response of European forests to the change in summer temperatures: a comparison between normal and warm years, from 1996 to 2006
263 Peng Wang (2012) Web-based public participation GIS application – a case

study on flood emergency management

264 Minyi Pan (2012) Uncertainty and Sensitivity Analysis in Soil Strata Model Generation for Ground Settlement Risk Evaluation

265 Mohamed Ahmed (2012) Significance of soil moisture on vegetation greenness in the African Sahel from 1982 to 2008

266 Iurii Shendryk (2013) Integration of LiDAR data and satellite imagery for biomass estimation in conifer-dominated forest

267 Kristian Morin (2013) Mapping moth induced birch forest damage in northern Sweden, with MODIS satellite data

268 Ylva Persson (2013) Refining fuel loads in LPJ-GUESS-SPITFIRE for wet-dry areas - with an emphasis on Kruger National Park in South Africa

269 Md. Ahsan Mozaffar (2013) Biogenic volatile organic compound emissions from Willow trees

270 Lingrui Qi (2013) Urban land expansion model based on SLEUTH, a case study in Dongguan City, China

271 Hasan Mohammed Hameed (2013) Water harvesting in Erbil Governorate, Kurdistan region, Iraq - Detection of suitable sites by using Geographic Information System and Remote Sensing

272 Fredrik Alström (2013) Effekter av en havsnivåhöjning kring Falsterbohalvön.

273 Lovisa Dahlquist (2013) Miljöeffekter av jordbruksinvesteringar i Etiopien

274 Sebastian Andersson Hylander (2013) Ekosystemtjänster i svenska agroforestrysystem

275 Vlad Pirvulescu (2013) Application of the eddy-covariance method under the canopy at a boreal forest site in central Sweden

276 Malin Broberg (2013) Emissions of biogenic volatile organic compounds in a Salix biofuel plantation – field study in Grästorp (Sweden)

277 Linn Renström (2013) Flygbildsbaserad förändringsstudie inom skyddszoner längs vattendrag

278 Josefin Methi Sundell (2013) Skötseleffekter av miljöersättningen för natur- och kulturmiljöer i odlingslandskapets småbiotoper

279 Kristín Agustsdottír (2013) Fishing from Space: Mackerel fishing in Icelandic waters and correlation with satellite variables

280 Cristián Escobar Avaria (2013) Simulating current regional pattern and composition of Chilean native forests using a dynamic ecosystem model

281 Martin Nilsson (2013) Comparison of MODIS-Algorithms for Estimating Gross Primary Production from Satellite Data in semi-arid Africa

282 Victor Strevens Bolmgren (2013) The Road to Happiness – A Spatial Study of Accessibility and Well-Being in Hambantota, Sri Lanka

283 Amelie Lindgren (2013) Spatiotemporal variations of net methane emissions and its causes across an ombrotrophic peatland - A site study from Southern Sweden

284 Elisabeth Vogel (2013) The temporal and spatial variability of soil respiration in boreal forests - A case study of Norunda forest, Central Sweden

285 Cansu Karsili (2013) Calculation of past and present water availability in the Mediterranean region and future estimates according to the Thornthwaite water-balance model

286 Elise Palm (2013) Finding a method for simplified biomass measurements on Sahelian grasslands

287 Manon Marcon (2013) Analysis of biodiversity spatial patterns across multiple taxa, in Sweden
288 Emma Li Johansson (2013) A multi-scale analysis of biofuel-related land acquisitions in Tanzania - with focus on Sweden as an investor
289 Dipa Paul Chowdhury (2013) Centennial and Millennial climate-carbon cycle feedback analysis for future anthropogenic climate change
290 Zhiyong Qi (2013) Geovisualization using HTML5 - A case study to improve animations of historical geographic data
291 Boyi Jiang (2013) GIS-based time series study of soil erosion risk using the Revised Universal Soil Loss Equation (RUSLE) model in a micro-catchment on Mount Elgon, Uganda
292 Sabina Berntsson & Josefin Winberg (2013) The influence of water availability on land cover and tree functionality in a small-holder farming system. A minor field study in Trans Nzoia County, NW Kenya
293 Camilla Blixt (2013) Vattenkvalitet - En fältstudie av skånska Säbybäcken
294 Mattias Spångmyr (2014) Development of an Open-Source Mobile Application for Emergency Data Collection
295 Hammad Javid (2013) Snowmelt and Runoff Assessment of Talas River Basin Using Remote Sensing Approach
296 Kirstine Skov (2014) Spatiotemporal variability in methane emission from an Arctic fen over a growing season – dynamics and driving factors
297 Sandra Persson (2014) Estimating leaf area index from satellite data in deciduous forests of southern Sweden
298 Ludvig Forslund (2014) Using digital repeat photography for monitoring the regrowth of a clear-cut area
299 Julia Jacobsson (2014) The Suitability of Using Landsat TM-5 Images for Estimating Chromophoric Dissolved Organic Matter in Subarctic Lakes
300 Johan Westin (2014) Remote sensing of deforestation along the trans-Amazonian highway
301 Sean Demet (2014) Modeling the evolution of wildfire: an analysis of short term wildfire events and their relationship to meteorological variables
302 Madelene Holmblad (2014). How does urban discharge affect a lake in a recreational area in central Sweden? – A comparison of metals in the sediments of three similar lakes